Review Article

Sara I. Ahmad*, Hicham Hamoudi, Ahmed Abdala, Zafar K. Ghouri, and Khaled M. Youssef

Graphene-Reinforced Bulk Metal Matrix Composites: Synthesis, Microstructure, and Properties

https://doi.org/10.1515/rams-2020-0007
Received Aug 12, 2019; accepted Dec 12, 2019

Abstract: This paper provides a critical review on the current status of graphene-reinforced metal matrix composites (GRMMCs) in an effort to guide future work on this topic. Metal matrix composites are preferred over other types of composites for their ability to meet engineering and structural demands. Graphene is considered an ideal reinforcement material for composites due to its unique structure and extraordinary physical, thermal, and electrical properties. Incorporating graphene as a reinforcement in metals is a way of harnessing its extraordinary properties, resulting in an enhanced metallic behavior for a wide variety of applications. Combining graphene with bulk metal matrices is a recent endeavor that has proven to have merit. A systematic study is needed to critically examine the efforts applied in this field, the successes achieved, and the challenges faced. This review highlights the three main pillars of GRMMCs: synthesis, structure, and properties. First, it discusses the synthesis techniques utilized for the fabrication of GRMMCs. Then, it highlights the resulting microstructures of the composites, including graphene dispersion and interfacial interactions. Finally, it summarizes the enhancements in the mechanical, electrical, thermal, and tribological properties of GRMMCs, while highlighting the effects of graphene type and content on those enhancements.

Keywords: graphene, metals, composites, interface, properties

***Corresponding Author: Sara I. Ahmad:** Department of Sustainable Development, Hamad Bin Khalifa University, Doha 5825, Qatar; Email: sahmed@mail.hbku.edu.qa; Tel.: +974 66633557
Hicham Hamoudi: Qatar Environment and Energy Research Institute, Doha 34110, Qatar
Ahmed Abdala, Zafar K. Ghouri: Department of Chemical Engineering, Texas A&M University, Doha 23874, Qatar
Khaled M. Youssef: Department of Materials Science and Technology, Qatar University, Doha 2713, Qatar

Table of Abbreviations

2D two dimensional
3D three dimensional
ARB accumulative roll bonding process
at% atomic %
BM ball milling
CMC ceramic matrix composites
CNT carbon nanotube
COF coefficient of friction
CP cold pressing
CS compressive strength
CTAB cetrimonium bromide
CVD chemical vapor deposition
CYS compressive yield strength
CTE coefficient of thermal expansion
DMD disintegrated melt deposition method
DI water deionized water
EC etyle cellulose
FLG few layer graphene
FS flexural strength
FSP friction stir processing
GNF graphene nanoflake
GNP graphene nanoplate
GNR graphene nanoribbon
GNS graphene nanosheet
GO graphene oxide
GQD graphene quantum dot
Gr graphene
GRMMC graphene-reinforced metal matrix composite
HP hot pressing
HPS hot press sintering
HRDSR high-ratio differential speed rolling
HRTEM High-resolution transmission electron microscopy
HV Vickers hardness
IACS international annealed copper standard
IPA isopropyl alcohol
LS laser sintering
MLG multilayer graphene

MLM molecular level mixing
MM mechanical mixing
MMC metal matrix composite
MO metal oxide
MS magnetic stirring
PASE particle-assisted shear exfoliation
PCA process control agent
PG pristine graphene
PM planetary milling
PMC polymer matrix composite
PMMA Poly (methyl methacrylate)
PVA polyvinyl alcohol
PVP polyvinyl pyrrolidone
RGO reduced graphene oxide
SAED selected area electron diffraction
SEM scanning electron microscopy
SLM selective laser melting
SPS spark plasma sintering
TC thermal conductivity
TEM transmission electron microscopy
TYS tensile yield strength
UTS ultimate tensile strength
UHP uniaxial hot pressing
VHP vacuum hot pressing
vol% volume %
wt% weight %
XRD x-ray diffraction
YM Young's modulus

1 Introduction

Graphene, known as "the wonder material of today's scientific world," is not only the strongest material to be discovered to date but also is the thinnest material [1, 2]. The two-dimensional (2D) structure of graphene is defined by its one-atom thick, 2D sp^2 hybridized carbon sheet consisting of hexagonal lattices with a height of 0.33 nm [3, 4]. For many decades, graphene has been identified by the scientific world as the basic structural unit of bulk graphite. Theoretically, it had been regarded as unstable to exist physically; hence, it attained no specific interest as an individual entity. However, the pioneering work of Geim and coworkers [5] in 2004, which led to the separation of single layers of graphite, led to rapidly growing attention to graphene, which would later be known as the wonder material. It has been proven to have exceptional properties as an isolated entity, such as excellent thermal and electrical conductivities of 5×10^3 W/m·K [6] and 6×10^3 S/m [7], respectively. It is harder than a diamond and 100 times stronger than steel, with a tensile strength and elastic modulus of 130 GPa and 1.2 TPa, respectively [8]. Yet it is flexible and can take any form or shape [9]. Moreover, it is capable of absorbing 2.3% of light [10], making it the first and only one-atom-thick material visible to the naked eye. Those exceptional properties elevated graphene from being the building unit of graphite to an independent material with countless possibilities to be used in a wide range of applied technologies. Applications of graphene include electronics, energy storage, sensors, biomedical devices, and as the newest member in bulk composites for structural applications [11–16].

Harnessing the extraordinary properties of graphene can be accomplished through the incorporation and dispersion of graphene as a reinforcement in bulk composites such as polymers, ceramics, or metal composites [17, 18]. Composites are advanced materials and are considered the most promising class of materials in the modern applied science world. Combining different materials to provide unique properties is highly attractive for all sorts of applications [19, 20]. Composite materials can be classified into metal matrix composites (MMCs), ceramic matrix composites (CMCs), and polymer matrix composites (PMCs). More research has been conducted on CMCs and PMCs than MMCs. This is mainly due to the simpler fabrication routes of such composites, which does not involve high temperature and pressure requirements. Yet MMCs have higher abilities to meet engineering demands and are the most widely used in manufacturing industries such as aerospace, automotive, and construction [21]. Even in small concentrations, the interaction of graphene as a reinforcement within the matrix is facilitated by its nanometric nature [18] and its large surface area of 2626 m^2/g [22]. The 2D structure of graphene provides a higher surface area than other carbon-based materials, thereby offering a larger area to interact with the matrix for enhanced mechanical stress and electrons or phonons transfer [1, 23]. In addition, its large specific area eliminates the need to use large fractions of the reinforcements, reducing the tendency for agglomeration within the matrix [24, 25], and it can also act as a barrier to dislocation motion, resulting in enhanced strengthening of materials [26]. Another feature that makes graphene suitable as a reinforcement is its flat morphology, which is more susceptible to withstand the high-pressure processing routes involved in the fabrication of composites [1]. Its lower production cost than carbon nanotubes (CNTs) and its availability in high-quality and bulk quantities adds to its potential as a reinforcement material [1, 27].

The alteration in the microstructure of metallic materials after adding nanoscale reinforcements allows for tai-

loring of the properties of those materials, which makes it highly suitable for structural and functional applications [20]. However, compared with graphene-based PMCs [22, 28–30] and CMCs [31–33], the field of graphene-based MMCs has been little researched. In addition, the majority of the existing literature in this field has focused on the deposition of metallic nanoparticles, metallic oxides, and metallic carbides on the surface of graphene and its derivatives to explore its applications in energy storage, sensory applications, and photocatalytic systems [34–43]. Increasing interest has been reported in using graphene and its derivatives as a reinforcement in bulk MMCs, yet the field is still at its early stages [44]. This can be attributed to many challenges in fabricating MMCs reinforced with graphene, such as the dispersion of the reinforcement in the matrix and the undesired interfacial reaction due to the metals' high reactivity [45]. Even with limited number of research studies, graphene has been proven to fulfill the requirements of an excellent nanofiller in MMCs, leading to the production of superior materials that are lightweight [24], demonstrate high strength [46, 47], have high ductility [48, 49], and have enhanced thermal [50, 51] and electrical conductivity [52, 53].

Graphene can be used to describe a graphene-based family of materials that have been produced with varying structures. In this paper, those materials will be referred to as graphene "Gr" unless specified otherwise and include graphene nanoplates (GNPs), graphene oxide (GO), reduced graphene oxide (rGO), graphene quantum dots (GQDs), and graphene nanoribbons (GNRs). It is important to note that unless single-layered graphene is mentioned, the abbreviation "Gr" is used often in this paper to represent all the above-mentioned graphene derivatives for simplicity. It is important to note that per the author's knowledge, no studies so far have reported the reinforcement of GQDs in MMCs. In addition, only one paper reported the fabrication of GNRs in MMCs [52]. The main focus of this field thus far had been on developing GNPs [18, 23–27, 54–57] and GO-reinforced MMCs [49, 58–73].

Figure 1 shows the increased attention toward utilizing Gr as a reinforcement material in bulk MMCs. According to Web of Science and Science Direct databases, the number of publications investigating Gr-reinforced MMCs per year has increased from 2010 to 2018. This increasing trend shows the increased scientific research interest in studying the effect of Gr as a reinforcement material in MMCs. Among the reported studies of MMCs, Gr-reinforced Al, Cu, and Mg matrix composites have gained the most interest.

Research on GRMMCs has developed in a short period of time and is still at its beginning. A systematic study

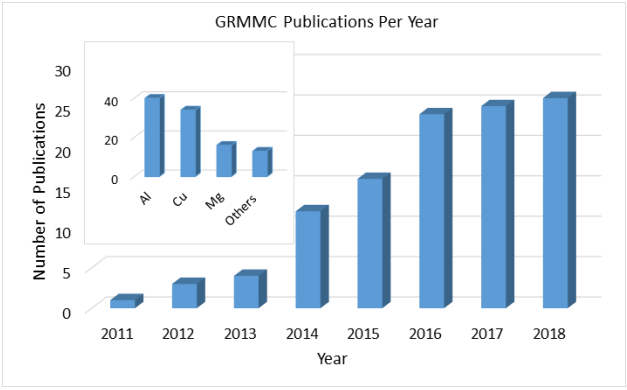

Figure 1: Number of publications on bulk GRMMCs per year based on Web of Science and Science Direct databases. The index shows the number of publications per metal type.

on the efforts applied in this field and the successes and challenges is required. The aim of this review paper is to provide a deeper insight into the status of the GRMMC research field and to serve as a comprehensive reference to guide future work on GRMMCs. It provides a full review on the work that has been performed in this field while focusing on the most studied metallic systems (Al, Cu, Mg). The review starts with a brief background introducing Gr and its derivatives. Then, it sheds light on the various processing techniques for GRMMCs, the microstructures of GRMMC and how it is affected by the dispersion and distribution of Gr in metal matrices, as well as the interfacial interactions between Gr and metals. Finally, the review discusses the effect of Gr addition on the mechanical, thermal, electrical, and surface properties of GRMMC.

2 Graphene Properties, Derivatives, and Synthesis

The research boom on Gr is directly related to its birth in 2004 when Geim *et al.* [5] successfully isolated it from graphite. It was regarded for the first time as a thermally stable entity regardless of its atomic thin structure [22, 45]. However, the history of Gr dates back to as early as the 19th century. A timeline of the history of Gr is presented in Figure 2. A more detailed historical background on Gr research can be found in Geim's 2012 review paper [74].

The fabrication of monolayer Gr requires overcoming the Van der Waals forces connecting the Gr layers in graphite. Exfoliating high-quality and large quantities of monolayers of Gr is still a challenging process. In contrast, attaining graphene nanoplatelets (GNPs), which consist of a few (10–40) Gr layers [1], is easier and faster

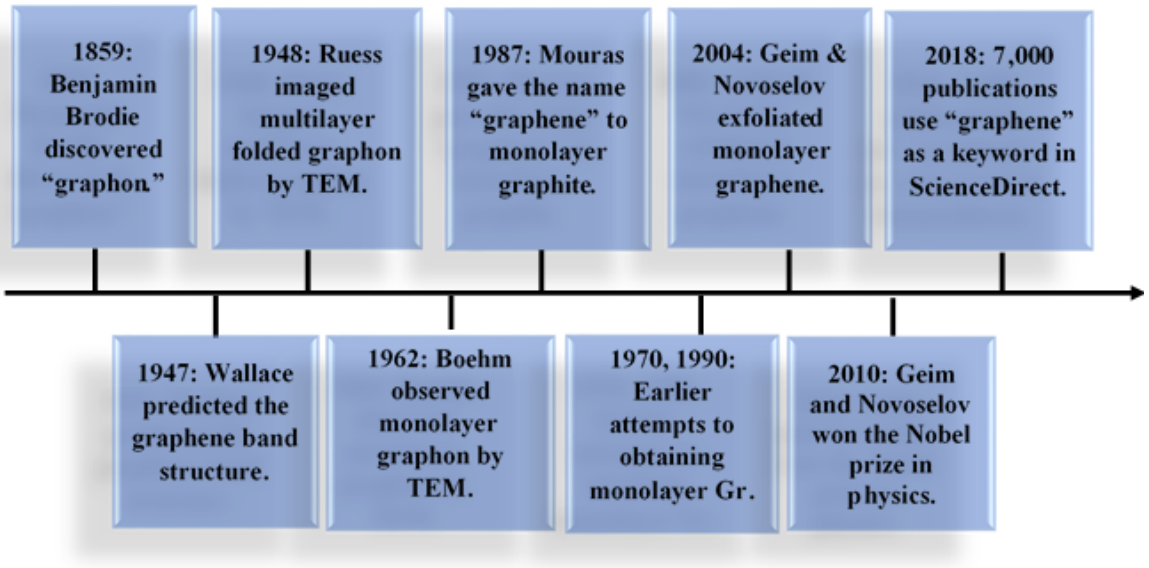

Figure 2: Timeline of the most important milestones in graphene history.

than exfoliating monolayer Gr [55, 75]. The thin structure of GNPs can retain the structural integrity and outstanding properties of monolayer Gr, such as its high surface area and excellent mechanical, electrical, and thermal properties [1]. In the literature, a variety of names are used to describe few layers Gr (FLGs) or GNPs such as graphene nanosheets (GNSs), graphene platelets, and graphene nanoflakes (GNFs).

Just like graphite, which consists of stacked layers of Gr connected via Van der Waals forces, graphite oxide consists of stacked layers of GO. In graphite oxide, the stacked GO sheets are functionalized with O, OH, or COOH groups. The rich presence of functional groups increases the interlayer spacing between the sheets to 6–10 Å, compared with 3 Å for unfunctionalized graphite [22, 70]. Graphite oxide was first prepared in the 19th century by Brodie [76] by treating graphite with strong materials such as potassium chlorate and nitric acid. However, graphite oxide possesses different properties than Gr. Today, a safer synthesis technique of graphite oxide is favored in laboratories, as reported by Hummers and Offeman [77]. It involves the mixing of graphite with sodium nitrate, sulfuric acid, and potassium permanganate. After the discovery of Gr in 2004, GO has been used in research as the starting material for large scale production of GNP through exfoliation of graphite oxide into GO and the reduction of GO into rGO [22]. The functional groups in GO allow for its dispersibility in water and other solvents. This produces monodispersed GNPs via chemical or thermal reduction of GO in colloidal suspensions [78, 79]. Unfortunately, an inversely proportional relationship exists between the physical properties of Gr and dispersibility [80]. The reduction of GO is an important process in order for the material to possess the outstanding properties of Gr, especially electrical properties, as GO is electrically nonconductive [22, 78].

GNRs are thin, elongated Gr sheets with nanometric width around 10–20 nm and a high aspect ratio [81]. GNR materials have attracted the attention of many research studies due to their capability of generating a band gap, which normal Gr sheets lack. This unique characteristic of GNRs is attractive for optoelectronic applications. However, controlling the quality and the type of the edge is the main challenge in utilizing Gr in electronic devices [81, 82]. GNRs have been produced by a variety of methods, such as lithography [83], chemical vapor deposition (CVD) [84], and unzipping CNTs by the plasma etching technique [85]. Figure 3 presents a collection of transmission electron microscopy (TEM) images of monolayer Gr, GNPs, GO, and GNRs.

The first successful fabrication method of Gr was performed in 2004 [5] using the micromechanical cleavage method. In this method, a scotch tape was used to exfoliate a single layer Gr from graphite. Several Gr synthesis processes have been developed, any of which can be categorized as a top-down or a bottom-up technique. Top-down techniques involve the isolation of Gr layers from graphite or graphite derivatives to produce single or multilayer Gr sheets. Graphene samples produced using top-down methods are usually of small sizes and large quantities. Bottom-up techniques involve building the Gr sheet atom by atom using specific substrates and carbon-containing compounds. Graphene samples provided by

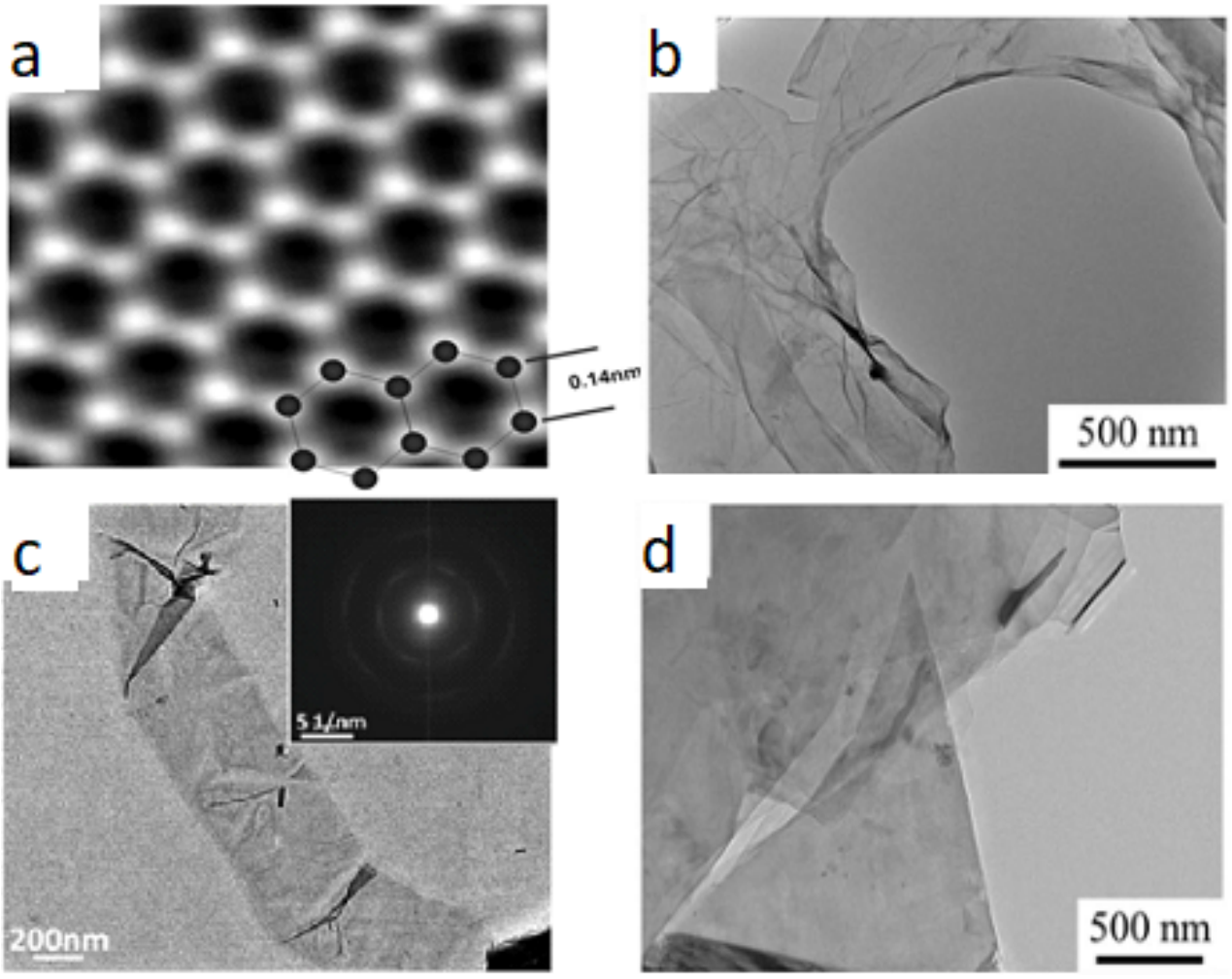

Figure 3: TEM images of (a) a graphene sheet, (b) GO, (c) GNR, and (d) GNP. Reproduced from References [52, 86–88], respectively.

such techniques are usually of small quantity, high quality, and large size [3, 28, 86].

A detailed explanation of all techniques is out of the scope of this work. Therefore, related references are included within the text. Top-down techniques have been used mainly in the fabrication of Gr for bulk GRMMCs [64, 67]. Only a few studies have used in-situ bottom-up Gr growing techniques [88–90]. Recent reviews on the synthesis of Gr and its derivatives can be found in References [91, 92]. Tables 1 and 2 summarize the information on commercially available Gr used in certain GRMMC studies and the main techniques adopted for the synthesis of Gr and its derivatives in other GRMMC studies, respectively.

3 Graphene-Reinforced Metal Matrix Composites (GRMMCs)

3.1 Synthesis Techniques

The synthesis of GRMMCs has faced several obstacles that challenge the successful fabrication of such composites. The first challenge is the poor affinity of Gr toward metals, suggesting poor resultant interfacial bonding. The second challenge is the agglomeration of Gr sheets within the metal due to the Van der Waals forces between Gr sheets [97] and its high surface energy [1], which restricts the homogenous distribution of Gr in the metal matrices. Thus, attaining high-quality GRMMCs is directly related to the synthesis technique of choice. Several authors have argued that the usual powder methodology techniques do not fully solve the dispersion problem of Gr in metal matrices, thus not capturing Gr's full potential and resulting

Table 1: Summary of Commercial Gr and its Derivatives Used in GRMMC Studies.

Product	Company	Size (μm)/Surface Area (m^2/g)	Thickness (nm)	Reference(s)
GNP, GNS, FLG, and multilayer graphene (MLG)	Tanfeng Tech Co. Ltd	5–30	5–10	[93]
	Skyspring Nanomaterials	—	5–10	[47]
	Qingdao Huagao Graphene Technology Corp. Ltd. (China)	—	10 layers	[94]
	Sixth Element Materials Technology Co. Ltd. (China)	14.17 SA	20 layers	[87]
	Ningbo Morsh Technology Co., Ltd., China.	5–15	2–10	[2, 71, 95–97]
	US Nano Company, (USA)	2	20	[98]
	XG Sciences, (USA)	1–15 120–750 SA	1–20	[23, 24, 54, 99–102]
	Angstron Materials	<14	10–100	[63, 103]
	Nanjing Xian Feng Nano Material Technology Co. Ltd (Jiangsu, China)	5–25	5–20	[11, 17, 55, 104–107]
	Nanografi Co. Ltd.	750 SA	5–8	[108]
	American Elements, USA	5–25	5–25	[109]
	XG Science, South Korea	—	6–8	[46]
	Chengdu Organic Chemistry Co. Ltd.	5–10	4–20	[48, 110, 111]
	Cheap Tubes, Inc.	<2	—	[112]
GO	Graphenea (Gipuzkoa, Spain)	—	>95% monolayer	[58, 59]
	Cheap Tubes, Inc.	0.3–0.8	0.7–1.2	[60]
	Institute of Coal Chemistry, Chinese Academy of Sciences	—	—	[61]
	Nanjing Xian Feng Nano Material Technology Co. Ltd (Jiangsu, China)	1–2	1–2	[62]
	Nanomaterials LS	<0.1	2–4	[63]

Table 2: Summary of Synthesized Gr and its Derivatives in GRMMC Studies.

Product	Synthesis	Reference(s)
GO	Modified Hummers' method	[49, 64–72, 113]
GNP, GNF, MLG, FLG, and GNS	Reduction of GO	[49, 57, 113–118]
	Exfoliation of graphite	[18, 56, 119–121]
	In-situ growing Gr in bulk metal matrix	[89]
	In-situ growing 3D Gr by CVD using NaCl template	[90]
	Ex-situ growing of Gr sheets by CVD	[122]
GNR	Facile chemical unzipping of multiwalled CNTs	[52]

in a direct negative impact on the fabricated Gr-metal composite properties [123]. Researchers are striving to discover and develop more advanced techniques for the fabrication of GRMMCs, aiming to produce higher-quality composites by achieving better Gr distribution within metal matrices. Table 3 summarizes the synthesis techniques used for the fabrication of GRMMCs. In this review, the synthesis section is divided into three main sections according to the steps involved in the synthesis technique: pretreatment, synthesis, and postsynthesis and consolidation.

Table 3: Summary of Synthesis Techniques Used for the Fabrication of GRMMC.

Synthesis Step	Techniques		Reference(s)
Pretreatment	Gr pretreatment	Mechanical mixing / sonication in a solvent	[11, 17, 24–27, 44, 49, 51, 52, 54, 58, 59, 64, 65, 68, 69, 71, 73, 93, 96, 99, 104, 107, 108, 115, 118, 120, 123–126, 128–131]
		Surface modification	[69, 71, 90, 96, 113, 127]
	Metal pretreatment	Mechanical mixing / sonication in a solvent	[11, 17, 52, 58, 59, 65, 104, 107, 116, 129, 130]
		Surface modification	[51, 64, 66, 68, 71, 73]
		Ball milling	[88, 128, 129]
Mixing Techniques	Ball milling		[18, 20, 23, 25, 27, 46, 48–50, 53–57, 63, 65, 70, 95, 99, 101, 109, 114–116, 118, 119, 131–133]
	Solution-assisted mixing	Sonication in a solvent	[24, 44, 50, 108, 115, 131]
		Mechanical mixing	[11, 17, 57, 58, 66, 68, 71, 73, 89, 93, 104–108, 117, 120, 125, 127, 130]
		Magnetic stirring	[51, 52, 58, 59, 69, 124, 126]
		Molecular-level mixing	[67, 72, 96, 97, 134, 135]
		High shear mixing	[121, 135, 136]
		Pestle and mortar	[137]
		Vortex mixing	[93, 128]
	Molten/liquid metal processes		[87, 94, 98, 103, 110, 111, 120, 138–141]
	Other techniques	In-situ synthesis	[88–90, 122, 140, 142–144]
		Rolling processes	[100, 123, 145]
Postsynthesis/ consolidation	Cold pressing followed by hot treatment		[11, 17, 18, 20, 26, 27, 44, 50, 58, 59, 65, 66, 73, 95, 104, 105, 107, 124, 125, 129, 130, 132, 137]
	Hot pressing		[23, 49, 51, 54, 55, 63, 64, 68, 70, 88, 99, 101, 108, 118–120, 126, 128]
	Hot extrusion		[11, 17, 48, 50, 55, 57, 73, 95, 104, 105, 107, 110, 111, 118, 130]
	Spark plasma sintering (SPS)		[24, 52, 69, 71, 72, 93, 96, 97, 109, 127, 134, 135]
	Hot rolling		[25, 52, 56]
	3D printing		[60, 112, 133]

3.1.1 Pretreatment of Graphene Reinforcement and Metal Matrix

Before mixing the composite components to fabricate the GRMMCs, several researchers treated the Gr and the metals separately for several reasons, such as to further exfoliate the Gr sheets, to prevent Gr agglomeration and enhance its dispersion in the metal matrix, or to enhance the attraction and attachment between the Gr and the metal matrix. Thus far, the main pretreatment processes that have been reported are either solvent dispersion of the Gr reinforcement [11, 17, 24–27, 44, 49, 51, 52, 54, 58, 68, 69, 71, 73, 99, 118, 123–126] and/or the metal matrix [11, 17, 52, 58], and the surface modification of the Gr reinforcement [69, 71, 90, 96, 127] and/or the metal matrix [51, 66, 68, 71, 73]. Certain mixing techniques have

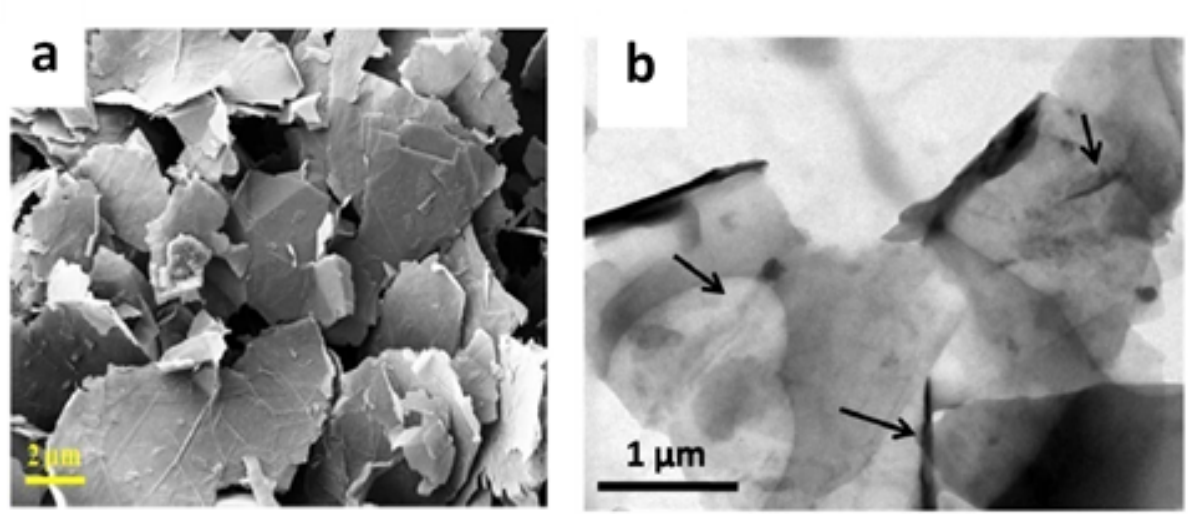

Figure 4: (a) SEM images of GNP powders and (b) TEM images of sonicated GNPs. Reproduced from Reference [24].

been associated with certain pretreatment steps. For example, mechanical mixing or sonication of metals or Gr in solvents is a step mainly used before solution-assisted mixing techniques or ball milling. Pretreatment steps involving surface modifications for metals or Gr have been reported mainly in studies utilizing solution-assisted mixing. Even ball milling has been used as a pretreatment step in some studies [88, 128, 129]. One study reported ball milling of Cu and poly (methyl methacrylate) (PMMA) as a carbon source before in-situ fabricating Cu-Gr composite via CVD [88]. Others used milling to modify the morphology of their metal, such as changing it from spherical to flake-like morphology [128, 129]. However, other studies did not report a pretreatment step because the mixing technique used did not require one or because the authors simply did not opt for one.

3.1.1.1 Graphene Pretreatment

Maintaining the structural integrity of Gr (that is, its high surface area and nanometric structure) is important to extrapolate its unique properties in metal matrices. Several researchers have reported the dispersion of Gr in different solvents in an aim to further exfoliate Gr sheets [68] and to enhance their dispersion and prevent their agglomeration in the metal matrix during the mixing step [58]. Different solvents have been used, such as water [51, 58, 68, 69, 71, 73, 125], ethyl alcohol [25, 118, 124], ethanol [11, 27, 49, 52, 54, 99], and acetone [17, 24, 26, 44, 123, 126], in order to disperse Gr using either ultrasonication, mechanical, or magnetic stirring. Bisht *et al.* [24] ultrasonicated GNPs in acetone before mixing it with Al matrix and consolidating it by SPS. Figures 4a and 4b show the scanning electron microscopy (SEM) and TEM images of the GNP before and after ultrasonication, respectively. The transparency of the GNPs shown in the TEM image suggested good reduction in the number of GNP layers and exfoliation during ultrasonication. In addition, ultrasonicating the GNPs has led to the formation of folds and wrinkles in the GNP sheets, which resulted in limited plastic deformation of the composite due to the mechanical interlocking of GNPs in the Al matrix provided by those features.

The nature of the Gr starting material directly affects the synthesis technique of choice and is critical to their interactions with the matrix material. Several researchers have preferred to start with GO as a precursor [70, 125] in order to avoid the agglomeration of Gr reinforcement. This is attributed to the hydrophilic functional groups in GO, which can successfully suspend GO in aqueous solutions and form chemical bonds with surface-modified metal particles [51, 66, 68, 73]. However, the reduction of GO is hard to control and is often incomplete, which introduces structural defects into the graphitic structure [127]. To avoid the need to reduce GO and eliminate any related structural damages while attaining good affinity of Gr toward metals, pretreating Gr by surface modification has been reported [69, 71, 90, 96, 113, 127]. Zhang *et al.* [127] performed electroless plating of GNP with Cu and Ni before mechanically stirring the modified GNPs with Cu powders and finally sintering the mixed powder composite via SPS. Electroless plating includes sensitizing and activating GNP by ultrasonicating in $SnCl_2$ and $PdCl_2$ solutions followed by washing and filtration before the electroless plating process takes place. At the end of the electroless plating, Ni and Cu were, respectively, adsorbed on the surface of GNPs.

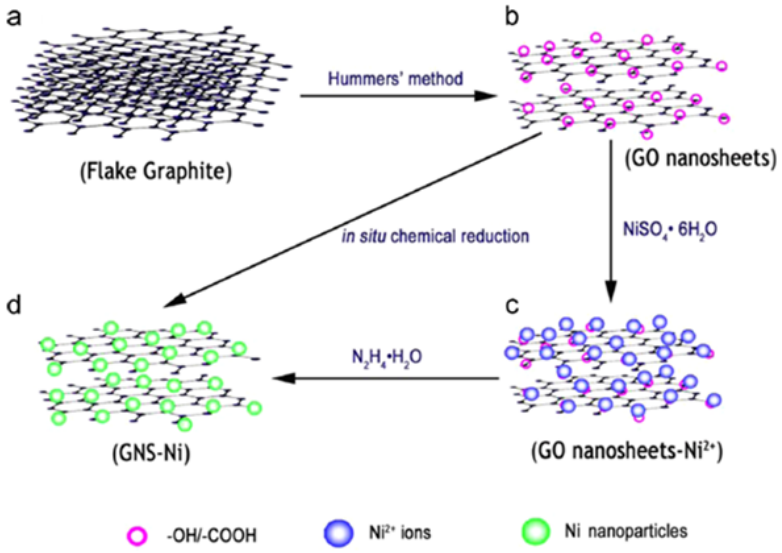

Figure 5: A schematic diagram of the in-situ chemical reduction steps for the fabrication of Ni-decorated GNS. Reproduced from Reference [113].

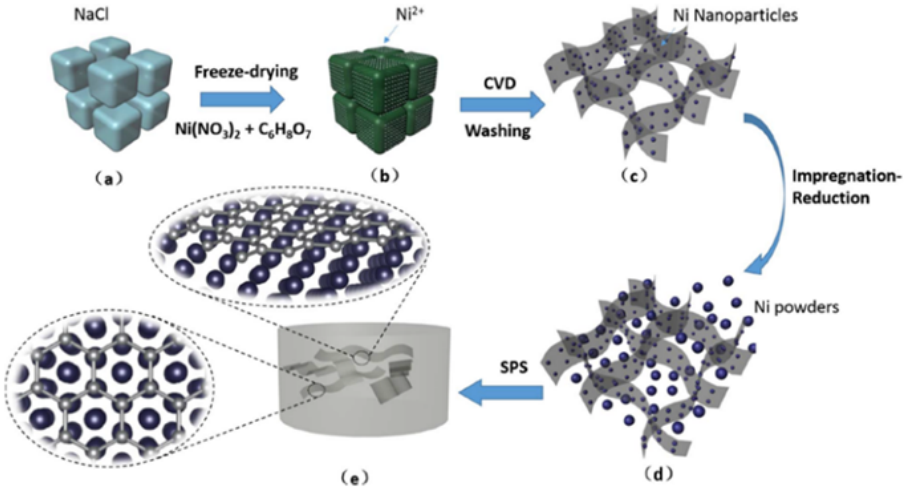

Figure 6: Schematic diagram of the process of 3D Ni-decorated GNS/Ni bulk composites: (a) NaCl crystals, (b) Ni(NO3)2-C6H12O6 coated NaCl by self-assembly after freeze-drying process, (c) Ni-decorated GNSs after CVD process and water washing, (d) Ni-decorated GNS/Ni composite powders after impregnation-reduction process, and (e) bulk composites fabricated by SPS. Reproduced from Reference [90].

Several studies [69, 90, 113] have reported the surface modification and in-situ synthesis of GNS. Tang *et al.* [113] produced Ni-decorated GNSs using an in-situ chemical reduction method. In their method, negatively charged GO is first mixed with Ni salts where Ni ions aggregate and nucleate at the functional group's sites of GO. The mixture then is treated with a reducing agent where nickel ions are reduced in situ to Ni nanoparticles, while the GO are simultaneously reduced to GNS. Finally, this Ni-decorated GNS was sonicated with Cu powders and consolidated via SPS. A schematic diagram of the in-situ chemical reduction steps is shown in Figure 5. A similar procedure was adopted by Ju *et al.* [69]. They used Mg ions as an anchor binding the GNS to Al. The GO sheets were mixed with the Mg salts and then chemically reduced to GNSs using ascorbic acid. The resultant Mg-decorated GNSs were mixed with Al and consolidated via SPS.

More recently, Fu *et al.* [90] synthesized 3D Ni-decorated GNSs by an in-situ high-temperature CVD technique using NaCl crystals, $C_6H_{12}O_6$, and $Ni(NO_3)_2$ as a template, a carbon source, and Ni precursor, respectively. This was followed by an impregnation-reduction process to produce Ni-decorated GNS-Ni composite powders. A schematic diagram of the process is shown in Figure 6. The final composite exhibited a 188% and a 26% increase in the tensile yield strength (TYS) and the ultimate tensile

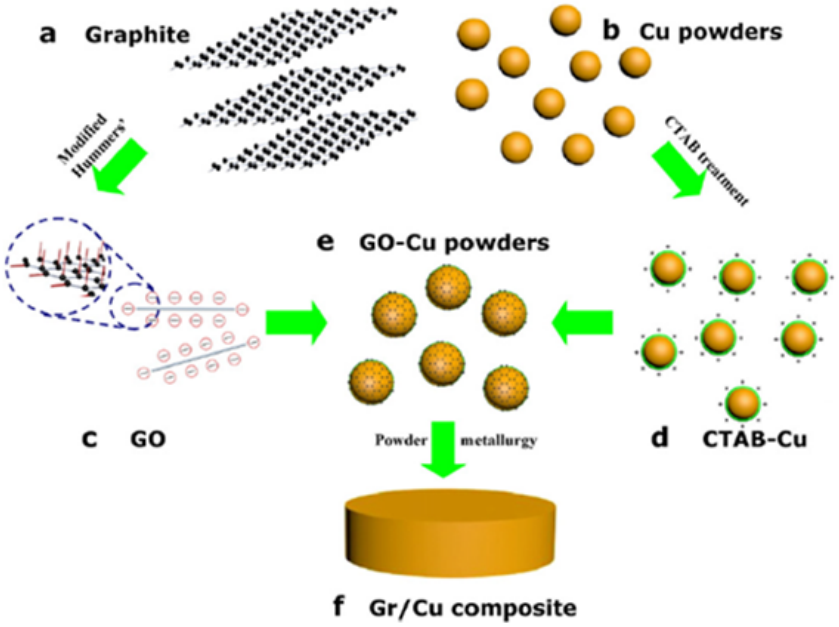

Figure 7: Schematic diagram of the fabrication process of Gr-Cu composite. (a) Graphite, (b) Cu powders, (c) GO with the negative charge, (d) CTAB-modified Cu powders, (e) GO-Cu powders, and (f) Gr/Cu composite. Reproduced from Reference [51].

strength (UTS), respectively. This result was attributed to the homogeneous distribution of GNS in the Ni matrix and the strong interfacial bonding.

3.1.1.2 Metal Pretreatment

Aside from dispersing the Gr-based reinforcement, several researchers reported the dispersion of the metal-based matrix powders in a similar manner. This step was then followed by mixing both reinforcement suspension and the metal slurry for enhancing the uniform dispersion of Gr reinforcement in the metal matrix. The solvents used for metal dispersion include acetone [17, 58] and ethanol [11, 52]. Yang *et al.* [52] used ultrasonication and magnetic stirring to disperse GNRs and Cu separately before mixing both solutions. Liu *et al.* [58] mechanically stirred Al in acetone before adding the ultrasonicated GO water dispersion. Rashad *et al.* [11] ultrasonicated and mechanically mixed GNPs and Al in ethanol, respectively, before mixing the ultrasonicated GNPs and the Al slurry via mechanical mixing.

Several researchers reported the surface modification of the metal matrices ahead of mixing the Gr reinforcement with the metal matrix to enhance the interaction affinity and binding capacity between Gr and metals [51, 64, 66, 68, 71, 73]. Gao *et al.* modified the surface charge of Cu and Al in separate studies ([51, 64] and [68], respectively) using the same technique to enhance the Gr-metal affinity via charge attraction. They mechanically stirred the negatively charged GO with the positively charged cationic surface agent (CTAB)-coated Cu and Al. In general, GO adheres to a negative surface charge due to its attached functional groups such as epoxide and hydroxyl groups on the basal plane and carboxyl groups at the edges. In contrast, CTAB is cationic in nature, which gives Cu and Al powders a positive charge after they are coated with it. As a result of charge attraction, the GO-Cu and GO-Al composite powders achieved uniform adsorption, and the process is referred to as electrostatic self-assembly. Figure 7 is a schematic diagram of the synthesis process of GO-reinforced CTAB-coated Cu. This process was followed by cold compaction of composite powders and sintering at high temperatures to thermally reduce GO. The authors suggested that this novel process eliminates the agglomeration of the GO sheets and preserves its large size as they uniformly adsorb on the surface of the metal.

Some researchers reported the surface modification of metal matrices by the use of polyvinyl alcohol (PVA) [66, 71, 73]. It is a water-soluble polymer used to introduce a hydrophilic membrane to metals' surfaces. Wang *et al.* [73] synthesized the GNS-Al composite by treating Al flakes by PVA aqueous solution before mechanically mixing it with GO aqueous dispersion dropwise, filtering and rinsing the GO-Al composite powders, and heating the GO-Al composite powders to decompose the PVA and reduce the GO nanosheets to GNSs. The same procedure was followed 5 years later by Ponraj *et al.* [66] using a Cu matrix instead of Al. Similarly, Jiang *et al.* [71] modified Cu powders with

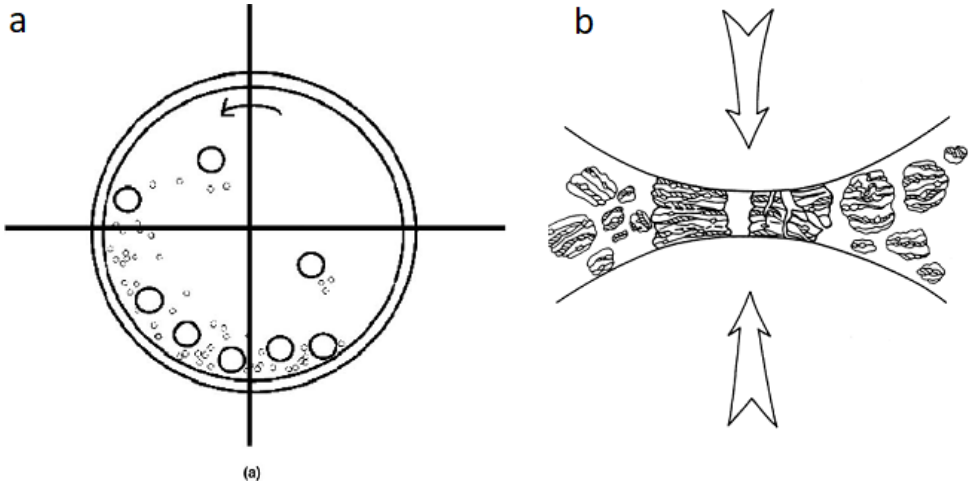

Figure 8: (a) Schematic diagram of the rotation of powders and milling balls inside the milling vial. (b) The crushing of materials as a result of ball collisions. Reproduced from Reference [6].

PVA to produce Gr-Cu composites, but they used Gr as precursor instead of GO. Because Gr lacks the hydrophilicity of GO and hence has no affinity toward the OH functional groups in PVA, Gr was treated with polyvinyl pyrrolidone (PVP) before mixing it with PVA-modified Cu. The two polymers were used to enhance the interactions between Gr reinforcement and the Cu matrix. Jiang *et al.* [71] explained that the PVP would interact with Gr via π-π interactions, while the carbonyl group in PVP would interact with the hydroxyl groups in PVA. Because Gr has lower defects and higher structural integrity than GO, it is expected to perform better as a reinforcement.

3.1.2 Mixing Techniques

Mixing the composite components is done using a variety of techniques and is considered the main step in the synthesis of GRMMCs. No systematic studies have compared mixing techniques and their effects on the structure and behavior of GRMMCs. Thus, it is impossible to categorize the mixing techniques based on effectiveness.

3.1.2.1 Mechanical Milling

Mechanical milling, which is also called ball milling or mechanical alloying, is a top-down synthesis technique used to produce materials with nanostructures. This is done by disintegrating the coarse-grained structure of those materials' elemental powders [146, 147]. In mechanical milling, which is represented in Figure 8, selected powders are sealed in a steel vial along with a number of steel balls of certain sizes under an inert atmosphere, typically argon. The high energy rotation of the balls inside the vial causes constant collision of the balls, which leads to crushing the powders trapped in between with a high impact force. The repeated mechanical deformation results in the formation of cell/subgrain structures with high dislocation density. These cellular structures transfer into high-angle grain boundaries with increasing milling time, forming nanocrystals [146, 147].

Mechanical milling has become a widely chosen technique for the mixing of Gr-reinforced MMCs due to its simplicity and scalability in Gr-reinforced Al [18, 20, 23, 25, 27, 50, 54–57, 70, 99, 118, 119, 132], Cu [49, 63], or Mg [48] matrix composites. In most cases where milling was used for the mixing of Gr and metals, a process control agent (PCA) is used to adsorb onto the surface of powders, minimize cold welding, and prevent particle agglomeration. Nonetheless, the structural integrity of Gr in MMCs prepared via milling is a point of debate. Some researchers have suggested that the structural integrity of Gr is damaged during mechanical milling due to its large surface area, which cannot withstand the high impact force from milling [51]. In addition, it was suggested that milling can cause interfacial reactions due to heat generation during milling [68, 104]. In most studies, the structural integrity of Gr in GRMMCs had been characterized using Raman spectra [18, 48, 49, 53, 55, 56, 70]. Ranges between 1333–1359, 1583–1603, and 2665–2727 cm^{-1} have been reported for typical D, G, and 2D bands, respectively, for GRMMCs synthesized via milling. Generally, the G and D bands are the most important for the evaluation of Gr. The I_D/I_G ratio represents the integrity of the Gr structure. It was reported that this ratio increases after milling, suggesting an increase in the defect-representing band [55, 56, 70]. Li *et al.* [53]

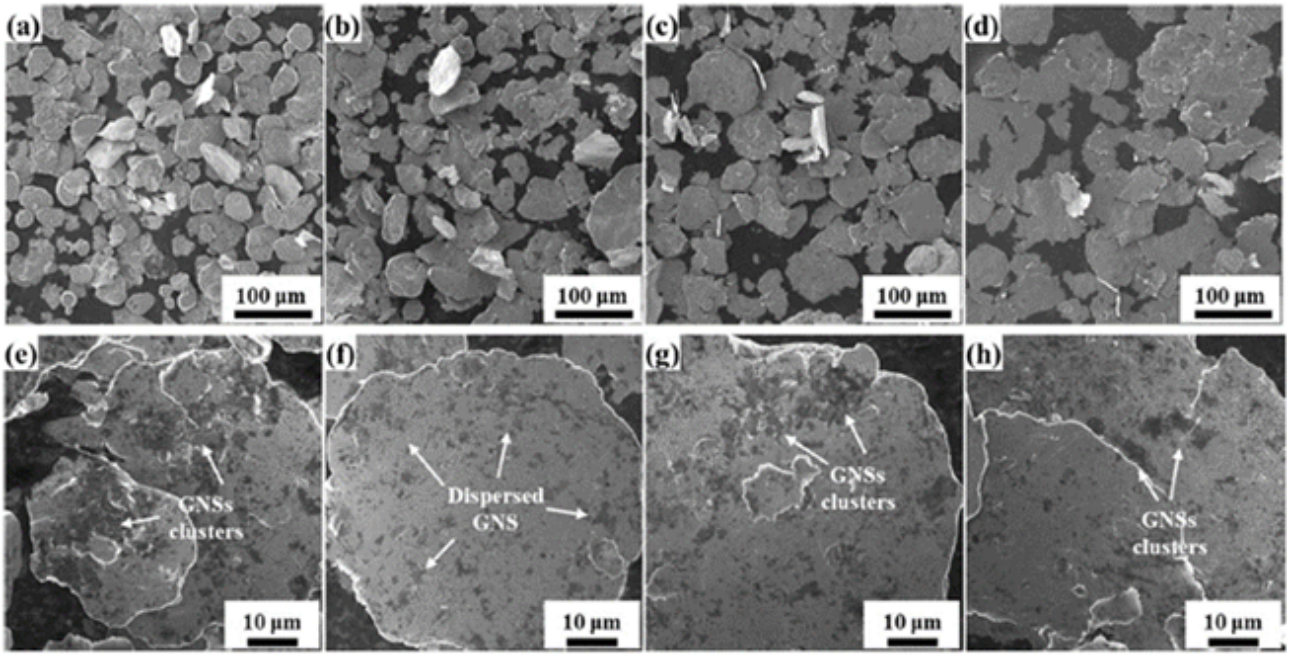

Figure 9: SEM images of GNS/Al flakes after low-speed milling (a, e) 4 h, (b, f) 6 h, (c, g) 8 h, (d, h) 10 h. Reproduced from Reference [95].

used milling to disperse 0.2 wt% GNPs with Al to form what they called the "master alloy" as the GNP carrier, before adding it to Al melts to form the composite through casting and rolling. The I_D/I_G ratio from the Raman spectrum for GNPs before and after milling of the master alloy and in the Al-0.2 wt% GNP composites was 0.13, 1.10, and 1.14, respectively. The ratio increases significantly after milling of GNPs, yet it remains almost the same with a slight increase after high-temperature melting, casting, and rolling. The result suggests that most of the structural damage occurred in the milling process.

The intrinsic structure damage of Gr and its derivatives may be unavoidable during milling, yet several researchers have reported a reduction in the damage degree by controlling the milling time [18, 49, 95] and the milling media size [55]. The ball-milling time is a main factor that greatly affects the milling synthesis and, hence, the structural integrity and dispersibility of Gr [49, 95]. Pérez-Bustamante *et al.* [18] mixed GNSs and Al powders via milling in methanol as a PCA to avoid agglomeration. They reported a reduction in the peak intensity of Raman spectra as the milling time increased. This finding was justified by the introduction of structural disorders and increase in amorphous fraction of the GNPs with increased milling time. However, crystallinity of GNPs was still preserved even after 5 h of high-energy milling, which was attributed to the protection provided by the ductile Al matrix against constant collision on the well-dispersed GNPs. Similar results were reported by Yue *et al.* [49], where the Raman spectra ratio of I_D/I_G increased from 0.84 to 1.42 with increasing the ball-milling time. The authors attributed this behavior to the large accumulated milling energy that results in breaking the weaker chemical energy of the C-C bonds.

Jiang *et al.* [95] reported that implementing an optimum milling time can eliminate the need for a tradeoff between achieving a uniform dispersion of Gr in metal matrices and the structural damage of Gr nanosheets, as well as the dilemma of achieving high strength at the expense of poor ductility. A shift-speed ball milling process, which consisted of various hours of low-speed milling and 0.5 h high-speed milling, was used to prepare 0.5 vol% Gr-reinforced Al composite. The dispersion of Gr in Al was studied via SEM images in Figure 9. It was reported that after 6 h of low-speed milling, Gr was well dispersed with no apparent clustering, compared with the obvious clustering of Gr after 4 h milling and reaggregation after 8–10 h of milling. In addition, a well-balanced combination of strength and ductility, of 295 MPa UTS, and 13.5% tensile elongation, were reported after 6 h low-speed milling and 0.5 h high-speed milling.

Zhang *et al.* [55] suggested that the use of smaller diameter milling balls or slower rotation speed can reduce the milling-induced degree of damage in the Gr intrinsic structure. It was explained that the reduction in milling collision energy is determined by these two factors, thus the 3-mm balls used in their study, compared with the 5- to 10-mm balls used in other studies, helped to minimize

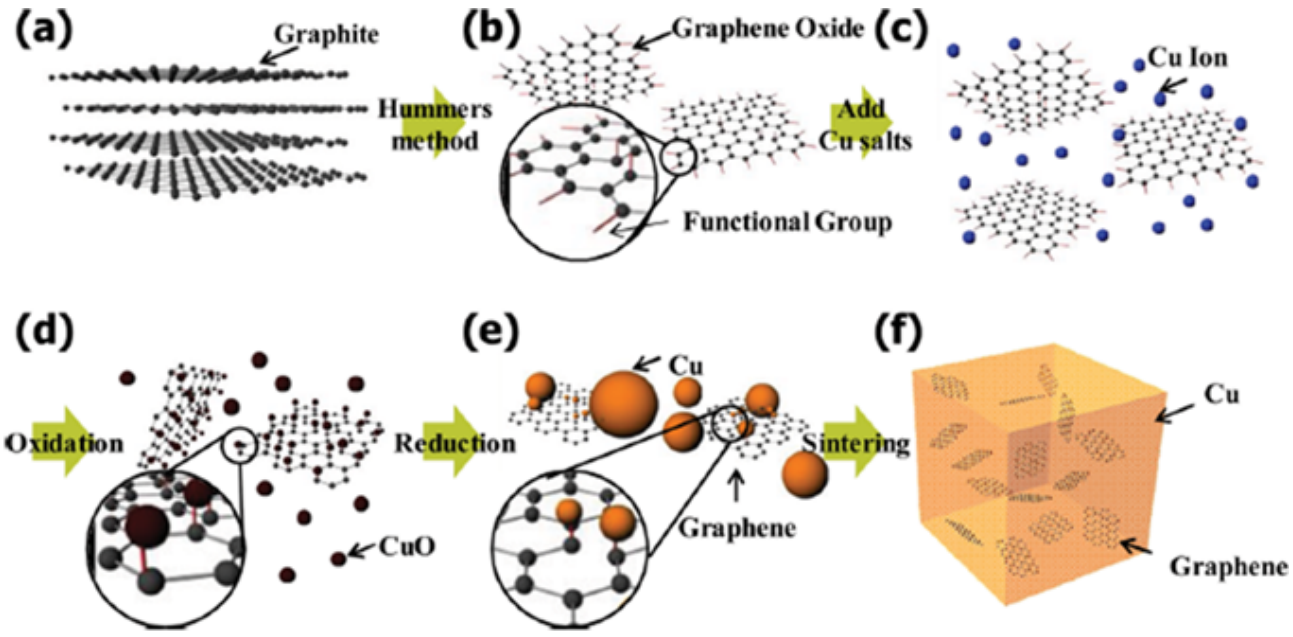

Figure 10: Schematic of the MLM process to fabricate rGO-Cu composite. (a) Graphite. (b) Graphene oxide prepared by Hummer's method. (c) Dispersion of Cu salt in GO solution. (d) Oxidation of Cu ions to CuO on GO. (e) Reduction of GO. (f) Sintered rGO-Cu composite powders. Reproduced from Reference [72].

the reduction in their I_G/I_D ratio to 0.9 only after 24 h of milling. Nevertheless, milling is the most widely used technique in the synthesis of GRMMCs due to its simplicity, low cost, and effectiveness in dispersing Gr into metal matrices [49, 95], as studies utilizing milling in the synthesis of GRMMCs have reported uniform and homogenous dispersion of Gr nanosheets in metals [18, 23, 25, 27, 54, 56, 57, 70, 95, 99, 119].

3.1.2.2 Solution-Assisted Mixing

The techniques in this category involve the mechanical mixing of Gr and metal powders in a solvent. The selection of solvents is based on certain criteria such as nonreactivity with Gr or metals, volatility, and ease of evaporation [1]. There have been several reports on wet powder mixing of Gr and metals using techniques such as ultrasonic dispersion [24, 44, 50], mechanical mixing [11, 17, 57, 58, 66, 68, 71, 73, 89, 93, 104–108, 117, 120, 125, 127, 130], and magnetic stirring [51, 58, 69, 124, 126]. Solution-assisted methods have several drawbacks to be considered. First, the liquid media can be a source of contamination, which if not treated properly can prevent the full densification of the powder composites. Second, these methods are not suitable for large-scale composite fabrication. This is because a large amount of liquid media is required to ensure the adequate mixing of a few grams of composite powders. In addition, a uniform dispersion of Gr and metals might not be possible to achieve in liquid media mixing with all types of metals. This is because of the much higher density of metals than Gr, which can cause metal powders to settle instead of mixing uniformly with Gr [1].

Molecular-level mixing (MLM) is a synthesis technique that involves the mechanical mixing of the Gr reinforcement and the metal matrix in a solvent, yet with an aim of enhancing the interfacial bonding between the composite's reinforcement and matrix through chemical bonding [72]. MLM has been used in the synthesis of Gr-reinforced Cu [51, 72, 96, 97, 134, 135] and Ni [67] matrix composites. Usually, the MLM synthesis technique involves several chemical steps. First, GO is mechanically mixed with the metal ions in a solvent, where the metal ions would attach to the GO sheets, which prevents its agglomeration. Second, metal ions are oxidized to form a chemical bond between the GO and the metal ions, thereby producing GO-reinforced metal oxide (MO) composites. This enhances the adsorption and dispersion of Gr in metals due to the decreased density difference between Gr and metal ions compared with Gr and metals. Finally, thermal reduction takes place to reduce GO-MO to GRMMCs [72, 134]. A schematic diagram of the MLM process adopted by Hwang *et al.* [72] for the synthesis of Gr-reinforced Cu matrix composites is shown in Figure 10. After preparing the GO from graphite using the Hummers method, an aqueous solution of Cu acetate was added to the GO suspension. NaOH was added after heating the

mixed solution to 80°C and the reaction reduced Cu ions to CuO, forming the GO-CuO mixture. Performing this step should enhance the dispersion between Cu and Gr through chemical bonding. Finally, the composite powders were thermally reduced at 450°C to Gr-Cu and consolidated by SPS. A Raman spectrometer was used to examine the effect of the synthesis process on the rGO structural integrity. The I_D/I_G ratio increased from 0.78 to 0.81 for GO and GO-Cu ions, respectively, then decreased to 0.40 for rGO-Cu composite. The authors related the increase in the ratio to the damage of the sp^2 network of Gr as a result of the interaction of the Cu ions with the GO surface. The reduction in the ratio was, however, related to the partially recovered structure of Gr in the composite after the reduction process.

Chen *et al.* [97], Si *et al.* [96], and Zhang *et al.* [134] used MLM to fabricate GNP-reinforced Cu composite by starting with GNPs instead of GO. Zhang *et al.* [134] reported a modified MLM process. They suggested that the NaOH used in Reference [72] can have an adverse effect on chemical bonding by rapidly reducing CuO and GO during heating. In their study, they activated GNPs by using a hydrochloric acid solution before dispersing it in deionized water via ultrasonication. Then, they added the aqueous solution of Cu acetate to the GNP suspension with continuous sonication to facilitate the adsorption of Cu^2 ions. Heating and magnetic stirring followed to evaporate the solvent and dry the composite powders. The Cu acetate was then decomposed and thermally reduced in a tube furnace. Finally, composite powders were sintered and densified via SPS. The I_D/I_G intensity ratio from Raman spectra before and after the reduction were found to be 0.25 and 0.20, respectively. The drop in the ratio after the reduction suggests the partial restoration of the original structure.

Another promising solution-assisted technique is the particle-assisted shear exfoliation (PASE) technique [121, 135, 136]. The operating mechanism in PASE requires a high-shear mixer to induce a high-shear force on materials in liquids. In the synthesis of GRMMCs, PASE had been reported to effectively exfoliate graphite into fewer Gr sheets and to positively influence a homogenous distribution of Gr sheets in the metal matrix. It is claimed that the resultant high-shear force is sufficient to successfully exfoliate Gr sheets and eliminates the need for Gr pretreatment steps such as intercalation to weaken the interlayer binding strength. Wang *et al.* [121] used PASE to synthesize a Gr-Cu bulk composite using graphite and Cu particles as the starting materials without any additional pretreatment steps. The starting materials were dispersed in 1,3-butanediol and mixed using a rotor-stator mixer. The mixed slurry was then centrifuged for 1 h, heated at 200°C, and consolidated by SPS to obtain a bulk composite. The successful exfoliation of Gr into Cu powders was verified using x-ray diffraction (XRD), SEM, and TEM. Most importantly, high resolution TEM (HRTEM) investigations revealed that the sheets were multilayered but with a thickness less than 20 nm. SEM images of the powder composite revealed that the Gr sheets were embedded in the copper powder, suggesting good distribution; the copper particles prevented the Gr sheets from restacking. In another study, Wang *et al.* [136] combined PASE with MLM to produce a rGO-reinforced Cu matrix composite. The authors compared the properties and strengthening efficiency of the rGO-Cu composite produced by combining PASE and MLM with that produced using MLM alone. The microstructural and mechanical results verified the positive effect the PASE method imposed on the final composite. The composite produced using MLM alone suffered from agglomeration, a nonhomogenous structure, thicker GO sheets, holes and cracks, and lower yield strength values when compared with the composite fabricated using PASE and MLM. The effective synthesis technique included a typical MLM process where a GO colloid was added to cuprammonia and sonicated for 30 min. The PASE step was introduced during the solution evaporation step where, instead of the usual magnetic stirring, a high-shear rotor-stator mixer was used to offer high-shear force in the solution, aiding in the exfoliation and distribution of the GO.

3.1.2.3 Rolling Processes

Kim *et al.* [100] and Liu *et al.* [123] prepared the Gr-metal composites using different rolling procedures that yielded uniform microstructures and enhanced the composite properties. Kim *et al.* [100] used a combination of ball milling and high-ratio differential speed rolling (HRDSR) processing for the synthesis of MLG-reinforced Cu matrix composites. It was reported that ball milling resulted in significant fragmentation of MLG followed by a large shear strain provided by HRDSR, which accelerated the breakage of MLG into nanosizes, resulting in a dense uniform dispersion of MLG in the Cu matrix. The yield strength of the 1 vol% MLG-Cu composite was reported to be 361 MPa and the strengthening mechanism was concluded to be Orowan strengthening due to the homogeneous dispersion of high-density nanosized MLG particles. Liu *et al.* [123] reported the effect of changing the number of cycles in the accumulative roll bonding (ARB) process on the dispersion of GNSs in the Cu matrix. As the number of rolling cycles increases, the tensile strength reaches a maximum of 496 MPa after 6 ARB cycles, which is higher than that of unrolled GNS-Cu by 275 MPa. However, elon-

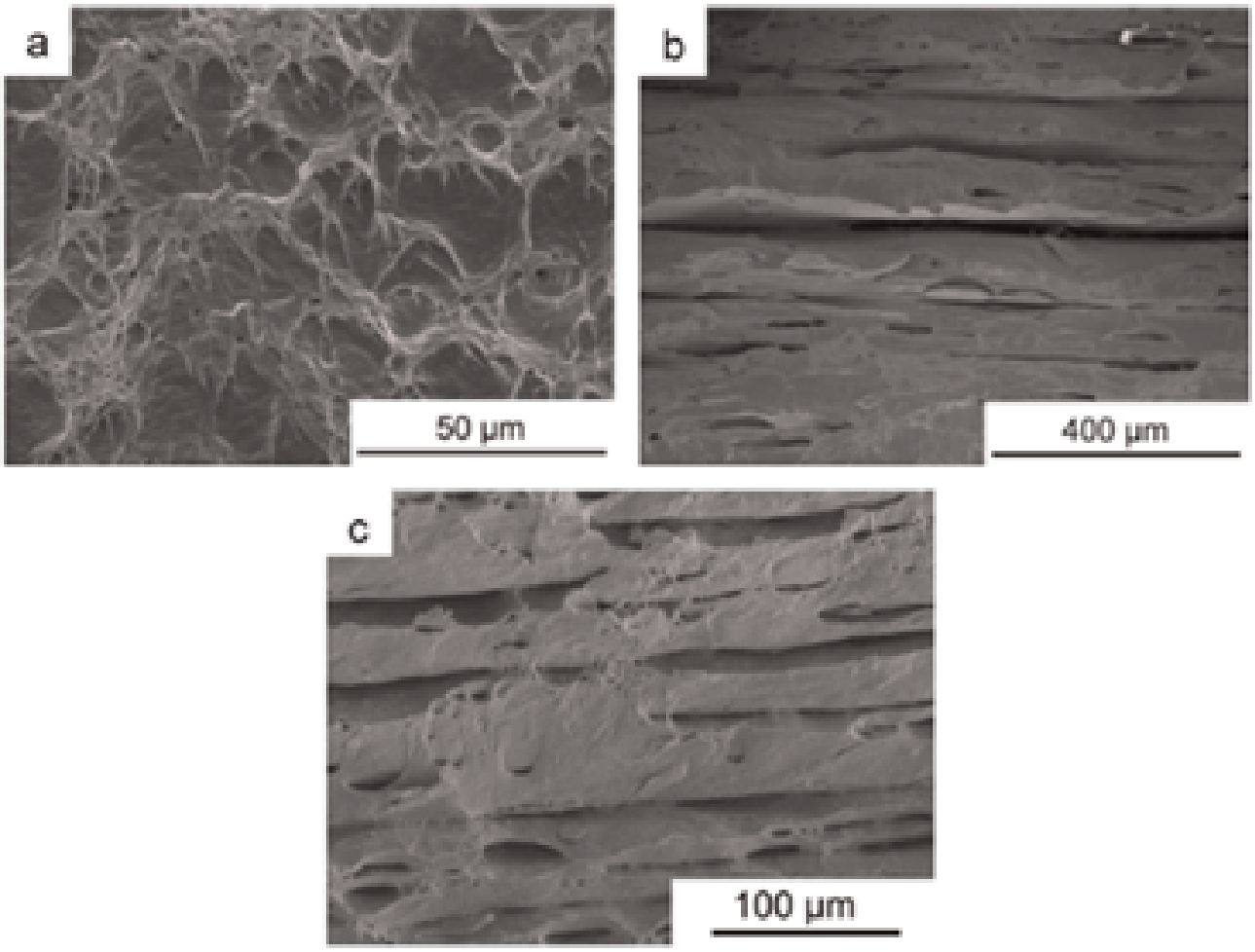

Figure 11: SEM images of tensile fracture of (a) annealed Cu showing ductile features, (b) accumulative roll bonded Cu, and (c) accumulative roll bonded GNS-Cu composite after 6 h rolling, where (b) and (c) show features of shallow dimples and shear zones. Reproduced from Reference [123].

gation drops significantly after the first cycle by 38% compared with annealed Cu and remains almost constant (5%) with increasing the cycle number. The sharp drop in elongation was attributed to the increment in the number of interfaces that act as sources for crack initiation after the first cycle. However, cycling was reported to enhance the uniformity of the GNS distribution within the Cu matrix, as well as the Cu-GNS and Cu-Cu bonding, leading to constant elongation with further cycling. This finding agrees with the SEM images in Figure 11, where the fracture surface of annealed Cu is represented by a typical ductile fracture with dimple-like morphology, while that of accumulative roll bonded Cu and accumulative roll bonded Cu-GNPs combines the features of shallow dimples and shear zones. Therefore, the authors [100, 123] concluded that rolling processes are effective methods for the fabrication of GRMMCs.

3.1.2.4 In-Situ Synthesis

In-situ synthesizing of Gr in metal matrices has been reported to be effective for enhancing the strengthening efficiency of GRMMCs. Recently in-situ synthesis of Gr has been reported in Cu [88, 142], Al [140, 143, 144], and Ni [89, 90] bulk metal matrices. Chen *et al.* [88] reported the fabrication of a bulk Gr-Cu composite by CVD. They suggested that the in-situ growing of Gr results in better dispersion of Gr and a stronger adhesion between Gr and the metal matrix. In addition, their in-situ method resulted in the fabrication of a 3D Gr structure, which has a better strengthening effect than the usual 2D Gr produced by other methods. Initially, PMMA was used as the carbon source and was milled with Cu powders. The PMMA distributes within the Cu powders during milling and prevents Cu welding by forming interspaces between the agglomerated Cu powders in which the Gr will be grown into during CVD. The milled powders went through a CVD pro-

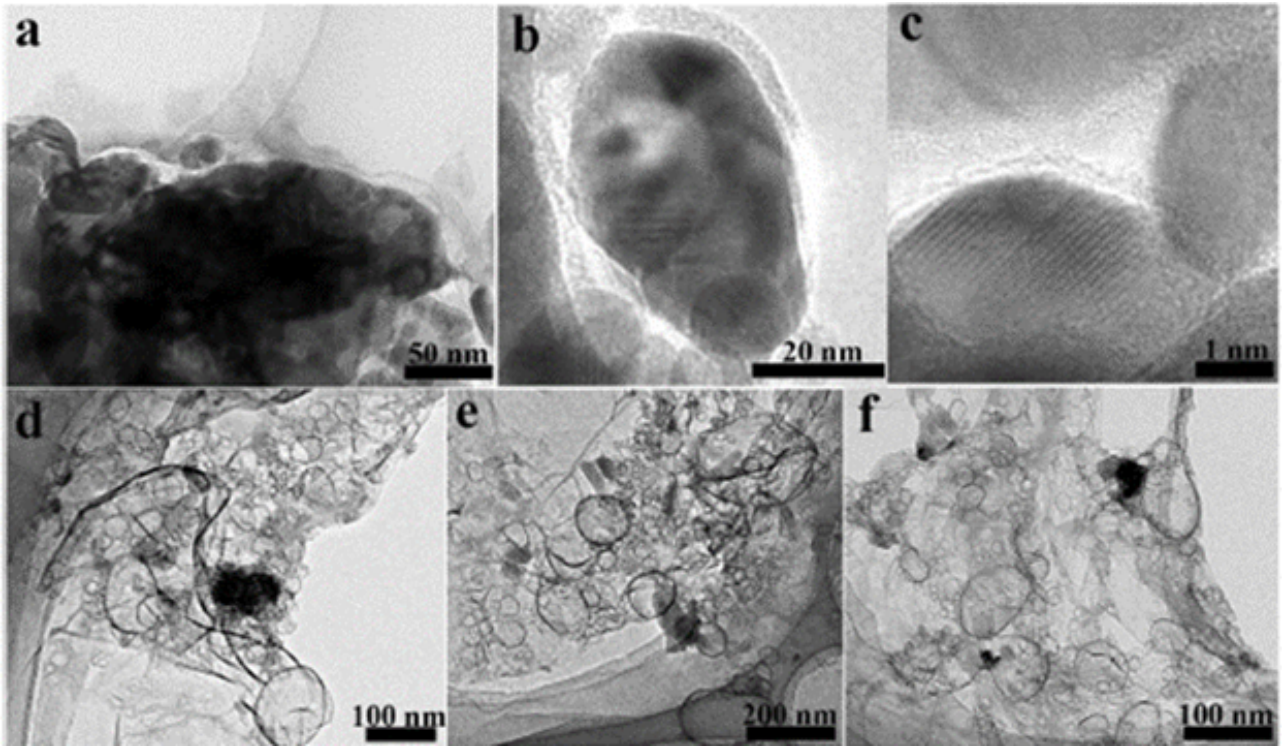

Figure 12: (a–c) TEM images of Cu powders coated by in-situ grown 3D Gr. (d–f) TEM images of porous 3D Gr after the removal of the Cu matrix with $CuCl_2$ solution. Reproduced from Reference [88].

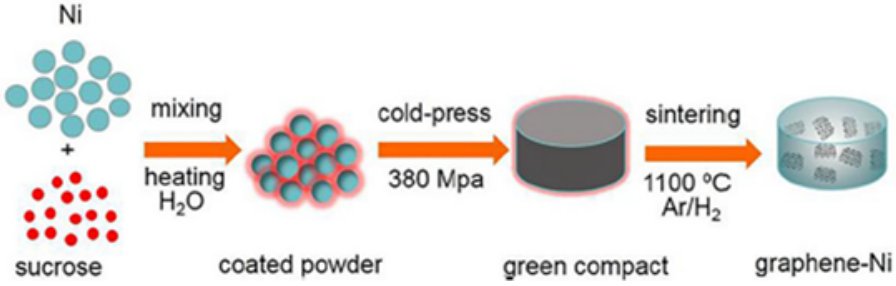

Figure 13: A schematic diagram of the in-situ fabrication process of Gr-Ni composite. Reproduced from Reference [89].

cess in a quartz tube during which carbon atoms decomposed from PMMA and diffused into the porous structure of the Cu powder agglomerates. This is attributed to the high temperature environment and low solubility of C in Cu. As a result, Gr copies the porous structure of the agglomerated Cu powders, and a 3D Gr structure is formed following the shape of the porous Cu framework. The Cu-Gr composite powders were then hot pressed under a vacuum. TEM images of in-situ grown Gr in Cu are shown in Figure 12(a–c). In addition, the 3D structure of Gr was demonstrated and captured by TEM, as shown in Figure 12(d–f). This was done by removing the Cu matrix via $CuCl_2$ solution acidized with hydrochloric acid, leaving the interconnected 3D framework of Gr with a porous structure corresponding to the empty spaces where the Cu matrix was placed.

Jiang *et al.* [89] reported the in-situ fabrication of Gr-reinforced bulk Ni matrix composites. They used simple powder metallurgy steps to fabricate in-situ grown Gr into Ni matrix. A schematic diagram of the in-situ fabrication process is shown in Figure 13. They used sucrose as Gr precursor and mechanically stirred it with Ni in water until the water evaporated. Later, the composite powders were green compacted and sintered. The composite achieved a 69.8% increase in hardness and 311% increase in UTS. This was attributed to the uniform distribution of Gr in Ni and the foreign impurity-free interface achieved with this in-situ synthesis leading to efficient load transfer.

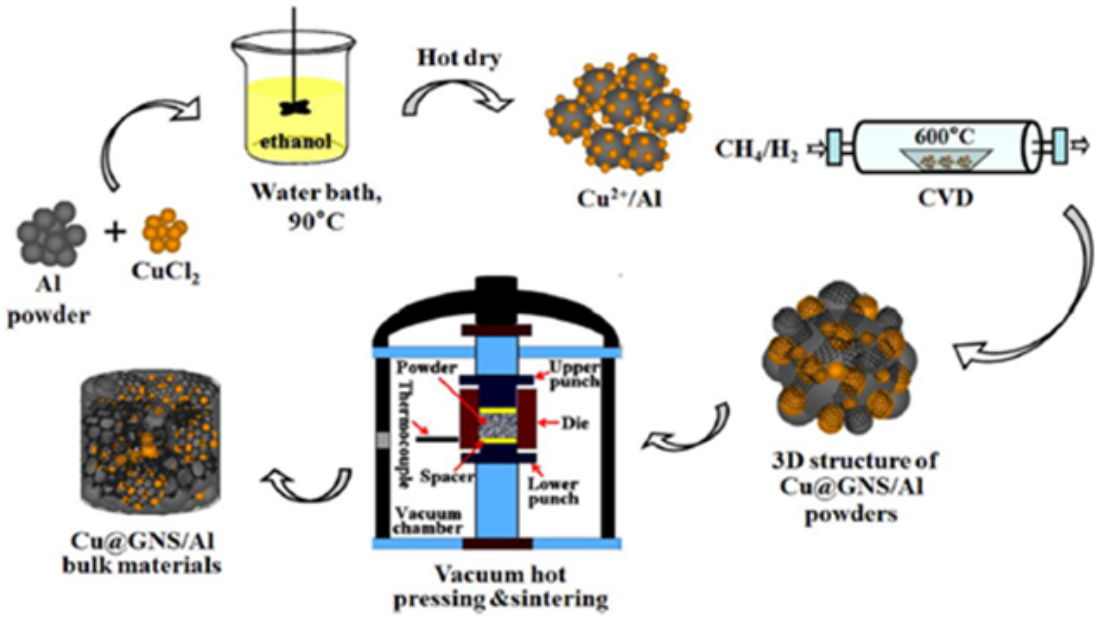

Figure 14: A schematic diagram of the preparation procedure of Cu-GNS-Al bulk composites. Reproduced from Reference [143].

Producing in-situ Gr grown in an Al matrix via CVD holds several challenges, such as the noncatalytic nature of Al, its pore wettability with carbon, and the Al_4C_3 formation reaction that can take place due to high-temperature processing. These challenges can be overcome by adding an intermediate material into the interface of Gr and Al to act as a catalyst, enhance interfacial bonding, and prevent carbide formation. Chen *et al.* [143] and Liu *et al.* [144] produced Cu-coated GNS-Al and Ni-decorated GNP-6061Al matrix composites, respectively. Both studies utilized CVD to incorporate the intermediate elements. Chen *et al.* [143] used Cu as the catalyst and methane as the carbon source. First, they used magnetic stirring and ultrasonication to mix Al and $CuCl_2$ and obtain a homogeneous Cu^{2+}-Al solution. The solution was then heated to dry the powders before loading it into a tube furnace for the CVD process to obtain Cu-Al powders followed by heating with methane-Ar atmosphere to obtain the Cu-coated GNS-Al powders. This was followed by vacuum hot pressing and sintering. The composite achieved a 200% increase in UTS. A schematic diagram of the process is shown in Figure 14.

3.1.2.5 Molten or Liquid Metal Processes

Fabricating bulk GRMMCs with steps involving metal melts processing, such as Mg [103, 110, 111, 138] and Al [87, 94, 98, 120, 139–141], has been reported. Rashad *et al.* [110, 111] used the disintegrated melt deposition (DMD) technique to fabricate 1.5 wt% GNP-reinforced Mg-6Zn alloy and 3 wt% GNP-reinforced AZ61 Mg alloy, respectively. The process involves the melting of a 1.3 Kg Mg ingot in a graphite crucible and a protective atmosphere, followed by the addition of the alloying elements and the GNP powders while maintaining the Mg melting temperature of 20°C. The molten mixture was allowed to cool and solidify in a steel mold preheated at 300°C. The solidified mixture was homogenized and hot extruded to 16-mm diameter rods of uniformly dispersed GNPs in Mg alloys. Yang *et al.* [94] and Du *et al.* [138] combined powder metallurgy with metallic melt processing to fabricate Gr-reinforced Al and Mg matrix composites, respectively. Yang *et al.* [94] used ball milling to mix the Al powders and GNPs followed by green compaction to compact the milled powders into a preform, before performing the pressure infiltration method. A schematic diagram of the synthesis is shown in Figure 15. The compacted preform is placed under molten Al while a pressure of 15 MPa is applied onto the molten Al, forcing it to penetrate the composite powder preform. The GNP-Al composite achieved a 228% increase in TYS and a 93% increase in UTS.

Du *et al.* [138] mechanically mixed GNPs and Mg-based alloy powders in ethanol under ultrasonication followed by centrifugation and vacuum drying. Mixed composite powders were extruded into rods before melting in an electromagnetic induction furnace with stirring to achieve homogeneity. The molten composite mixture was allowed to solidify under atmospheric conditions followed by hot extrusion. The composite achieved a 62% increase in TYS. Seventy-two percent of the strength enhancement was attributed to load transfer due to the efficient interfacial

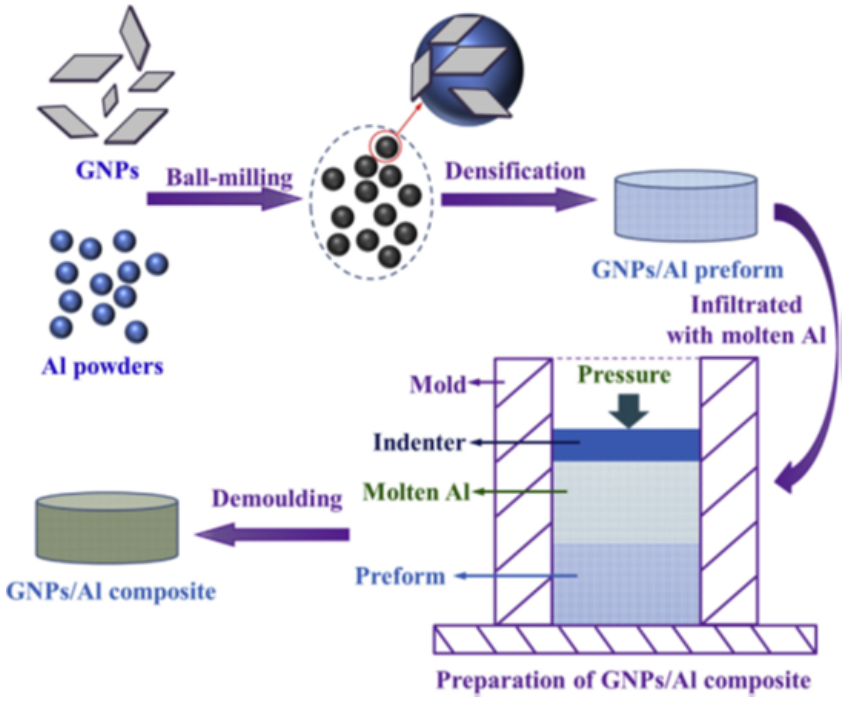

Figure 15: The schematic preparation process of the GNP-Al composites via the pressure infiltration method. Reproduced from Reference [94].

bonding and homogenous distribution of GNPs in the Mg alloy matrix.

In 2012, Chen *et al.* [103] combined liquid-state processing of metal melts with solid-state stirring to develop a novel GNP-reinforced Mg matrix composite technique. The process consists of three main steps. In the first step, GNPs were dispersed into Mg by adding GNPs into the ultrasonicated Mg melt at 700°C using an automatic feeding system and a high-powered ultrasonic probe. The second step was to solidify the ultrasonicated GNP-Mg melt by casting it onto a plate mold to obtain a plate-shaped composite. The presence of large clusters within the composite was captured by SEM images, suggesting poor dispersion of GNPs into the Mg matrix. This was attributed to the large aspect ratio of the GNP, which makes it difficult to achieve homogenous dispersion of GNP into the Mg melt using ultrasonication only. Thus, the third step in the process was needed: solid-state processing. Friction-stir processing (FSP) was the solid-state technique applied to further distribute the GNPs into the Mg matrix. FSP is an emerging solid-state metal working technique, which involves mixing the sample in the solid state, imposing severe plastic deformation on the processed zone. In addition, friction is created between the rotating tool and the processed sample, which leads to localized heating [148, 149]. FSP is a proven technique for homogenous dispersion of reinforcements in metal matrices and homogenizing structures of cast alloys [150, 151]. During FSP, the composite plate prepared by step 2 was treated with a special rotating tool that has a pen-shaped end, which interacts with the plate by heating and mixing it, thus processing it in the solid state. Recently, FSP was employed in several studies for the fabrication of Gr-reinforced Al matrix composites [98, 120, 139]. Zhang *et al.* [120] reported the fabrication of 1 wt% GNP-reinforced 2009Al alloy matrix composite via a combination of powder metallurgy and the FSP technique. The effect of increasing the number of FSP passes on the distribution of GNPs in the metal composite was studied. It was reported that two passes were enough to achieve homogenous distribution of GNPs and to decrease the number and size of GNP clusters in the matrix. The above investigations indicate that the molten metal-based synthesis techniques are feasible and effective for the fabrication of bulk GR-MMCs.

3.1.3 Postsynthesis/Consolidation

The consolidation step is important to fabricate GRMMCs. It provides the final product to be studied and controls the extent of the sample's densification. This step is mostly needed when the composite obtained is in the powder form after the mixing step. This applies to mixing techniques including ball milling, solution-assisted mixing, a

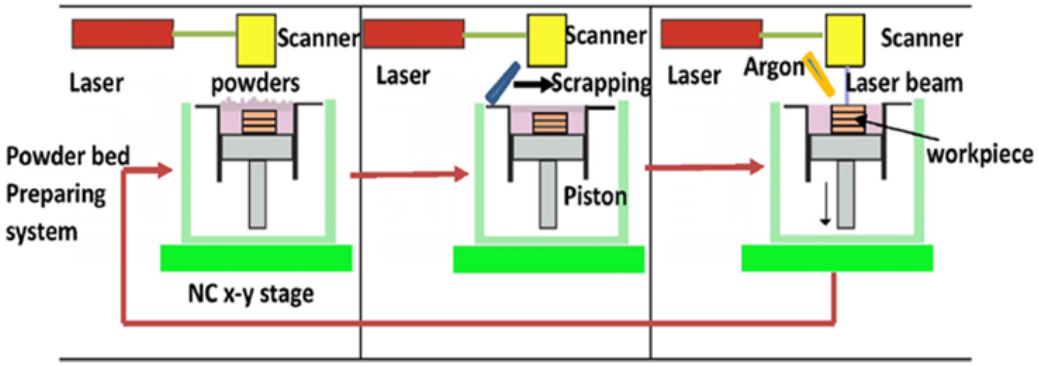

Figure 16: Schematic diagram of the laser 3D printing graphene aluminum process. Reproduced from Reference [133].

few in-situ synthesis techniques, and after some molten metal mixing procedures. The consolidation step can be divided into three categories: pressing and sintering methods, full densification methods, and the most recently developed, 3D printing.

Pressing/sintering consolidation techniques involve two steps: the pressing of the mixed composite powders (which can be done at room temperature and is known as green compaction, or it can be done simultaneously with heating) followed by sintering or annealing [11, 17, 18, 20, 26, 27, 44, 50, 58, 65, 66, 73, 124, 125, 132, 137]. Composite powders are placed into a steel die, and a vertical pressing motion is applied onto the mixed powders for pressing. Limitations exist such as the size and shape of the final sample as it is controlled by the size and shape of pressing tools, the pressing capacity, and the powder compressibility. Although this technique is a simple approach for composite compaction, full densification is hardly achieved [152].

Achieving approximately full density in samples can be achieved through the second category of consolidation techniques: full densification methods. Several techniques have been developed and applied for the synthesis of GRMMCs, such as hot pressing [23, 49, 51–55, 63, 68, 70, 88, 99, 108, 118, 119, 126], hot rolling [25, 52, 56], extrusion [11, 17, 50, 55, 57, 73, 118], and SPS [24, 52, 69, 71, 72, 97, 127, 134]. Relative densities between 98% and 99.8% have been achieved for GRMMCs via full-densification consolidation techniques [11, 17, 24, 26, 88, 113, 125–127].

3D laser printing techniques have been used for the synthesis of Gr-reinforced Ni [112], Ti [60, 153], and Al [133] matrix composites. Most recently, Hu *et al.* [133] fabricated for the first time a Gr-reinforced Al matrix composite by 3D printing using the selective laser melting (SLM) technology. First, ball milling was used to disperse Gr into Al without the use of process control agents or protective gases. Then, SLM was used to consolidate the ball-milled powder composite and fabricate a 3D bulk composite. A schematic diagram of the 3D printing process is presented in Figure 16. Raman spectra of the laser-melted composite showed an increase in the I_D/I_G ratio from 0.053 to 0.48 for as-received Gr and Gr in the laser-sintered Gr-Al composite. The increase in structural defects was attributed to the thermal damage from the high temperature of the SLM process and to the reaction between Gr and aluminum, leading to the formation of Al_4C_3.

Ayyappadas *et al.* [137] compared the effects of two sintering techniques on the densification of their Gr-Cu composite prepared by powder metallurgy and cold pressing. Microwave sintering resulted in higher relative density than conventional tube furnace sintering for their 0.9 vol% Gr-Cu composite. Sintering in a microwave field allowed for higher heating rates, which led to shorter processing times and gave more refined structure of the composite. Similarly, Ghasali *et al.* [102] studied the effect of different sintering techniques, such as conventional, microwave, and SPS, on the densification and performance of 1 wt% GNP-Al composite. Each sintering technique had a different effect on the formation of Al_4C_3 and thus resulted in a different structure and mechanical performance. The highest relative density was reported after SPS thanks to its vacuum environment.

A few observations have been made regarding density after consolidation in GRMMCs. One observation is the density of the GRMMCs compared with the pure metal prepared in the same way. In several reports, the density of the GRMMCs was found to be less than that of the pure metal due to the contribution from Gr, which has a lower density than that of metals [11, 17, 24, 27, 58, 108, 129, 140]. However, several authors reported a higher density for the GRMMCs compared with the pure metal [26, 137]. Ayyappadas *et al.* [137] suggested that Gr acting as a lubricant during cold pressing enhanced the densification and increased the density of the composite compared with pure

Cu processed the same way. Alam *et al.* [26] reported a poor relative density of 77% for pure Al compared with 98% for 3 wt% GNP-Al composite. They justified the poor Al density to the poor powder compressibility of Al as a result of the Al_2O_3 layer on the Al surface, which hindered the direct contact between Al powders. In contrast, the addition of GNP particles helped in filling those pores and resulted in a much higher composite densification. Because the density of Al_2O_3 is higher than the density of Al and Gr, Rashad *et al.* [17] reported higher experimental densities than theoretical densities and attributed it to Al oxidation and formation of Al_2O_3 during sintering.

The density of GRMMCs has been reported to vary with Gr content [11, 17, 24, 26, 27, 47, 58, 65, 97, 99, 104, 108, 126, 127, 140]. A decrease in experimental density was reported at higher Gr additions. Some authors attributed this behavior to the lower density of Gr than the metal matrix, thus lowering the density of the composite via Gr addition [11, 17]. Ayyappadas *et al.* [137] suggested that this behavior is a result of Gr acting as a barrier to Cu diffusion, resulting in lower densification. Li *et al.* [27] attributed the drop in the relative density of their GNS-Al composite when adding GNSs to the increased air gaps that form in the composite as a result of the absorption of GNSs to gas elements such as O, N, and CO. Alam *et al.* [26] reported an enhancement in the density of the Gr-Al composite up to 3 wt% GNP addition, after which a sharp decrease in density is observed. The enhancement was attributed to the filling of the voids between Al particles by GNPs. However, beyond 3 wt% GNP addition, authors suggested that the agglomeration of the GNPs in the composite and the formation of Al_4C_3 phase resulted in poor densification and sinterability [26]. The agglomeration of GNPs in GRMMCs at higher GNP addition and its effect on poor densification and porosity has been reported in other GRMMC studies as well [24, 65, 127].

3.2 Structure and Morphology of GRMMCs

During the processing of GRMMCs, the Gr sheets tend to agglomerate. This is caused by the high surface energy of the nanometer-thick sheet that stems from the weak Van der Waals forces that hold the Gr layers. This results in inhomogeneous dispersion of Gr in metal matrices [69]. Enhancing the properties of metals depends on the integrity of the interface between the Gr reinforcement and the metal matrix. Thus, uniform distribution and homogenous dispersion of the reinforcement within the metal matrix must be achieved without sacrificing the structural integrity of the Gr [73]. This is basically controlled by the type and amount of reinforcement material used and the synthesis technique of the composite. The morphology of GRMMC is usually investigated through the atomic-scale resolution images of SEM and TEM, and other analytical tools such XRD and Raman spectroscopy, as they offer detailed morphological and structural information [56].

3.2.1 Dispersion of Graphene in MMCs

One of the main structural features investigated in all prepared GRMMCs is the degree of dispersion of Gr in the metal matrix. A homogenous and good dispersion of Gr and its derivatives has been reported in Al [18, 23–25, 27, 44, 53–57, 69, 70, 94, 139, 141], Cu [51, 52, 66, 71, 88, 93, 97, 123–127, 134, 137], and Mg [65, 103–105, 108, 110, 138], where good dispersion is usually attributed to the effectiveness of the composite's fabrication technique [48, 56, 71, 103, 127]. In some cases, it was difficult to observe Gr by electron microscopic means, suggesting that Gr was well dispersed throughout the metal matrix [18, 48, 56, 70]. Shin *et al.* [56] produced FLG with an Al matrix using planetary milling followed by attrition milling. Their analysis concluded that FLG can be observed after planetary milling, as the sheets were thin enough to transmit the electron beam and show the Al particles below the Gr sheets. However, those thin sheets were no longer visible on the Al powder surface after attrition milling, which suggests its effectiveness in embedding and dispersing the sheets inside the Al matrix. Similar results were reported by Rashad *et al.* [48]; they used ball milling to fabricate GNP-reinforced AZ31 Mg alloy. GNPs were not traced via TEM in the milled composite powders, suggesting that they are well embedded and uniformly distributed within the metal matrix.

Surface modification of Gr and/or the metal before composite fabrication is suggested to enhance Gr dispersion in metal matrices [66, 71, 73, 127]. Zhang *et al.* [127] attributed the homogenous distribution of GNPs in the Cu matrix composite to the electroless plating of GNPs by Cu and Ni before the ultrasonication of the treated GNPs with Cu powders. Compared with the treated GNP-Cu composite, the untreated GNP-Cu composite showed heavy agglomeration and clustering. Jiang *et al.* [71] used PVP and PVA in the surface modification of pristine graphene (PG) and Cu, respectively. The affinity of the carbonyl groups in PVP to the hydroxyl groups in PVA compensates for the lack of affinity between PG and Cu, realizing a homogenous dispersion of PG in Cu. Compared with their modified PG-Cu composite, PG sheets agglomerated and separated from Cu particles in the unmodified sample.

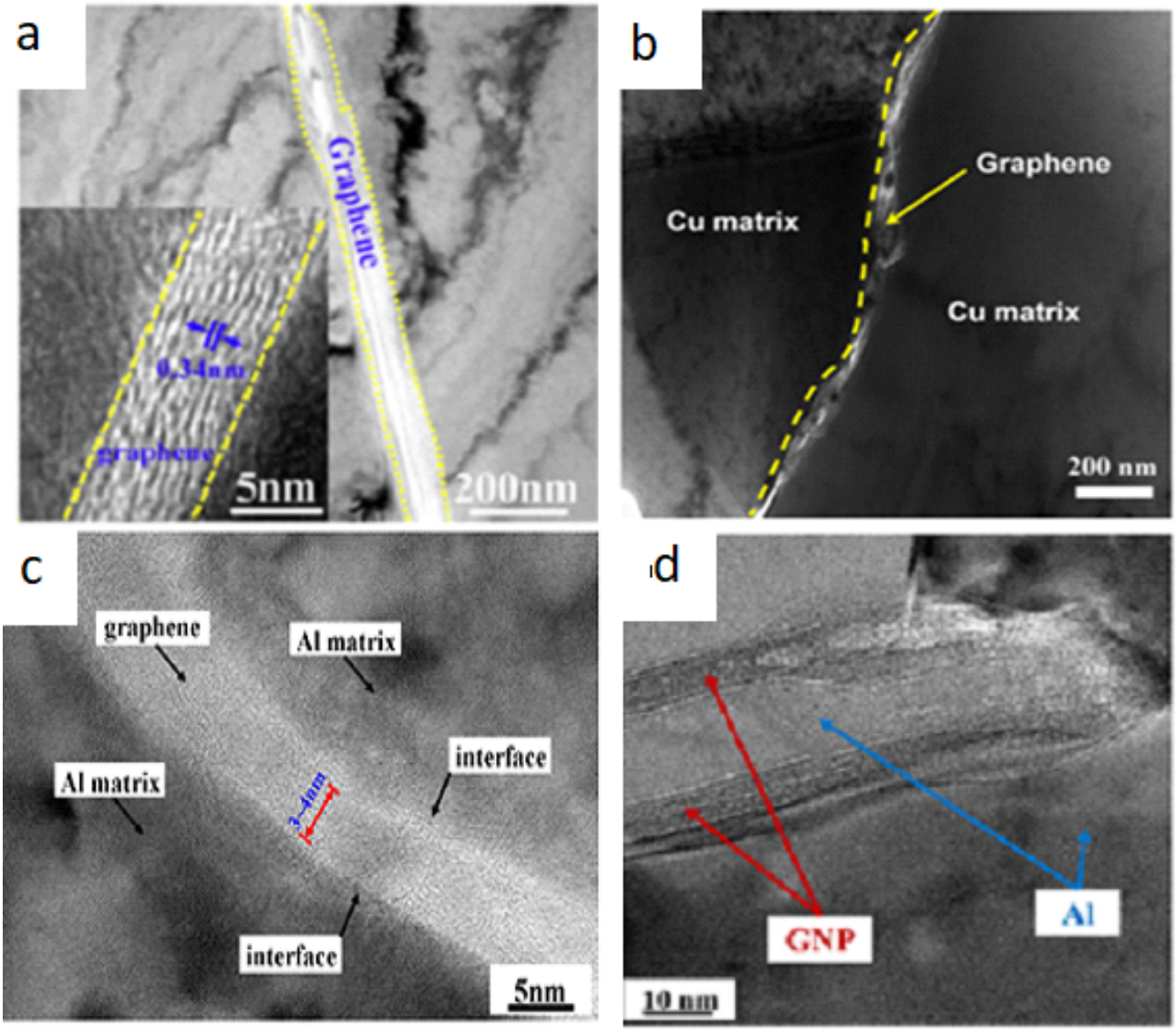

Figure 17: TEM images showing distribution of Gr sheets in (a, b) Cu matrix, and (c, d) Al matrix. Reproduced from References [49, 51, 57], and [54], respectively.

Many reports have indicated that Gr was distributed around or along the grain boundaries of metal matrices such as Al [47, 53–55, 57, 59, 68, 69, 98, 140] and Cu [49, 51, 63, 66, 100, 124, 126, 134, 137, 142]; see Figure 17. This feature suggests good dispersion of reinforcement in the matrix. Ju *et al.* [69] confirmed the distribution of Gr along the grain boundaries of Al particles for their 0.3 wt% GO-Al composite through HRTEM, where Gr sheets with three to five layers were observed to surround the Al particle. Gao *et al.* [51] reported the homogenous distribution of rGO along the grain boundaries of Cu matrix, which was attributed to their successful electrostatic self-assembly technique.

3.2.2 Interfacial Interactions and Carbide Formation

Another challenge in synthesizing Gr-reinforced MMCs is the high reactivity of metals and the possibility of interfacial interactions at the Gr-metal interface [44]. Good interfacial bonding has been reported in GRMMCs prepared by several synthesis techniques [49, 51, 52, 63, 64, 66, 71, 72, 88, 93, 97, 105, 108, 110, 111, 123–127, 134]. However, metals have different interactions with Gr, and many challenges still persist regarding the interfacial interactions.

In Gr-reinforced Al matrix composites, the formation of Al_4C_3 phase has been highly investigated. XRD has been used to determine the phase compositions of Gr-Al composite and to investigate the presence of interfacial reac-

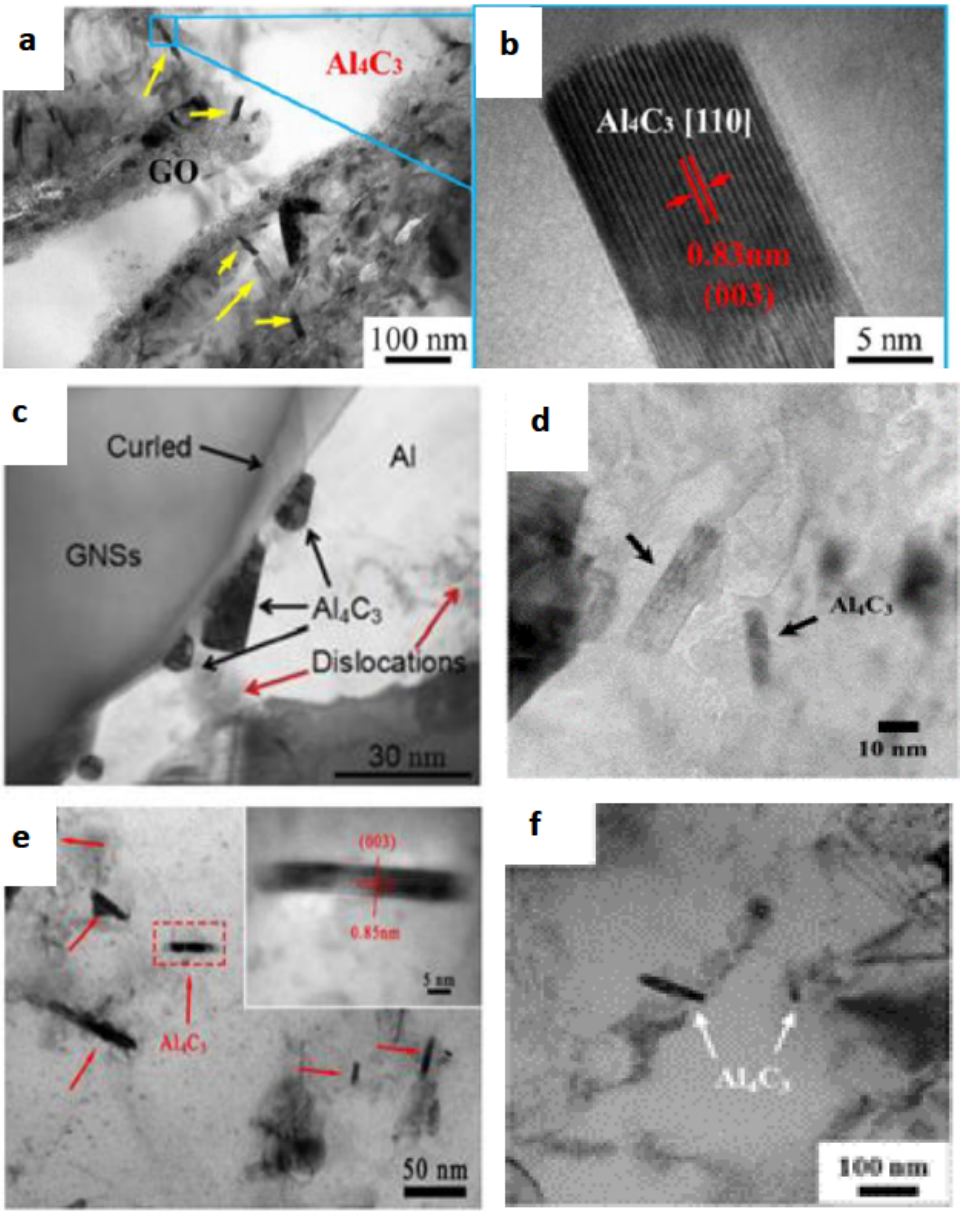

Figure 18: A collection of TEM images showing rod-like structure of Al_4C_3 phase. Reproduced from the following references: (a, b) [87], (c) [27], (d) [23], (e) [55], and (f) [95].

tions [18, 24, 27, 44, 54, 55, 57, 69, 70, 133, 139]. The presence of Al_4C_3 has been identified by XRD in some cases [18, 27, 55, 102, 133], while in other cases, XRD was not able to detect any interfacial reactions, such as forming the Al_4C_3 [24, 44, 54, 69, 70, 94]. The undetectability of Al_4C_3 by XRD was attributed to the low content of carbides formed, making it beyond the detection limit of XRD; the absence of any residual carbon in the starting reinforcement material; and the passivation of Al due to the formation of thin stable aluminum oxide preventing any chemical contact between Al and carbon. Furthermore, investigating the presence of second phases and interfacial reactions between Gr and Al was based on TEM images, SAED analysis, and EDX in some studies [23, 24, 27, 55, 57, 87, 94, 95, 120, 133, 154, 155]. Figure 18 shows TEM images that have reported the presence of Al_4C_3 phase in Gr-Al composites. The Al_4C_3 phase was described to have a needle-like or rod-like appearance [23, 27, 55, 87, 95, 120, 133, 154, 155].

Li *et al.* [27] reported the absence of Al_4C_3 in XRD patterns of Al-0.25 wt% GNS composite prepared by ball milling and hot pressing (HP). However, rod-like Al_4C_3 phases were identified by TEM. Hence, the absence of

Al_4C_3 peaks was attributed to the XRD detection limit. In the same study, Al_4C_3 peaks were detected by XRD for high Gr wt%, and it was reported that the intensity of those peaks increased with increasing the Gr content from 0.5 wt% to 1.0 wt%. This suggests that the Gr content plays a significant role in the intensity of the Al_4C_3 phase.

There seems to be a debate surrounding the formation of Al_4C_3 in Gr-Al composites regarding whether it is caused by the exposure of the composite to high temperatures during synthesis, or it is initiated due to disorder of the graphitic structure induced by synthesis regardless of the temperature. It has been reported that the formation of carbides in Al-C systems can be controlled by thermodynamic and kinetic approaches. Thermodynamically, the reactivity of Al-C systems can be lowered by using carbonaceous materials with fewer defect sites or by adding alloying elements to change the Gibbs free energy of the reactions. Kinetically, controlling the rate of reaction by controlling synthesis temperature or time of exposure to high temperature can inhibit Al_4C_3 formation [94, 102]. The phase diagram of the Al-C system [26] suggests that a facial interaction in Gr-Al composites can occur at a temperature of 550°C with a stochiometric ratio of 4:3. When it comes to Al-Gr in the literature, some studies have used synthesis routes such as sintering, HP compaction, or SPS, at temperatures in the range of 300–600°C, yet no formation of Al_4C_3 was detected by XRD [44, 54, 57, 69, 70], TEM [94], or EDX [53, 59].

It has been reported that defect-free Gr platelets are known to be chemically inert to the Al reaction even at temperatures above the Al melting temperature [87, 94, 154, 156]. However, structural defects on Gr can serve as initiation sites for the interfacial reaction with the Al matrix even at temperatures below the Al melting point [26, 55, 94]. The formation of Al_4C_3 has been attributed to the quality and structural integrity of the Gr reinforcement in the Al-matrix composites [26, 44, 55, 57, 69, 94, 156]. Li *et al.* [53] used both ball milling and high-temperature melting, in addition to rolling and casting, to fabricate their 0.2 wt% GNP-Al composite. No traces of Al_4C_3 were detected at the interface by EDX [53]. Yang *et al.* [94] fabricated Al_4C_3-free 0.54 wt% GNP-Al composite using the pressure infiltration method; the composite was subjected to high pressures and temperatures. The author suggested that the use of low-defect Gr can hinder the Gr-Al reaction. Jiang *et al.* [95] reported an increase in structural damage of Gr with milling time as well as higher content of Al_4C_3 at higher milling times. This result showed the relationship between the structural integrity of Gr and carbide formation in Gr-Al composites synthesized by ball milling. Al_4C_3 peaks were detected at all milling times in Raman spectroscopy with significantly higher relative peak intensities at higher milling times. In addition, rod-like phases corresponding to Al_4C_3 were only identified by TEM at higher milling times.

Not only is there a lack of understanding regarding the formation mechanism of Al_4C_3 in Gr-Al composites, but there is also a debate on the role the phase plays on the properties of the composites. Several studies have reported that the carbide phase exhibits a detrimental effect on the mechanical behavior of Gr-Al composites due to the structural damage involved with the formation of Al_4C_3. Other studies attributed the enhancement in mechanical properties (such as strength and hardness) to the Al_4C_3 interfacial product. Ghasali *et al.* [102] suggested that the amount of carbide formed at the Gr-Al interface determines the effect this phase has, whether positive or negative, on the mechanical behavior of the Gr-Al composites. A more systematic approach toward producing and characterizing these composites is required in order to achieve a better and more comprehensive understanding of the issue.

In studies involving Gr-reinforced Cu composites, second phase formation between Cu and Gr has not been reported [51, 63, 64, 71, 97, 123–127, 134, 137]. This is attributed to the lack of a solid-solution phase in the Cu-C phase diagram [71, 123, 137], resulting in physical bonding only and no chemical reactions between Gr and Cu. However, several researchers have reported the formation of Cu-O-C bonding at the interface between Gr and copper. Several advantages has been related to such bond formation including the enhanced load transfer between the matrix and reinforcement, and the enhanced distribution of the Gr reinforcement in the Cu matrix [49, 52, 72, 97, 127, 134, 137]. Other researchers have suggested decorating Gr sheets with metal or carbide coatings that have better affinity with Cu to achieve a strong interface between Gr and Cu. Several coatings, such as Ni [2, 127], TiC [96], and VC [96], have been reported to have a positive effect on the interfacial bonding and mechanical properties of Gr-Cu composites [128].

While carbides such as MgC_2 and Mg_2C_3 are known in Mg-C systems, the formation of such metal carbides in Gr-Mg studies has not been reported [109]. Similar to Cu, a big challenge in the field of fabricating Gr-reinforced Mg matrix composites is the poor wettability between Mg and carbonaceous material such as Gr [105]. As a result, an alloying element, which possesses better wettability with Gr, is usually added to the Mg matrix before mixing it with the Gr reinforcement in an attempt to increase the wettability between Gr and Mg [48, 104, 105, 110, 111]. Al and Zn have been reported as efficient alloying elements in Mg matrices that enhance the wettability of Mg and Gr and result in

excellent bonding and uniform dispersion of Gr within the metallic matrix [105, 110].

3.3 Properties of GRMMCs

3.3.1 Mechanical Properties

The main purpose behind incorporating Gr or its derivatives as a reinforcement in metals is to enhance their mechanical behavior [1]. The main challenge in the development of GRMMCs is to improve strength without sacrificing good ductility. It is important to note that enhancement in the mechanical properties of GRMMCs vary from one study to another because of the difference in the starting materials used, Gr concentrations, fabrication methods, or synthesis parameters used; hence, different structures and morphologies are obtained [1, 129]. This section outlines the latest GRMMC research and the reported mechanical behavior. Tables 4, 5, 6, and 7 summarize the reported studies in the field of Gr-reinforced Al, Cu, Mg, and other metals and their resultant mechanical properties.

3.3.1.1 Strength and Hardness

The mechanical properties of GRMMCs vary from one study to another. The two most reported factors to affect the mechanical properties in the same study are the Gr content and Gr type used as a reinforcement.

Effect of Graphene Content

Relatively small amounts of Gr have been used in the majority of reports, with weight percentages ranging from 0.05% to 5% [18, 20, 24, 26, 27, 44, 49–51, 54, 55, 57–59, 63–66, 69, 71, 88, 94, 105, 108, 110, 124, 125, 133, 138, 141], and volume percentages ranging from 0.1% to 10% [23, 25, 52, 56, 70, 72, 97, 98, 109, 126, 127, 134, 137, 154]. Improved tensile and compressive strengths and hardness have been reported in the majority of fabricated and studied Gr-Al [18, 20, 23–25, 27, 44, 50, 54–58, 68–70, 94, 133, 140, 141], Gr-Cu [49, 51, 52, 63, 64, 66, 71, 72, 88, 93, 96, 97, 123–128, 134, 137] and Gr-Mg [48, 65, 103–105, 108–111, 138] composites. In these studies, the concentrations of Gr were optimized; above this level, the mechanical properties gradually decreased with observed deterioration in the behavior. Such behavior was attributed to the difficulty in achieving a homogenous distribution of reinforcement in the matrix at a high reinforcement content. In addition, agglomeration of Gr or its derivatives at a high Gr content can form microvoids and, hence, poor contact between the reinforcement and the matrix. In the case of Al, the deterioration in mechanical strength was related to the formation of interfacial reactions such as Al_4C_3, which had been reported to increase with increasing the Gr content. The enhancement in the strength and hardness of GRMMCs occurred for several reasons, such as the homogenous dispersion of the reinforcement in the matrix, the successful load transfer between the reinforcement and the matrix, and the resultant strong interfacial bonding [18, 23, 49, 51–53, 57, 65, 66, 72, 88, 94, 96, 97, 101, 108, 120, 123, 125–130, 134, 137, 138], dislocation pinning by Gr and grain refinement [20, 27, 49, 54, 56, 57, 65, 70, 71, 88, 93, 96, 97, 101, 108, 123–129, 138, 139], Orowan strengthening [24, 52, 129, 130, 134], the increase in dislocation density due to mismatch in coefficient of thermal expansion (CTE) [18, 27, 48, 49, 52, 97, 103–105, 110, 111, 124, 126, 127, 129, 130, 134, 138], the formation and presence of carbides [102] as obstacles to dislocation motion [44], and the formation of twin boundaries that act as barriers resulting in the discontinuity of the slip systems [137].

Kumar *et al.* [44] studied the effect of Gr concentrations in GNP-reinforced Al6061 matrix composite. The increase in hardness was attributed to the homogenous dispersion of Gr in the Al alloy matrix at 0.5 wt% concentration, whereas the reduction in hardness was attributed to agglomeration and initiation of microvoids at higher Gr weight concentrations. Similar observations have been reported in References [24, 49, 59, 133]. Hu *et al.* [133] reported that the hardness increased after adding Gr to the Gr-Al composite. Compared with pure aluminum, Al-2.5 wt% Gr had the highest hardness value, with a 75% increase in hardness. The increase was attributed to the significant intrinsic mechanical properties of Gr. The larger error bars reported for the average hardness values at a higher Gr content suggest that a higher graphene content leads to Gr agglomeration and results in scattering of the hardness values. Dasari *et al.* [59] reported a higher porosity content in the Al-GO composite at higher GO concentrations and attributed that to the agglomeration of GO sheets. Similarly, Ayyappadas *et al.* [137] reported a decrease in the density of the GNF-Cu composite with increasing Gr content, which was correlated with the increase in porosity when increasing the GNF content. The authors reported that the GNFs acted as barriers to Cu diffusion throughout the sintering process. Hence, the higher the GNF content, the larger the barrier to Cu diffusion, and the higher the porosity in the composite, which resulted in lower density [137].

Table 4: Summary of Reported Gr-Reinforced Al Matrix Composites Studies.

Matrix	Reinforcement	Pretreatment	Mixing	Compacting	% Increase				%	Ref.
					Strength TS	YS	Hardness	Others	Elongation (original)	
Al6061	GNP 0.70 wt%	In-situ CVD synthesis of Ni-decorated GNPs	Ball milling (BM)	HP	30% (213 MPa)	75% (140 MPa)	33.7% (67.2 HV)	–	22.1%	[144]
Al	GNP 0.2 wt%	–	BM	Cold pressing (CP) / electromagnetic induction heating of CP powders and Al melt / casting and rolling	36.8% (156 MPa)	–	16.5% (43.6 HV)	–	4%	[53]
Al	GNP 1.00 wt%	BM in ethanol of GNPs Ultrasonication of GNPs with SDS in ethanol	BM	SPS	–	–	≈109 HV	–	–	[102]
Al	GNP 0.54 wt%	–	BM	HP / Infiltration of molten Al and pressed powder Extrusion / annealing	93%	228%	–	–	–	[94]
Al5083	GNP 1.8 wt%	–	BM	HP / Infiltration of melted alloy and pressed powder Extrusion / annealing	11.07% (331MPa)	19.12% (186.9 MPa)	–	–	6.3% (21.3%)	[87]
Al5083	GO 1.8 wt%	–	BM	HP / Infiltration of melted alloy and pressed powder Extrusion / annealing	–	17.6% (184.5 MPa)	–	–	9%	[87]
Al	MLG 2.50 wt%		BM	3D printing by SLM processing	–	–	75.3% (66.6 HV)	–	–	[133]
AA2124	GNP 5.00 wt%	–	Mechanical mixing (MM) BM	CP / sintering / hot extrusion	21.6% (425.6 MPa)	127.3% (200 MPa)	–	69% (120 GPa) Young's modulus (YM)	–	[47]
AlMg5	GO 1.00 vol%	–	BM	Uniaxial HP (UHP)	113.8% (556 MPa)	53.8% (200 MPa)	137% (166 HV)	287.14% (813 MPa) Flexural strength (FS)	10% (25%)	[70]
Al	GNS 0.50 vol%	–	BM	CP / sintering / hot extrusion	20% (295 MPa)	18.6% (230 MPa)	–	5.5% YM	13.5% (19.3%)	[95]
Al	GNS 1.00 wt%	GNP sonication in ethanol	BM	HP	56.19% (164 MPa)	38.27% (112 MPa)	16.13% (72HV)	–	15% (16%)	[27]

Table 4: ...continued

Matrix	Reinforcement	Pretreatment	Mixing	Compacting	% Increase Strength TS	% Increase Strength YS	Hardness	Others	% Elongation (original)	Ref.
Al2024	FLG 0.50 vol%	–	BM	HP / sintering	–	≈200% (100 MPa)	–	–	–	[23]
Al5083	GNP 1.00 wt%	–	BM	UHP / hot extrusion	50% (470 MPa)	50% (332 MPa)	–	–	3% (6.6%)	[55]
Al	GNP 0.50 wt%	GNP sonication in anhydrous ethanol	BM	CP / HP / annealing	–	–	8.81%	–	–	[54]
Al	GNP 1.00 wt%	GNP sonication in ethanol	BM	CP / HP	–	–	12.6% drop (97 HV)	–	–	[99]
Al	FLG 0.70 vol%	BM of graphite in isopropyl alcohol	BM	Hot rolling	–	71.8% (440 MPa)	–	–	–	[56]
Al2024	GNP 0.70 vol%	GNP sonication in ethyl alcohol	Planetary milling (PM) BM	Hot rolling	100% (700 MPa)	–	–	–	4%	[25]
Al-1.5 wt% Mg-3.9 wt% Cu	GNF 0.50 wt%	Sonication of GNFs in ethyl alcohol	BM MM	HIP / hot extrusion	25.5% (467 MPa)	50% (319 MPa)	–		–	[118]
Al	GNP 1.00 wt%	–	BM	CP / sintering	–	–	130% (92 HV)		–	[18]
Al6061	FLG 1.00 wt%	–	BM	CP / HP	–	–	–	47% (760 MPa) FS	–	[119]
Al	GNF 1.00 wt%	–	MM BM	Hot extrusion / annealing	68.7% (248 MPa)	55.2% (194 MPa)	–	–	8.3% (17.3%)	[57]
Al	rGO 0.5 wt%	–	Sonication in ethanol BM	CP / sintering	–	–	85.7% (31.6 HV)		–	[50]
Al-1.5 wt% Sn	FLGO 1.00 wt%	–	MM Sonication	CP / sintering	–	26.3% (120 MPa)	43% (≈60 MPa)	–	–	[129]
Al	GO 0.30 wt%	Sonication of GO in water MM of Al in acetone	MM	Filtration / thermal reduction CP / sintering	–	–	32% (34.5 HV)	–	–	[58]

Table 4: ...continued

Matrix	Reinforcement	Pretreatment	Mixing	Compacting	% Increase Strength TS	YS	Hardness	Others	% Elongation (original)	Ref.
Al	GO 0.30 wt%	Sonication and mixing of Al in CTAB Sonication of CTAB-coated Al in H2O Sonication of GO in H2O	MM	CP Sintering	30% (110 MPa)	–	–	–	–	[68]
Al	GNP 1.00 wt%	GNP sonication in ethanol Al MM in ethanol	MM	CP / sintering / hot extrusion	9.14% (203 MPa)	29.5% (145 MPa)	18.4% (90 HV)		–	[11]
Al	GNP 0.3 wt%	Sonication of GNPs in water MM of Al in acetone	MM in ethanol	CP / sintering / hot extrusion	11.1% (280 MPa)	14.7% (195 MPa)	11.8% (85 HV)		9.53% (13.4%)	[17]
Al	GNS 0.30 wt%	BM of Al Al dispersion in PVA aqueous solution	MM of PVA / Al and GNSs in H2O	HP / hot extrusion	62% (249 MPa)	–	–		13%	[73]
Al	GO 0.20 wt%	GO sonication in H2O Magnetic stirring (MS) of Al in IPA	Magnetic stirring	CP / sintering	–	–	29%	–	–	[59]
Al-1.5 wt% Sn	GO 1.00 wt%	MS of Al in ethanol GO sonication in ethanol / H2O	MS Sonication	CP / sintering		26% (120 MPa) compressive yield strength (CYS)	43% (≈58 HV)	–	–	[129]
Al	GNS 0.15 wt%	Dispersion of GNSs in EC / IPA Dispersion of Al in EC / IPA	MS	Filtration / CP / sintering	–	–	43% (37.7 HV)	–	–	[58]
Al	GNP 1.00 wt%	GNP sonication in acetone	Sonication	SPS	54.8% (105 MPa)	84.5% (65 MPa)	21.4%	–	–	[24]
Al6061	Gr 0.50 wt%	GNP sonication in acetone	Sonication	CP / sintering	–	–	≈24% (≈84 HV)	–	–	[44]
AA5052	GNP 3.00 vol%		FSP		35.7% (224 MPa)	112.4% (148.7 MPa)	53% (84 HV)	–	20% (28.5%)	[98]
Al	MLG 40.0 at%	–	FSP (8 passes)	–	75% (147 MPa)	88% (94 MPa)		–	26%	[139]

Table 4: ...continued

Matrix	Reinforcement	Pretreatment	Mixing	Compacting	% Increase Strength TS	% Increase Strength YS	Hardness	Others	% Elongation (original)	Ref.
Al2009	GNP 1.00 wt%	–	FSP	–	23.3% (514 MPa)	30.5% (398 MPa)	–	–	–	[120]
AA5052	GNP 3.00 vol%		FSP		18.6% (244 MPa)	112% (148.7 MPa)	40% (84 HV)	–	20% (28.5%)	[154]
Al	GNS 2.50 vol%	Magnetic stirring of Al and Cu in ethanol	In situ synthesis of Gr by CVD with methane as C source	VHP / sintering	200% (318 MPa)	–	–	–	–	[143]
Al	GNS 2.00 wt%	–	One step in-situ synthesis in molten Al under alkali halides melt	–	16% (48.1 MPa)	51.6% (93.78 MPa)	242% (57.19 HV)	45.1% (87.9 GPa) YM	24.2% (13.04)	[140]

Table 5: Summary of Reported Gr-Reinforced Cu Matrix Composites Studies.

Matrix	Reinforcement	Pretreatment	Mixing	Compacting	% Increase Strength		Hardness	Others	% Elongation (original)	Ref.
					TS	YS				
Cu	rGO 2.5 vol%	Sonication of GO collide in DI water	MLM	SPS	32.4% (748 MPa)	–	–	–	1.45%	[135]
Cu	FLG 0.5 vol%	Dip FLGs in Cu(OAc)2 Dry and calcination	PM	HP	–	15.2% (612 MPa) CYS	–	–	–	[101]
Cu	GNS 0.50wt%	GO sonication in ethanol	BM	Hot press sintering (HPS)	≈24% (≈230 MPa)	–	–	–	≈24% (≈20%)	[49]
Cu	rGO & GNP 1.00 wt%	–	BM	HP	–	–	HV(rGO/Cu)-> HV(GNP/Cu)> HV (Cu)		–	[63]
Cu	MLG 1.00 vol%	–	Sonication in ethanol BM	HRDSR	16.4% (425.5 MPa)	14% (360.5 MPa)	–	–	16.4% (24.1%)	[100]
Cu	Graphite 0.5 vol%	–	Attrition milling	HP	–	–	–	14.4% (841 MPa) CYS	–	[101]
Cu	GO 0.20 wt%	Treating Cu with PVA	MM	Heating/CP/sintering	–	–	–	10% (280 MPa) Compressive strength (CS)	–	[66]
Cu	rGO 0.30 wt%	Sonication of GO in H2O Treating Cu with PVA	MM	Heating/SPS	22% drop (163 MPa)	64.2% (156 MPa)	–	73% (208 MPa) CS	–	[71]
Cu	GNP 0.30 wt%	Treating GNP with PVP Treating Cu with PVA	MM	Heating/SPS	10.5% drop (187 MPa)	81.1% (172 MPa)	–	90% (228 MPa) CS	–	[71]
Cu	rGO 5.00 wt%	MM of GO in H2O with N2H4.H2O addition	MM	CP/SPS	–	35.3% (121.2 MPa)	–	–	21.5%	[125]
Cu	GNP 0.50 wt%	GNP activation in SnCl2 and PdCl2 GNP electroless plating with Ni	MM	SPS	–	64.5% (181 MPa)	–	–	–	[127]

Table 5: ...continued

Matrix	Reinforcement	Pretreatment	Mixing	Compacting	% Increase Strength TS	YS	Hardness	Others	% Elongation (original)	Ref.
Cu	GNS 1.00 vol%	In-situ chemical reduction Ni-decorated GNSs	Sonication	SPS	94% increase in TYS (268 MPa)	–	–	61% (132 GPa) YM	–	[113]
Cu	GNP 0.13 wt%	GNP sensitization in PVP, activation in SnCl2 and PdCl2, electroless plating with Ni	Sonication	SPS	12% increase in UTS (232 MPa)	–	–	–	60%	[2]
Cu	GNP 0.60 vol%	–	MLM (sonication of GNPs in Cu(NO3)2.3H2O	SPS	–	118.3% (310 MPa)	75% (1.75 GPa)	65% (147 GPa) YM	–	[97]
Cu	GNP 0.10 wt%	GNP activation in SnCl2 and PdCl2 GNP sonication in H2O	MLM (sonication of Cu acetate and GNPs in H2O)	SPS	–	52.9% (208 MPa)	–	–	–	[134]
Cu	rGO 0.10 wt%	GO sonication in H2O	MLM (sonication of Cu acetate and GO in H2O)	SPS	–	25% (170 MPa)	–	–	–	[134]
Cu	rGO 2.50 vol%	Sonication of GO in H2O	MLM (sonication of Cu acetate and GO in H2O)	SPS	30% (335 MPa)	80% (284 MPa)	–	30% (131 GPa) YM	–	[72]
Cu	GNR 1.00 vol%	GNR sonication in ethanol MS of Cu in ethanol	Stirring	SPS/hot rolling	–	55% (216 MPa)	–	–	6.4%	[52]
Cu	GO 0.3 wt%	Sonication of GO in H2O Sonication and stirring of Cu in CTAB and H2O	Stirring of GO and Cu	CP/sintering	–	–	18.5% (51 HV)	–	–	[64]
Cu	GO 0.30 wt%	GO sonication in H2O MS of Cu in CTAB/H2O	MS	CP/sintering	13.5% (210 MPa)	≈18.6% (≈51 Hv)	–	–	–	[51]
Cu	GNP 0.5 wt%	GNP sonication in ethyl alcohol	MS	CP/sintering/HP	–	–	≈44.7% (≈97 HV)	–	–	[124]
Cu	GNS 7.50 vol%	GNS sonication in acetone	MS	HP	–	–	44% (97.4 HV)	–	–	[126]

Table 5: ...continued

Matrix	Reinforcement	Pretreatment	Mixing	Compacting	% Increase Strength TS	YS	Hardness	Others	% Elongation (original)	Ref.
Cu	Gr	–	CVD	–	–	–	–	1.5 GPa flow stress at 5% strain	–	[122]
Cu	GNP 10 vol%	–	VM	SPS	26% (265 MPa)	–	–	–	–	[93]
Cu-0.2 at.%Cr & rGO 2.50 vol%	–	VM	Annealing/HP	82% (352 MPa)	–	–	–	–	[128]	
Cu	GNF 3.6vol%	–	Mixing by pestle and mortar	CP/microwave sintering	–	–	93.5% (89 HV)	–	–	[137]
Cu	GNP	Coating GNP with TiC and VC via a controlled reaction in molten salts	MLM	Compaction via SPS	40% (470MPa) for TiC-GNP/Cu	–			133% increase for VC-GNP/Cu	[96]
Cu	Gr (0.50 wt%)	Ball milling of Cu and PMMA	In-situ growth of Gr in Cu by CVD with PMMA	HPS	35.7% (308 MPa)	233.3% (290 MPa)	–	–	–	[88]
Cu	Gr 0.95 wt%	BM Cu and PMMA	In-situ growth of Gr in Cu by CVD with PMMA	HP	27.4% (274 MPa)	177% (244 MPa)	16.2% (143 HV)	–	–	[142]
Cu	GNS	GNS sonication in acetone	ARB (6 cycles)	–	7.13% (496 MPa)	–	–	–	5% (43%)	[123]

Table 6: Summary of Reported Gr-Reinforced Mg Matrix Composites Studies.

Matrix	Reinforcement	Pretreatment	Mixing	Compacting	% Increase Strength TS	YS	Hardness	Others	% Elongation (original)	Ref.
AZ31 Mg	GNP 0.30 wt%	–	BM	Sintering / hot extrusion	3.5% drop (275 MPa)	11.3% drop (173 MPa)	22.4% (71 HV)		21.7% (14.5%)	[48]
Mg	GNP 2.00 vol%	–	BM	SPS	–	–	36.9% (63 HV)	8.6% drop CS		[109]
AZ31Mg	rGO 0.40 wt%	Sonication of GNPs and alloy in hexane	MM BM	CP	–	–	HV(rGO / Mg) > HV(alloy)	–	–	[65]
Mg-10 wt% Ti	GNP 0.18 wt%	MM of Mg and Ti in ethanol GNP sonication in ethanol	MM	CP / sintering / hot extrusion	41.1% (230 MPa)	22.13% (160 MPa)	–	–	14% (3.2%)	[104]
Mg-1 wt% Al	GNP 0.30 wt%	–	MM	CP / sintering / hot extrusion	139.8% (446 MPa)	49.6% (178 MPa)	34.15% (55 HV)	131.4% (13.84) YM	16.9% (9.7%)	[105]
Mg-1 wt% Al	GNP 0.18 wt%	MS of Al Sonication of GNPs MM of Mg (All in ethanol)	MM	CP / sintering / hot extrusion	30.3% (254 MPa)	17.3% (190 MPa)	–	319% (15.5%) Failure strain		[130]
Mg	GNP 0.30 wt%	MM of Mg in acetone GNP sonication in acetone	MM	CP / sintering / hot extrusion	8% (238 MPa)	5% (197 MPa)	19.3% (68.5 HV)	10.6% (14.6 GPa) YM	3.11%	[106]
Mg-1 wt% Al-1 wt% Sn	GNP 0.18 wt%	Sonication of GNPs in ethanol Mixing of alloy in ethanol	MM	CP / sintering / hot extrusion	14% (269 MPa)	29.2% (208 MPa)	–		10.9% (16.7%)	[107]
Mg	GNP 0.50 wt%	Sonication of GNPs in ethanol	Sonication MM	HP / sintering	–	–	20.6% (48.5 HV)	–	–	[108]
Mg	GNP 1.20 vol%	–	Sonication / solid state stirring	–	–	–	78% (66 kg mm-2)	–	–	[103]
ZK60 Mg	GNP 0.05 wt%	Sonication of GNPs in ethanol	Sonication Hot extrusion to rod Facile melt stirring	Solidification of hot melt Hot extrusion	–	62% (256 MPa)	–	–	–	[138]
Mg-6Zn	GNP 1.50 wt%	–	DMD	Casting of molted metal Hot extrusion	13.4% (313 MPa)	34.6% (214 MPa)	43.3% (75.8 HV)	–	21% (17%)	[110]
AZ61 Mg alloy	GNP 3.00 wt%	–	DMD	Casting of molted metal Hot extrusion	11.7% (335 MPa)	26.1% (232 MPa)	15.9% (87.5 HV)	–	10.7% (11.5%)	[111]

Table 7: Summary of Reported Gr-Reinforced Other Metals Matrix Composites Studies.

Matrix	Reinforcement	Pretreatment	Mixing	Compacting	% Increase Strength TS	YS	Hardness	Others	% Elongation (original)	Ref.
Ni	GNP 1.00 vol%	–	BM	SPS	–	131.2% (370 MPa)	112.85% (165 HV)	–	43% (50%)	[46]
Ni	MLG (sucrose as C source)	–	MM	CP / sintering	311% (370 MPa)	–	69.8% (107 HV)	–		[89]
Ni	GNS 1.00 vol%	GNS synthesized via CVD using NaCl template	Impregnation and reduction	SPS	26% (546 MPa)	188.4% (474 MPa)	–	–	25.5% (36.7%)	[90]
Ni	rGO 1.50 wt%	–	MLM	SPS	95.4% (948 MPa)	328% (826 MPa)			12.1% (34.2%)	[67]
Ni	rGO	–	Electrodeposition	–	25% (864 MPa)	–	–	–	20.6% (15.1%)	[61]
Ni	GNP 5.00 wt%	MS of GNPs	Coating AISI4140 with GNPs, PVA, and Ni in water	LS	–	–	175.1% (605.2 HV)	–	–	[112]
Ti	GO 2.50 wt%	Sonication of GO	Coating AISI4140 with GO and Ti in water	LS	–	–	312.2% (742 HV)	–	–	[60]
Ti	GNS 2.50 wt%	Sonication of GNS	Coating AISI4140 with GNSs and Ti in ethanol	LS	–	–	161.1% (470 HV)	–	–	[153]
Ti	MLG 0.20 wt%	–	BM	SPS / hot rolling	91.7% (1050 MPa)	134.9% (1010 MPa)	–	–	5% (27%)	[114]
Ti	MLG 0.50 wt%	Sonication of MLG in water	Sonication BM	SPS	–	94.1% (918 MPa)	71.4% (15.39 HV)	6.4% (264.3 GPa) YM		[131]
Ti	GNP 0.10 wt%	GNP sonication	Sonication BM	SPS / hot rolling	54.2% (887 MPa)	57.1% (817 MPa)	–	–	10% (30%)	[115]
Ti	MLG 0.80 wt%	BM of MLG MM of Ti	BM	SPS / hot rolling	–	280% (2 GPa)	96%	16% YM	–	[116]
Ti6Al4V	GNF 0.50 wt%	–	MM	HIP Forging	12.3% (1058 MPa)	20.1% (1021 MPa)		14.7% (125 GPa) YM	9.3% (9.4%)	[117]

On the high concentration side of Gr reinforcement, several studies have reported its effect on the mechanical properties. One study reported the use of 10 wt%, 15 wt%, and 20 wt% GNPs as reinforcement in the AA2900 alloy [132]. In this study, the Gr-Al composite failed and broke during a standard Brinell hardness test because of the large amounts of Gr particles used. This led to a switchover in the roles of Gr and the metal alloy, where the reinforcement behaved as the matrix and the matrix became the reinforcement. Chu *et al.* [93] reported interesting results for the GNP-Cu composite. Adding 10 vol% GNPs led to a 26% increase in strength, which significantly dropped to −7.1% when the GNP addition was increased to 20 vol%. The TEM results suggested that GNP debonding occurred during tensile testing for both 10 vol% and 20 vol% GNP additions. At lower volume fractions, the enhancement in strength was attributed to grain refinement and dislocation strengthening. However, the enhancement was hindered by the poor Cu-GNP bonding, which weakened the load transfer ability and resulted in the unsatisfied strength enhancement of the composites. At 20 vol% GNP content, the GNP delamination played a dominant role over grain refinement and dislocation strengthening, which led to low load transfer efficiency and caused weakening in the composite strength.

Rashad *et al.* [110] studied the effect of GNP concentration on the mechanical behavior of Mg–6Zn prepared via DMD and hot extrusion. Vickers hardness was measured in the directions longitudinal and perpendicular to the extrusion direction. The hardness values measured in the longitudinal direction were higher than those in the perpendicular direction at any GNP content [110]. However, the effect of changing the GNP content on the hardness measurements was related to the direction in which the hardness was measured. In the longitudinal direction, the hardness increased only until the GNP content was 0.5 wt%, after which the hardness started to decrease. In the perpendicular direction, however, the hardness increased continuously with increasing GNP content up to 1.5 wt%.

Effect of Graphene Type

The reinforcement materials (type of Gr) play an important role in the synthesis of GRMMCs. Various reports have shown that the thickness, number of layers, lateral size, and chemical structure of the Gr reinforcement directly affect the mechanical behavior of GRMMCs [51, 58, 63, 71, 87, 124, 126, 129, 134, 140].

The effect of the chemical nature of the Gr derivative used as a reinforcement has been reported by several studies [58, 71, 87, 129, 134] in which authors have compared the use of unfunctionalized Gr, such as GNPs, with functionalized Gr, such as GO. These studies reported contradicting results as to which Gr derivative exhibited better performance as a reinforcement in GRMMCs. Jiang *et al.* [71] compared the use of GNPs and rGO in a Cu matrix. The results demonstrated that GNP outperformed rGO and offered a better performance as a reinforcement. The GNP-Cu and rGO-Cu composites achieved a 90% and 72% increase in yield strength, respectively, compared with pure Cu. According to the author's remarks, the absence of oxygen-containing functional groups in GNPs caused fewer structural defects than that in the rGO. Thus, GNP performed better as a reinforcement and enhanced the strength of the metal composite by blocking the dislocation motion. Similarly, Shao *et al.* [87] and Liu *et al.* [58] reported that unfunctionalized Gr performed better than rGO as a reinforcement; it achieved higher increases in hardness and strength of the composite for the same content of reinforcement added. In contrast, high mechanical properties of the MMCs reinforced with functionalized Gr were reported in several studies. Zhang *et al.* [134] produced GNP-Cu and rGO-Cu composites via MLM synthesis. The tensile behavior of both composites at different reinforcement contents is shown in Figure 19. The GNP-Cu composite exhibited higher strength at a lower GNP content, while the rGO-Cu composite exhibited a continuous increase in strength and a higher mechanical performance with increasing rGO content. This is because GNP has fewer structural defects than rGO, which enabled the GNPs to disperse uniformly and achieve better stress transfer and higher strength at a low reinforcement content. Increasing the reinforcement content led to the agglomeration of GNPs and

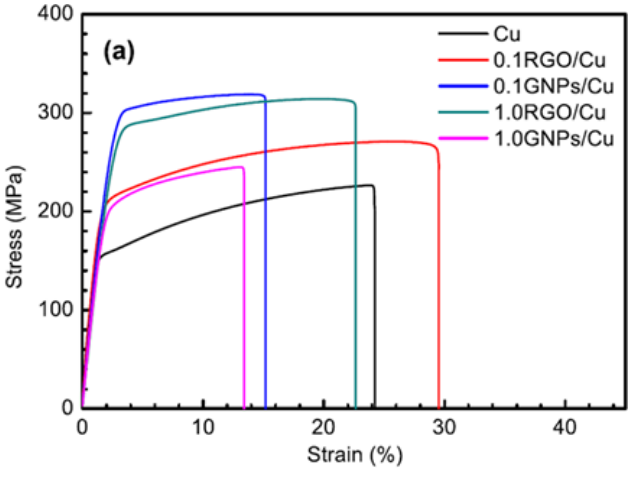

Figure 19: Tensile stress-strain behavior of GNP-Cu and rGO-Cu composites at different reinforcement content. Reproduced from Reference [134].

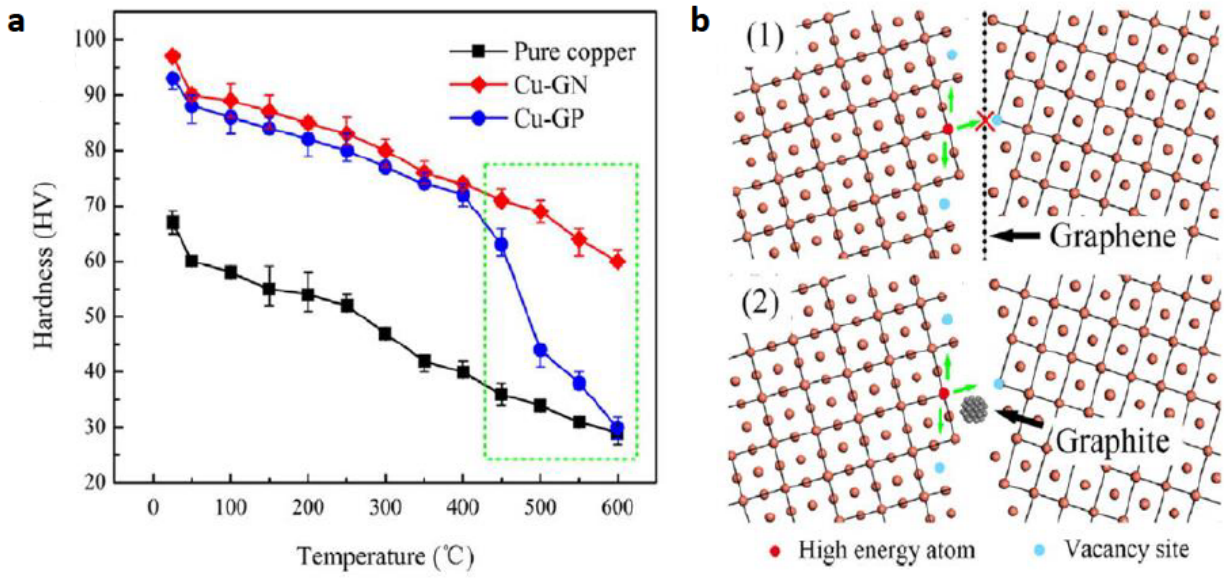

Figure 20: (a) Hardness vs. temperature curves of copper matrix composites. (b) Schematic diagrams of the hindrance of atom diffusion generated by graphene and graphite. Reproduced from Reference [124].

hence increased porosity, which restricted stress transfer and decreased mechanical strength. However, no aggregates were found in the rGO-Cu composite at a higher reinforcement content because of its hydrophilic functional groups, which aided in forming stronger interfacial bonding between GO and the Cu matrix. Similar observations and reasoning were given by Asgharzadeh *et al.* [129].

The thickness and lateral size of Gr have been shown to affect the mechanical behavior of GRMMCs [63, 124, 126]. Dutkiewicz *et al.* [63] used two grades of GNPs varying in thickness and in lateral dimensions in the Cu matrix. The composite contained GNPs with 2- to 4-nm thickness and size less than 100 nm showed a 50% improvement in hardness compared with that with GNPs of 10- to 20-nm thickness and lateral size less than 14 μm. In addition, SEM images revealed a highly uniform microstructure of the composite with finer GNPs than those containing coarse GNPs. Wang *et al.* [124] studied the effect of temperature on the hardness of GNP-Cu and graphite-Cu composite (referred to as Cu-GN and Cu-GP, respectively); see Figure 20a. The authors concluded that the hardness of both composites with the same reinforcement content is the same in the range between room temperature and 450°C. At 600°C, however, the hardness of GNP-Cu was found to be twice that of graphite-Cu. They attributed that to the higher efficiency of 2D GNPs to hinder atom diffusion and grain boundary motion at higher temperatures than when using the discontinuous interphase formed by the isolated graphite particles. The mechanism of hindering the grain boundary motion is schematically shown in Figure 20b.

Layered GRMMCs

In addition to bulk GRMMCs with homogenously and randomly distributed Gr reinforcements, layered structured GRMMCs have been investigated and have shown promising results [135, 157–159]. Kim *et al.* [122] reported the synthesis of a Gr-Cu nanolayered composite that consisted of alternating layers of Cu and monolayers of Gr. They used CVD to grow the monolayers of Gr before transferring it onto the deposited Cu layer to fabricate the Cu-Gr–layered structure. Nanopillar compression tests revealed that the nanolayered composite exhibited an ultra-high compression strength of 1.5 GPa when the repeat layer spacing was 70 nm. TEM investigations indicated a higher density of dislocations was present in the upper Cu layer, while the lower Cu layer showed dislocation starvation. This result was attributed to the strong Cu–Gr interface, which acted as a barrier to dislocation propagation across the interface. The authors explained that Gr acted as an impermeable interface to dislocations, preventing its propagation to the lower layers. This was a result of Gr's high intrinsic mechanical strength, which prevented its rupture and shearing. The compression tests revealed that Gr was not sheared during deformation up to a total compressive strain of 23%.

Yang *et al.* [135] synthesized another high-strength layered composite using MLM and SPS techniques. The authors investigated the effects of certain synthesis parameters, such as pH and temperature, on the structure and tensile properties of a rGO-Cu composite. Their analysis suggested that changing the pH value during the MLM process

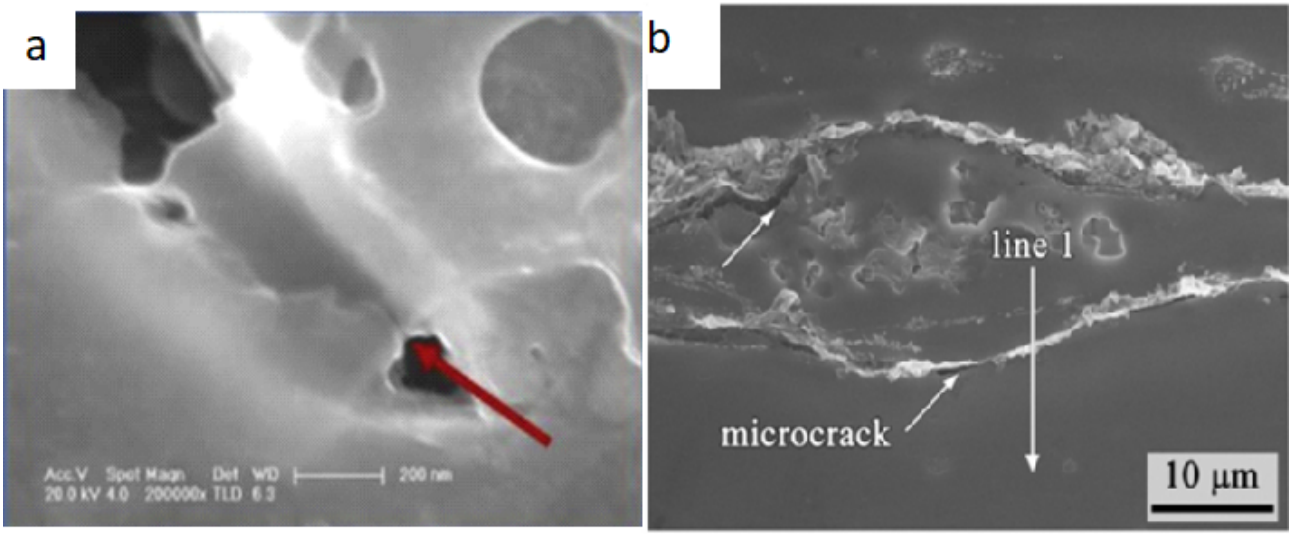

Figure 21: (a) TEM image showing the arrest of a microcrack by a graphene sheet. (b) SEM image showing microcracks in the composite rods along the rolling direction. Reproduced from References [139] and [53], respectively.

and the reaction temperature highly influenced the structure of the composite and its tensile properties. The tensile strength of the 2.5 vol% rGO-Cu composite was reported to be as high as 748 MPa for the composite fabricated at a pH of 13.6 and a reaction temperature of 20°C. The authors concluded that at high pH values and low reaction temperatures, the composite attained a hierarchical layered structure that was damaged when the synthesis was conducted at a lower pH and higher temperatures. These results highlight the importance of structural design and suggest that the formation of a hierarchical layered structure can play a crucial role in enhancing the mechanical properties of GRMMCs.

3.3.1.2 The Ductility and Deformation Mechanisms

Attaining high strength in GRMMCs without compromising good ductility is a challenge that has yet to be overcome. Mechanical deformation behavior in GRMMCs was reported to vary based on the metal matrix. The majority of the Gr-Al studies have reported a decrease in the ductility of the composites compared with the initial ductility of the metal [11, 18, 20, 24, 25, 27, 53–57, 70, 94]. The deterioration in ductility has been attributed to the pinning of dislocations by the reinforcement [24] and to the agglomeration of the reinforcement along the grain boundaries with increasing Gr content, resulting in weak interface bonding [11, 57]. Nonetheless, some studies have reported promising results in ductility at certain Gr concentrations along with an enhanced strength of the composite [11, 20, 27, 57, 139, 140].

Recently, Dixit *et al.* [139] reported a high ductility of 26% tensile elongation for their MLG-Al composite fabricated via FSP. The high ductility was attributed to the good bonding between the Al matrix and Gr reinforcement. In addition, the TEM analysis of a quasi-static crack growth proved that Gr was acting against propagation during the ductile fracture test. Figure 21a shows a Gr sheet arresting a microcrack that was developed upon loading. Yan *et al.* [118] synthesized 0.5 wt% GNF-reinforced aluminum matrix composite by ball milling followed by HIP and extrusion. An increase in the tensile strength from 373 MPa to 467 MPa was reported for pure Al and Gr-Al composite, respectively, without affecting the uniform elongation and ductility of the metal. This finding was attributed to the wrinkled structure of Gr that was preserved even after milling. Upon plastic deformation, the wrinkled structure of Gr straightens and flattens, thereby preserving the good ductility of the metal. Li *et al.* [53] observed wrinkling of GNP sheets after fabrication, which included ball milling. However, the 0.2 wt% GNP-Al witnessed a reduction in tensile elongation from 11% to 4% due to the formation of microcracks; see Figure 21b. The authors explained that the wrinkles and folds in the GNPs would partially unfold with initial stretching. However, the GNPs couldn't keep up with the ductile Al, which further deforms with increasing the load, leading to the rapid expansion of the microcracks at the interface and deterioration of the composite's elongation. In contrast, promising results have been reported by Yolshina *et al.* [140], who synthesized Gr-Al composites through a one-step process that took place directly in molten aluminum under alkali halides melt. The compos-

ites exhibited simultaneous increase in hardness, elastic modulus, tensile and yield strength with increasing the Gr content up to 2 wt%. Additionally, the authors reported an increase in tensile elongation to reach 24.2% for their 2 wt% Gr-Al composite compared with 13% elongation for pure Al.

Similar to Al, the ductility of pure, ductile, malleable, and easily processed Cu has been reported to drop significantly when adding Gr [49, 51, 71, 93, 97, 123, 125, 127, 134]. The deterioration in ductility has been attributed mainly to the pinning of dislocations by the reinforcement [71] and the agglomeration of the reinforcement along the grain boundaries with increasing Gr content, resulting in weak interface bonding [97]. In addition, several studies have attributed the deterioration in ductility to cracking, which tends to initiate in the grain boundaries where Gr is mostly located and/or at the interface between Gr and Cu, before cracks extend and propagate to the matrix [51, 71, 123]. Nevertheless, unprecedented enhancement in ductility of Gr-Cu compared with pure Cu was reported by Yang *et al.* [52]. They achieved a 39% increase in ductility over pure Cu for the 3 vol% GNR-reinforced Cu matrix composites prepared via the facile solution-based method followed by SPS and hot rolling. It is crucial to note that the study utilized GNR rather than rGO or GNSs; hence, the promising enhancement in ductility had been associated with the type of Gr derivative used and its distribution. The authors attributed the ductility to the uniform distribution of the GNRs inside the grains, which provided rigid interfacial areas that acted both as dislocation initiation sites and dislocation sinks pinning dislocation motion at the same time. This allows for achieving high strength by dislocation pinning without sacrificing the good ductility of the matrix by generating new dislocations. In addition, the intergrain uniform distribution of the GNRs avoided aggregation at the grain boundaries and alleviated the tendency to induce large stress concentrations and microcrack generations at grain boundaries. This behavior has been reported several times with the use of GNSs [51, 71, 123]. Other studies maintained decent ductility or tensile elongation percentages along with the associated strength enhancement of the composites. Jiang *et al.* [2] produced Ni-plated GNP-Cu composite and reported a 60% elongation, which is better than that of unreinforced Cu. Yue *et al.* [49] produced rGO-Cu by ball milling and HP using varying GO content. The optimized GO concentration was reported to be 0.5 wt%, which resulted in a 28% increase in UTS over pure Cu and a 24% tensile elongation. This had been attributed to the good interface bonding as a result of the successful distribution of rGO nanosheets in copper. The authors explained that with low GO content, GO sheets can hinder crack propagation by shielding the cracks. This is facilitated by their high aspect ratio and large contact area with the matrix. However, increasing the GO content more than 0.5 wt% resulted in rGO aggregation, providing sites for composite cracking. The same behavior and justification had been reported by Zhang *et al.* [134] for a 0.1 vol% rGO-Cu composite. SEM images showed the ductile behavior of the composite prepared by molecular-level mixing and SPS. Dimples were clearly distributed on the fracture surface, demonstrating a typical plastic deformation fracture behavior. The ductility behavior of the samples in References [2, 49, 52], and [134] are shown in Figures 22a, 22b, 22c, and 22d, respectively.

Unlike the face-centered cubic metals (Al and Cu) discussed previously, in which the increase of reinforced mechanical strength and hardness is mostly accompanied by a deterioration in ductility, the Gr-reinforced Mg matrix composites showed a significant improvement of ductility and strength compared with pure Mg or its alloys processed at the same conditions [48, 104, 105, 110, 111]. Rashad *et al.* [104, 105, 110] reported a significant increase in the ductility of the Mg matrix composites by adding GNPs. They reported an increase in tensile fracture strain from 17% for Mg-6Zn to 21% for Mg-6Zn-1.5 wt% GNPs [110], from 9.7% for pure Mg to 16.9% for Mg-1Al-3 wt% GNPs [105], and from 3.2% for pure Mg to 14% for Mg-10Ti-0.3 wt% GNPs [104]. SEM images of the tensile fracture surfaces of Mg-6Zn-1.5 wt% GNP are shown in Figure 23, where ductile fracture features are represented by dimples and tear ridges. An improvement in ductility has been attributed to the high surface area of GNPs and good adhesion to metal matrix [104] as well as the uniform dispersion of GNPs throughout the matrix [110].

3.3.2 Thermal and Electrical Properties

3.3.2.1 Thermal Behavior

Different parameters can affect the thermal properties of Gr-reinforced metals, such as the composite's thermal conductivity, thermal diffusivity, and CTE. Yolshina *et al.* [140] studied the effect of Gr content on the melting point of the Gr-Al composites. They reported a decrease in the melting point of the Gr-Al composite with an increase in the Gr content. Enhancements in the thermal conductivity of metal matrices after adding Gr have been reported for Cu [51, 160, 161] and Al [50]. Reddy *et al.* [50] investigated the effect of rGO content on the thermal conductivity (TC) of a rGO-Al composite. The TC is reported to increase from 48.5 W/mk to 58.5 W/mk for Al and 0.5 wt% rGO-Al composite, respectively. Gao *et al.* [51] reported an increase of the TC

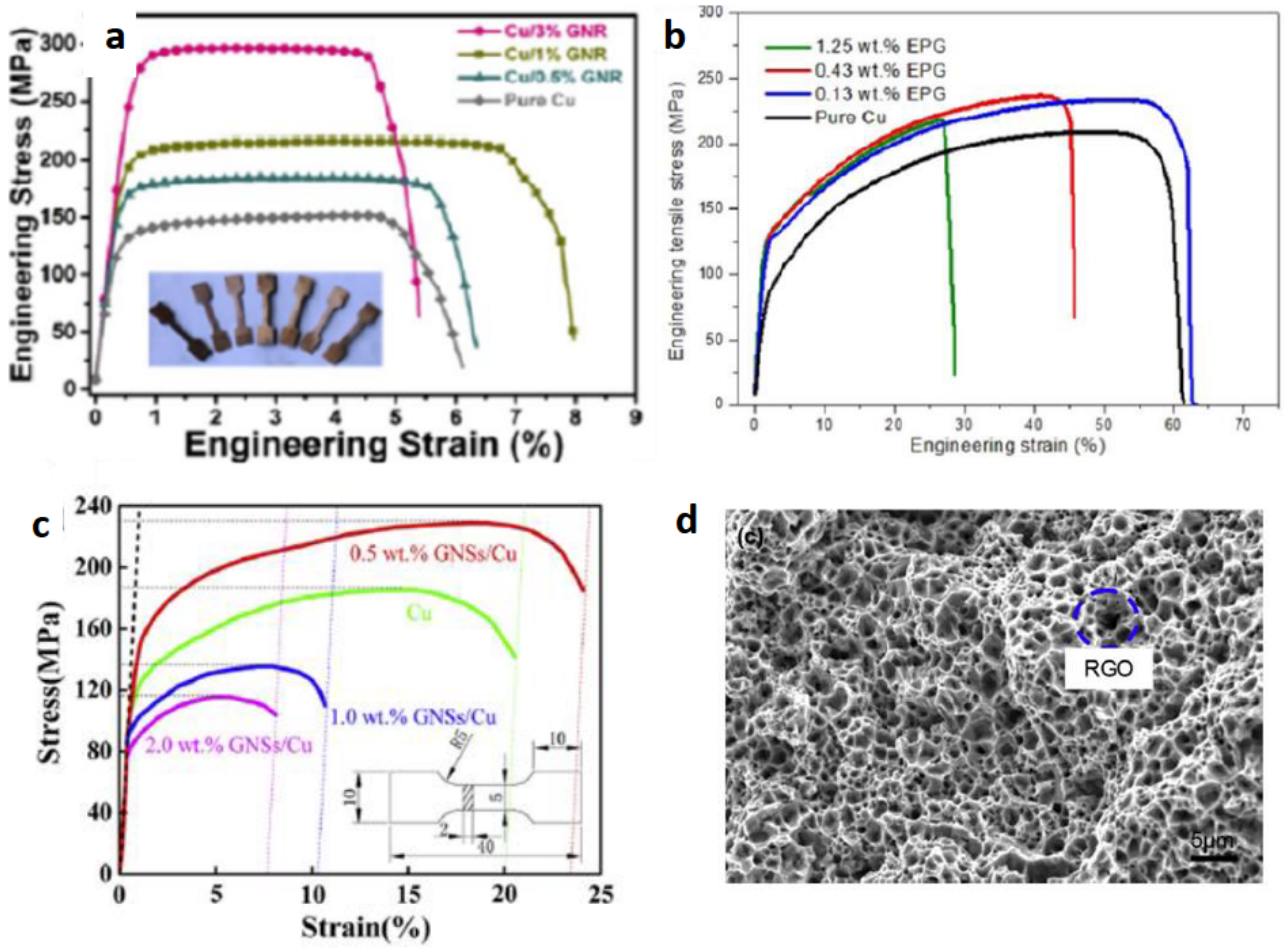

Figure 22: Tensile engineering stress-strain curves for (a) GNR-, (b) GNP-, and (c) GNS-reinforced Cu matrix composites. (d) SEM of fracture surfaces of 0.1 vol% RGO/Cu composites. Reproduced from Reference [52].

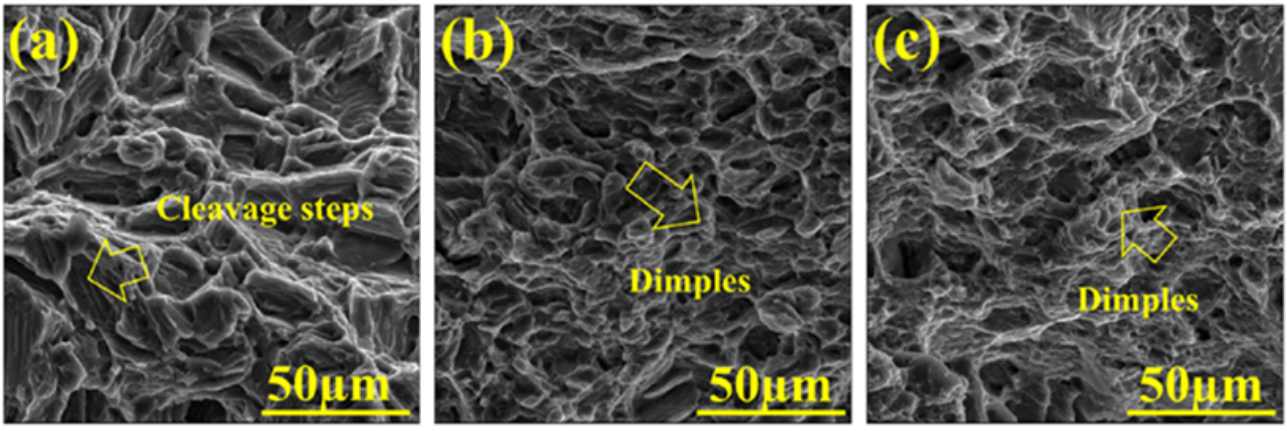

Figure 23: Tensile fracture images of as extruded (a) Mg–6Zn alloy, (b) Mg–6Zn–0.5GNP, and (c) Mg–6Zn–1.5GNP composites. Reproduced from Reference [110].

of their Gr-Cu composite with an increase in Gr content to reach a maximum value of 396 $Wm^{-1}K^{-1}$ at 0.3 wt%, after which a decrease in the TC was measured. The enhancement of the TC was ascribed to various reasons, such as the higher TC of Gr over pure Cu as well as the electrostatic self-assembly synthesis technique, which allowed for a uniform distribution of Gr in Cu and resulted in a lower interface thermal resistance. However, a higher Gr content resulted in Gr agglomeration in the composite and, hence, formed structural defects such as porosities and voids. These structural defects interfered with the phonon transfer between the Cu matrix and the Gr reinforcement, leading to a decrease in the TC of the composite [51, 97]. The effects of Gr alignment in the Gr-Cu composite on the TC of the composite are reported in References [160–162]. In these studies, the experimental and modeling results proved that achieving the highest possible TC requires the GNPs to be highly aligned in the metal composite. The studies concluded that the TC of GRMMCs is highly anisotropic, such that the enhancement achieved is different based on the conductivity's direction—whether perpendicular or parallel to the direction of alignment. In addition, the enhancement of the TC in one direction of the alignment was attained at the expense of the conductivity in the other direction [160, 161]. Chu *et al.* [161] controlled the alignment of GNS in the Cu-GNS composites via vacuum filtration and SPS. They reported a substantially higher in-plane (perpendicular) TC than through-plane (parallel) TC with a 35% increase in the in-plane TC than that of pure unreinforced Cu.

The thermal diffusivity of Gr-Cu composites has been studied. Chen *et al.* [97] and Si *et al.* [96] reported a decrease in the thermal diffusivity after adding GNPs to the Cu matrices. Chen *et al.* [97] reported a constant deterioration of thermal diffusivity measured in both the horizontal and parallel consolidation directions with increasing the GNP content. This behavior was attributed to the poor bonding and large mismatch in the CTE between Gr and Cu, which formed voids and increased the interfacial thermal resistance. Si *et al.* [96] explained that the increase in thermal resistance is due to the poor interfacial structure of Gr-Cu composites. This led to poor electron-phonon coupling, which is considered to be the main thermal transport mode in Gr-Cu composites. The CTE for Gr-Cu composites has also been studied [101, 124, 161]. It was reported to decrease after adding Gr. Wang *et al.* [124] attributed this decrease in CTE to the distribution of Gr in the composite and the effective drag force it applied on the grain boundary motion, which hindered grain growth at elevated temperatures.

3.3.2.2 Electrical Behavior

The effects of varying Gr content on the electrical conductivity of GRMMCs have been reported. The electrical conductivity was reported to decrease with increasing the Gr content [2, 52, 63, 96, 97, 137]. However, several studies have suggested that the excellent electrical conductivity of metals can be maintained after adding Gr. Li *et al.* [53] studied the effects of adding GNPs on the electrical conductivity of Al and reported a trivial 0.7% reduction in electrical conductivity for their 0.2 wt% GNP-Al composite. This finding was attributed to the low GNP content, suggesting that the Al matrix dominates the conductivity behavior and that phase interface scattering between Al and GNPs is very limited. A similar behavior was reported by other studies, where the electrical conductivity of Gr-Cu composite is trivially reduced and high conductivity is still achieved [63, 71, 72, 96, 97, 124, 135, 137]. The decrease in the electrical conductivity of Cu was justified by the presence of the Gr-Cu interface, resulting in a reduction of the electrons' mean free path as well as the scattering of electrons at the interface [71, 97].

Recent attempts have successfully reported enhanced electrical conductivity of Gr-Cu composites over pure Cu [52, 137, 163]. Yang *et al.*'s [52] results proved that enhancing the strength of metal composites by adding Gr does not have to be at the expense of electrical conductivity. Their composite achieved a 5% enhancement in the electrical conductivity of GNRs over pure Cu for 1 vol% addition of GNRs. When the GNR content was increased to 3 vol%, the electrical conductivity dropped below that of 1 vol%. However, this value is still 2.7% higher than that of pure Cu. The enhanced electrical conductivity was attributed to the unique geometry of the GNRs as well as its direction in the metal matrix, which was controlled via the hot-rolling process. In addition, the authors suggested that the clean and closely bonded interface reduced the electron scattering and, hence, minimized interfacial impedance. Last, the addition of GNRs in this study resulted in extra paths for electron transport. The electrical conductivity of Ayyappadas *et al.*'s [137] GNF-Cu microwave-sintered composite was reported to increase from 92% to 94% compared with pure Cu when the addition of GNFs was 0.9 vol%. This result was attributed to the homogenous distribution of the highly conductive GNFs in the matrix. Increasing the Gr content to 1.8 vol% led to maintaining a 92% electrical conductivity, which is similar to that of pure Cu. However, further increasing the GNFs content to 3.6 vol% achieved an 86% electrical conductivity, which is 6% less than that of pure Cu. The decrease in electrical conductivity was correlated to the introduction of porosities in the compos-

ite with increasing the GNF content, which interrupted the continuity of the conductive path necessary to achieve high electrical conductivity values. Recently, more promising results were reported by Cao *et al.* [163] for a layered Gr-Cu composite that was synthesized using CVD and hot pressing. The layered composite achieved the highest electrical conductivity for a Gr-Cu composite of a 117% International Annealed Copper Standard (IACS) with the addition of only 0.008 vol% Gr. The authors used first-principles calculation results based on the density functional theory to understand the resultant significant electrical conductivity. They attributed the high electrical conductivity of the embedded Gr to a doping effect that resulted in an increased carrier density and an unaffected, very high carrier mobility in Gr. Furthermore, the authors investigated the effect of changing the number of Gr layers on the electrical behavior of the composite through a careful control of the carbon source concentration and the growth time during the CVD process. The results suggested that the electrical conductivity in the Gr layers decreases with increasing the number of layers.

The effects of varying the Gr type in the composite on the electrical behavior of Gr-Cu composites have also been noted [63, 71, 124]. Wang *et al.* [124] compared the electrical conductivity when using GNPs and graphite in Cu composites. Compared with the 74.1 IACS% reported of graphite-Cu, the GNP-Cu composite was able to maintain 95.9% IACS. Jiang *et al.* and [71] and Dutkiewicz *et al.* [63] investigated the effect of reinforcing Cu with rGO and GNPs on the electrical conductivity and resistivity, respectively. Jiang *et al.* [71] reported a better electrical performance for the GNP-Cu with 84.2% IACS compared with 73.4% IACS for the rGO-Cu composite. Dutkiewicz *et al.* [63] reported a better electrical performance for rGO-Cu with only a 28% increase in electrical resistivity, compared with 57% for the GNP-Cu composite. While Dutkiewicz *et al.* [63] gave no justification, Jiang *et al.* [71] ascribed their results to the already better inherent electrical performance of GNPs compared with GO due to the inevitable defects in GO sheets after oxidation.

3.3.3 Surface Properties

3.3.3.1 Corrosion Behavior

The effects of the added reinforcement on the corrosion-resistant behavior of Gr-metal composites have been reported for Al [11, 140], Mg [108], and Cu [164–166]. The influence of the added reinforcement on the corrosion resistance is a main challenge in the fabrication of metal composites, especially in Al composites. Al is known for its corrosion-resistant properties due to its protective oxide film formed on the surface. The addition of another phase to Al, such as Gr, can cause discontinuities in the protective film, creating corrosion-initiating sites. Rashad *et al.* [11] and Yolshina *et al.* [140] studied the corrosion behavior of the Gr-Al composite after immersing the composite in 3.5 wt% NaCl solution. In this study [11], the potentiodynamic polarization measurements for the composite synthesized via powder metallurgy and hot extrusion showed an increase in the corrosion rate after adding GNPs. The authors suggested that the cathodic nature of Gr compared with the Al matrix leads to galvanic corrosion in the presence of the electrolyte. Yolshina *et al.* [140] reported similar observations for the Gr-Al synthesized by a one-step in-situ synthesis in molten Al under an alkali halides melt. The corrosion rate increased with increasing GNP concentration compared with the corrosion rate of pure Al. However, the authors suggested that the increase in corrosion rate from 0.0016 g/m^2h to 0.0048 g/m^2h for pure Al and 2 wt% GNP-Al composite, respectively, is minimal and that the composite is still classified as a class 4 corrosion-resistant material. SEM images of clean and corroded pure Al and 0.5 wt% Gr-Al composites are shown in Figure 24.

More recently, Jin *et al.* [164] studied the corrosion behavior of a Gr-Cu composite prepared by growing Gr on Cu by heating PMMA-coated Cu at 900°C followed by HP of the powder flakes to form a bulk composite. The corrosion rate of the composite was reported to decrease by 50% in NaCl. Several tests were conducted to evaluate the enhanced corrosion behavior of the synthesized Gr-Cu composite including etching behavior test in $FeCl_3$ solution, salt spray corrosion test, and electrochemical corrosion test. According to the results, Gr clearly showed anticorrosive advantages, but its performance was anisotropic; its orientation in the Cu matrix influenced the corrosion pathway. In addition, it was concluded that the defects present in the Gr structure are detrimental to its corrosion protection behavior and act as sources that promote corrosion. Finally, the tests confirmed that the corrosive media had to penetrate more Gr layers if the corrosion proceeded in the in-plane direction, offering higher corrosion resistance than when the corrosion proceeded in the cross-plane direction where more Cu channels were present. These results demonstrate the potential applications of such composites, especially when the enhancement in corrosion behavior is associated with substantial mechanical hardening and good electrical conductivities.

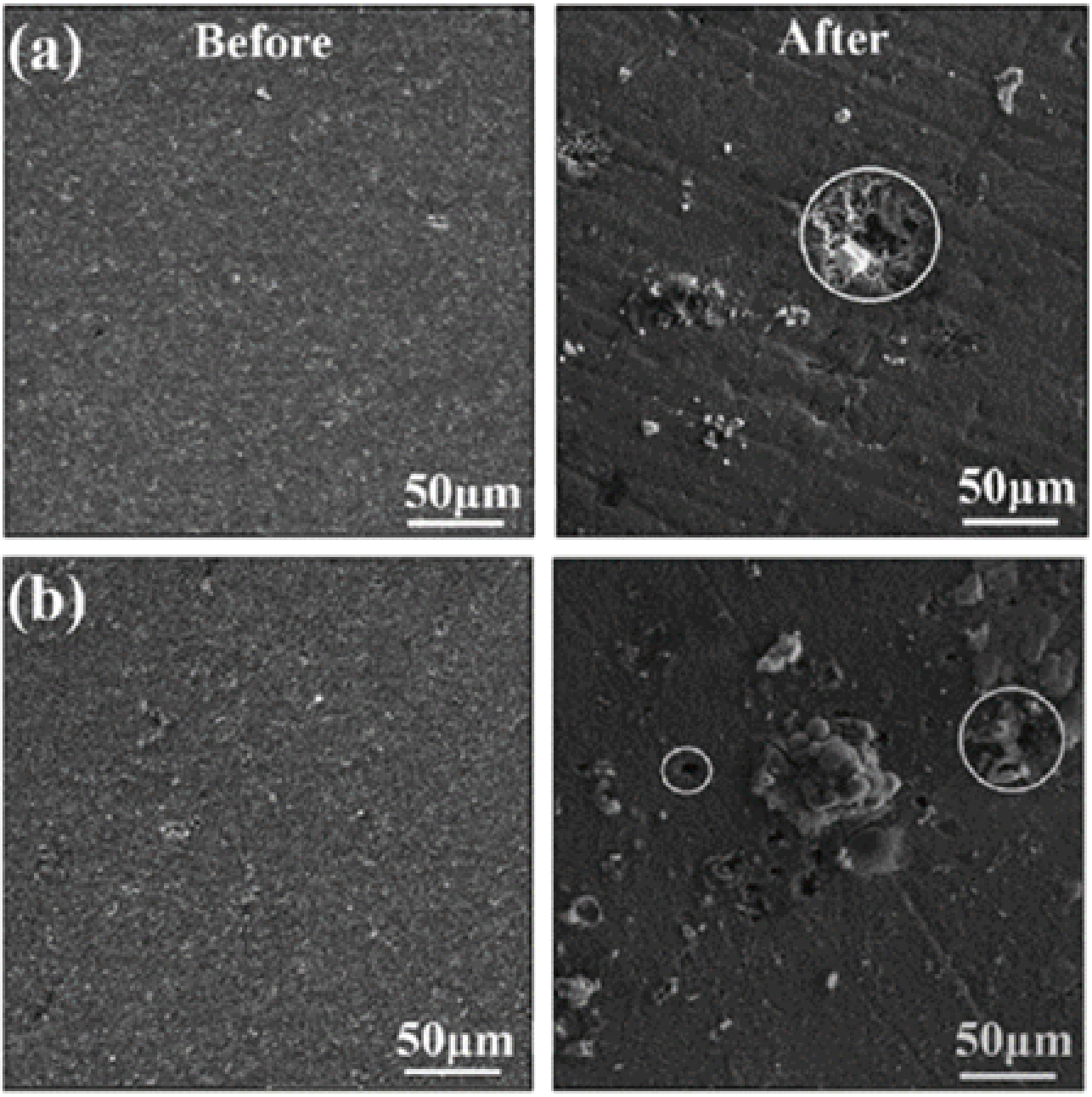

Figure 24: Before and after SEM images of (a, b) pure Al and (c, d) 0.5 wt% GNP-Al composite. Reproduced from Reference [140].

3.3.3.2 Tribological Behavior

Graphene and its derivatives are expected to have a positive influence on the tribological properties of MMCs, such as wear and friction behavior. This is attributed to its self-lubricating nature that stems from the squeezing of the Gr sheets in between sliding surfaces and its loadbearing capability, which reduces the wear rates of metal matrices [47].

The effects of changing the Gr content on wear rates and coefficient of friction (COF) have been investigated [47, 99]. It has been reported that the wear rates and COF decrease for Gr-Al composites compared with plain Al-based matrices [47, 99] and for Cu matrices [96, 97, 137] up to certain Gr content, after which an increase in wear rates and COF is reported [64, 126]. El-Ghazaly *et al.* [47] studied the tribological properties of hot-extruded GNP-reinforced AA2124. They reported superior wear behavior of the composite compared with the alloy. The authors reported a 34% reduction in the wear rate and a 22.5% reduction in the COF for the 0.3 wt% GNP-AA2124 composite

compared with plain AA2124. They also investigated the effects of GNP content on the tribological properties of the alloy and reported an increase in wear rate and COF with increasing the GNP content. This finding was attributed to the distribution of the GNPs within the metal matrix where GNPs were observed to segregate within the Al matrix with the increasing GNP content. This resulted in the release of nonuniform graphene thick films on the Al-matrices, which were delaminated between the rubbing surfaces. This finding is in contrast to the 3 wt% GNP content, where GNPs were mainly allocated at the grain boundaries and hence were smeared out uniformly on the sliding surfaces, providing a continuous graphene layer between the rubbing surfaces and hence increasing wear resistance.

Tabandeh-Khorshid *et al.* [99] reported a decrease in COF and an increase in wear rate with increasing the GNP content from 0.1 wt% to 1 wt%. They suggested that higher wear rates mean exposing more GNPs to the surfaces and thus higher lubrication during sliding, which led to a lower COF. Chen *et al.* [97] reported that the COF did not change when small amounts of GNPs, below 0.8 vol%, were added to Cu. However, increasing GNPs to 4.0 vol% led to a 60% reduction in COF over pure Cu. The trivial decrease in COF at a lower Gr content was justified by the quick wearing of the Gr thin film that forms at the worn surfaces. In contrast, increasing the Gr content formed a thick continuous film that prohibited oxidation and reduced friction. Si *et al.* [96] reported a drastic reduction in wear rates of the Gr-Cu composite with GNP concentrations starting from 0.9 vol%, with a minimum wear rate of 0.28×10^{-5} g/m for their 3.6 vol% GNP-Cu composite at a load of 30 N. This was attributed to the interlayer shearing mechanism of Gr that prevented metal-to-metal contact and led to lower wear rates and COFs.

Gao *et al.* [64] and Li *et al.* [126] reported that there is a critical Gr content above which the tribological behavior of the Gr-Cu composite deteriorates. In their work [64], the COF is first decreased to 65% lower than that of pure Cu by adding 0.3 wt% GNP, and then it increases when the GNP is increased to 0.5 wt%. The authors explained that at a high GNP content, GNPs were located at the grain boundaries, which led to the poor sintering ability of the 0.5 wt% GNP-Cu composite and resulted in Cu grains separating during the friction test. Li *et al.* [126] reported a similar behavior for the wear rate of the GNS-Cu composite, which decreased from 13.6×10^{-4} to 2.3×10^{-4} mm^3/m as the volume fraction increased from 2.5 vol% to 7.5 vol%, but later it increased as the GNS content increased to 10 vol%. This was justified by the poor mechanical behavior and the load-bearing ability of the 10 vol% GNS-Cu composite, where the hardness dropped from 97.4 Hv to 56.8 Hv when the GNS content increased from 7.5 vol% to 10 vol%, respectively. Similarly, the relationship between the wear behavior and the mechanical properties was referred to and addressed by El-Ghazaly *et al.* and Si *et al.* [47, 96].

4 Summary

This review focused on the three main pillars in bulk GRMMC studies: synthesis, structure, and properties. First, the variety of techniques used to produce GRMMC have been summarized and categorized based on the steps involved in the synthesis: pretreatment of metal and Gr, mixing, and postsynthesis/consolidation. Regardless of the synthesis route chosen, a synthesis technique was assumed to be successful when the composite attained two main structural features: a homogenous distribution of Gr within the metal matrix and a defect-free clean matrix-reinforcement interface. These two features facilitate mechanical load, electron, or phonon transfer between the metal matrix and the Gr reinforcement, all of which directly affect the enhanced response and behavior of the GRMMCs. In addition, studies showed that different metals have different interactions with Gr, and many challenges persist regarding the interfacial interaction formation. For example, the lack of second-phase formation had been attributed to the poor solid solubility between Cu and C in Cu-Gr systems, and to the poor wettability between Mg and Gr in Mg-Gr systems. Nonetheless, the formation of a second phase between Al and C in Al-Gr systems has been highly investigated and is considered a point of debate among researchers (*i.e.*, whether the formation of the Al_4C_3 is caused by the exposure of the composite to high temperatures during synthesis or is initiated by the disorder and defect points in the graphitic structure regardless of temperature). Furthermore, the role such phase played in the behavior of the composites is also a point of debate. Some studies suggested that it caused detrimental effects on the mechanical behavior of Al-Gr composites due to the structural damage involved with the formation of Al_4C_3, while other studies suggested that it enhanced the mechanical strength and hardness by pinning dislocations.

Impressive enhancements in the tensile and compressive strengths and hardness have been reported in studies utilizing relatively small concentrations of Gr, regardless of the metal type. In these studies, there were optimized concentrations of Gr, above which an observed deterioration in the behavior was reported. Such behavior had been attributed to the difficulty in homogenously distributing larger reinforcement content in the matrix, lead-

ing to agglomeration and poor contact between the reinforcement and the matrix. The ductility or mechanical deformation behavior in GRMMCs was reported to vary based on the metal type. In Al-Gr and Cu-Gr systems, most studies reported a decrease in the ductility of the composites compared with the initial ductility of the metal. In Mg-Gr systems, a simultaneous improvement in ductility and strength compared with pure Mg or its alloys processed at the same conditions has been reported. Another point of investigation highlighted in this review is the effect of the Gr derivative type and morphology on the overall behavior of the GRMMCs. Various reports have shown that the thickness, number of layers, lateral size, and chemical structure of the Gr reinforcement has directly affected the mechanical behavior of GRMMCs. So far, the main interest has been comparing the use of unfunctionalized Gr, such as GNPs, with functionalized Gr, such as GO. Some researchers have suggested that GNPs performed better as reinforcement due to the absence of oxygen-containing functional groups in GNPs, which would result in lower structural defects. Other researchers concluded that the hydrophilic functional groups in GO aided in stronger interfacial bonding between GO and the metal matrix, allowing the composite to withstand higher concentrations of the reinforcement without aggregation.

With the technological advancements in every known area, the demand for high-performance materials is more pressing than ever. Combining Gr into bulk metals promises enhanced mechanical performances and superior strength-to-weight ratios, as well as the expected enhancements in thermal and electrical performances. The field of GRMMCs is still in its early stages, but the increasing number of publications on this topic annually and the reported results prove both its merit and future. At the end of this review, it is important to highlight that inconsistent experimental findings with regard to the behavior and response of GRMMCs are reported and explained throughout the literature. Discrepancies arise largely from the large number of variables involved in different studies, such as the different Gr derivatives used, the metal type investigated, the handling of the materials, the synthesis technique of choice, and the amount of Gr reinforcement used. Thus, a more systematic approach toward producing and characterizing these composites is required to achieve a more comprehensive understanding of the behavior and response of these composites.

Acknowledgement: This work was made possible by NPRP Grant no. NPRP9-180-2-094 from the Qatar National Research Fund (a member of the Qatar Foundation). The statements made herein are solely the responsibility of the authors.

References

[1] Nieto, A., A. Bisht, D. Lahiri, C. Zhang, and A. Agarwal. Graphene reinforced metal and ceramic matrix composites: A review. *International Materials Reviews*, Vol. 62, No. 5, 2017, pp. 241–302.

[2] Jiang, R., X. Zhou, and Z. Liu. Electroless Ni-plated graphene for tensile strength enhancement of copper. *Materials Science and Engineering A*, Vol. 679, 2017, pp. 323–328.

[3] Whitener, K. E., Jr., and P. E. Sheehanb. Graphene synthesis. *Diamond and Related Materials*, Vol. 46, 2014, pp. 25–34.

[4] Novoselov, K. S., D. Jiang, F. Schedin, T. J. Booth, V. V. Khotkevich, S. V. Morozov, and A. K. Geim. Two-dimensional atomic crystals. *Proceedings of the National Academy of Sciences of the United States of America*, Vol. 102, No. 30, 2005, pp. 10451–10453.

[5] Novoselov, K. S., A. K. Geim, S. V. Morozov, D. Jiang, Y. Zhang, S. V. Dubonos, I. V. Grigorieva, and A. A. Firsov. Electric field effect in atomically thin carbon films. *Science*, Vol. 306, No. 5696, 2004, pp. 666–669.

[6] Balandin, A. A., S. Ghosh, W. Bao, I. Calizo, D. Teweldebrhan, F. Miao, and C. N. Lau. Superior thermal conductivity of single-layer graphene. *Nano Letters*, Vol. 8, No. 3, 2008, pp. 902–907.

[7] Du, X., I. Skachko, A. Barker, and E. Y. Andrei. Approaching ballistic transport in suspended graphene. *Nature Nanotechnology*, Vol. 3, No. 8, 2008, pp. 491–495.

[8] Lee, C., X. Wei, J. W. Kysar, and J. Hone. Measurement of the elastic properties and intrinsic strength of monolayer graphene. *Science*, Vol. 321, No. 5887, 2008, pp. 385–388.

[9] Geim, A. K. Graphene: Status and prospects. *Science*, Vol. 324, No. 5934, 2009, pp. 1530–1534.

[10] Nair, R. R., P. Blake, A. N. Grigorenko, K. S. Novoselov, T. J. Booth, T. Stauber, N. M. R. Peres, and A. K. Geim. Fine structure constant defines visual transparency of graphene. *Science*, Vol. 320, No. 5881, 2008, p. 1308.

[11] Rashad, M., F. Pan, Z. Yu, M. Asif, H. Lin, and R. Pan. Investigation on microstructural, mechanical and electrochemical properties of aluminum composites reinforced with graphene nanoplatelets. *Progress in Natural Science: Materials International,* Vol. 25, 2015, pp. 460-470.

[12] Feng, L., and Z. Liu. Graphene in biomedicine: Opportunities and challenges. *Nanomedicine (London)*, Vol. 6, No. 2, 2011, pp. 317–324.

[13] Guo, C. X., H. B. Yang, Z. M. Sheng, Z. S. Lu, Q. L. Song, and C. M. Li. Layered graphene/quantum dots for photovoltaic devices. *Angewandte Chemie*, Vol. 49, No. 17, 2010, pp. 3014–3017.

[14] Yoon, H. J., J. H. Yang, Z. Zhou, S. S. Yang, and M. M. Cheng. Carbon dioxide gas sensor using a graphene sheet. *Sensors and Actuators. B, Chemical*, Vol. 157, No. 1, 2011, pp. 310–313.

[15] Avouris, P., and F. Xia. Graphene applications in electronics and photonics. *MRS Bulletin*, Vol. 37, No. 12, 2012, pp. 1225–1234.

[16] Zhu, Y., S. Murali, W. Cai, X. Li, J. W. Suk, J. R. Potts, and R. S. Ruoff. Graphene and graphene oxide: Synthesis, properties, and applications. *Advanced Materials*, Vol. 22, No. 35, 2010, pp. 3906–3924.

[17] Rashad, M., F. Pan, A. Tang, and M. Asif. Effect of Graphene Nanoplatelets addition on mechanical properties of pure aluminum using a semi-powder method. *Progress in Natural Science: Materials International,* Vol. 25, 2015, pp. 460-470.

[18] Pérez-Bustamante, R., D. Bolaños-Morales, J. Bonilla-Martínez, I. Estrada-Guel, and R. Martínez-Sánchez. Microstructural and hardness behavior of Graphene nanoplatelets/aluminum composites synthesized by mechanical alloying. *Journal of Alloys and Compounds*, Vol. 615, Supplement 1, 2014, pp. S578–S582.

[19] Sharma, R., S. Jhap, K. Kakkar, A. Kamboj, and P. Sharma. A review of the aluminium metal matrix composite and its properties. *International Research Journal of Engineering and Technology*. Vol. 4, 2017, pp. 832-842.

[20] Konakov, V. G., O. Y. Kurapova, I. V. Lomakin, I. Y. Archakov, E. N. Solovyeva, and I. A. Ovid'ko. Fabrication of aluminum-graphene and metal-ceramic nanocomposites. A selective review. *Reviews on Advanced Materials Science*, Vol. 44, 2016, pp. 361-369.

[21] Hu, Z., G. Tong, D. Lin, C. Chen, H. Guo, J. Xu, and L. Zhou. Graphene-reinforced metal matrix nanocomposites – a review. *Journal of Materials Science and Technology*, Vol. 32, No. 9, 2016, pp. 930–953.

[22] Abdala, A. A. Polymer graphene nanocomposites. Proceedings of the The Sixth Jordan International Chemical Engineering Conference, 2012, Jordan.

[23] Shin, S. E., Y. J. Ko, and D. H. Bae. Mechanical and thermal properties of nanocarbon-reinforced aluminum matrix composites at elevated temperatures. *Composites. Part B, Engineering*, Vol. 106, 2016, pp. 66–73.

[24] Bisht, A., M. Srivastava, R. M. Kumar, I. Lahiri, and D. Lahiri. Strengthening mechanism in graphene nanoplatelets reinforced aluminum composite fabricated through spark plasma sintering. *Materials Science and Engineering A*, Vol. 695, 2017, pp. 20–28.

[25] Shin, S. E. and D.H. Bae. Deformation behavior of aluminum alloy matrix composites reinforced with few-layer graphene. *Composites Part A: Applied Science and Manufacturing*, Vol. 78, 2015, pp. 42–47.

[26] Alam, S. N., and L. Kumar. Mechanical properties of aluminium based metal matrix composites reinforced with graphite nanoplatelets. *Materials Science and Engineering A*, Vol. 667, 2016, pp. 16-32.

[27] Li, G., and B. Xiong. Effects of graphene content on microstructures and tensile property of graphene-nanosheets / aluminum composites. *Journal of Alloys and Compounds*, Vol. 697, 2017, pp. 31–36.

[28] Kim, H., A. A. Abdala, and C. W. Macosko. Graphene/Polymer Nanocomposites. *Macromolecules*, Vol. 43, No. 16, 2010, pp. 6515–6530.

[29] Zeranska-Chudek, K., A. Lapinska, A. Wroblewska, J. Judek, A. Duzynska, M. Pawlowski, A. M. Witowski, and M. Zdrojek. Study of the absorption coefficient of graphene-polymer composites. *Scientific Reports*, Vol. 8, No. 1, 2018, p. 9132.

[30] Du, J., and H. M. Cheng. The Fabrication, Properties, and Uses of Graphene/Polymer Composites. *Macromolecular Chemistry and Physics*, Vol. 213, No. 10-11, 2012, pp. 1060–1077.

[31] Walker, L. S., V. R. Marotto, M. A. Rafiee, N. Koratkar, and E. L. Corral. Toughening in graphene ceramic composites. *ACS Nano*, Vol. 5, No. 4, 2011, pp. 3182–3190.

[32] Porwal, H., S. Grasso, and M. Reece. Review of graphene–ceramic matrix composites. *Advances in Applied Ceramics*, Vol. 112, No. 8, 2013, pp. 443–454.

[33] Zhou, M., T. Lin, F. Huang, Y. Zhong, Z. Wang, Y. Tang, H. Bi, D. Wan, and J. Lin. Highly Conductive Porous Graphene/Ceramic Composites for Heat Transfer and Thermal Energy Storage. *Advanced Functional Materials*, Vol. 23, No. 18, 2013, pp. 2263–2269.

[34] Mahale, N. K., and S. T. Ingle. Electrocatalytic hydrogen evolution reaction on nano-nickel decorated graphene electrode. *Energy*, Vol. 119, 2017, pp. 872–878.

[35] Liu, Y., Y. Zhu, X. Fan, S. Wang, Y. Li, F. Zhang, G. Zhang, and W. Peng. (0D/3D) MoS2 on porous graphene as catalysts for enhanced electrochemical hydrogen evolution. *Carbon*, Vol. 121, 2017, pp. 163–169.

[36] Yu, X., B. Qu, Y. Zhao, C. Li, Y. Chen, C. Sun, P. Gao, and C. Zhu. Growth of Hollow Transition Metal (Fe, Co, Ni) Oxide Nanoparticles on Graphene Sheets through Kirkendall Effect as Anodes for High-Performance Lithium-Ion Batteries. *Chemistry (Weinheim an der Bergstrasse, Germany)*, Vol. 22, No. 5, 2016, pp. 1638–1645.

[37] Zhu, X., X. Jiang, X. Liu, L. Xiao, X. Ai, H. Yang, and Y. Cao. Amorphous CoS nanoparticle/reduced graphene oxide composite as high-performance anode material for sodium-ion batteries. *Ceramics International*, Vol. 43, No. 13, 2017, pp. 9630–9635.

[38] Yousef, A., M. H. El-Newehy, S. S. Al-Deyab, and N. A. M. Barakat. Facile synthesis of Ni-decorated multi-layers graphene sheets as effective anode for direct urea fuel cells. *Arabian Journal of Chemistry*, Vol. 10, No. 6, 2017, pp. 811–822.

[39] Tian, Z., H. Dou, B. Zhang, W. Fan, and X. Wang. Three-dimensional graphene combined with hierarchical CuS for the design of flexible solid-state supercapacitors. *Electrochimica Acta*, Vol. 237, 2017, pp. 109–118.

[40] Shabnam, L., S. N. Faisal, A. K. Roy, E. Haque, A. I. Minett, and V. G. Gomes. Doped graphene/Cu nanocomposite: A high sensitivity non-enzymatic glucose sensor for food. *Food Chemistry*, Vol. 221, 2017, pp. 751–759.

[41] Wei, Y., H. Wang, S. Sun, L. Tang, Y. Cao, and B. Deng. An ultrasensitive electrochemiluminescence sensor based on reduced graphene oxide-copper sulfide composite coupled with capillary electrophoresis for determination of amlodipine besylate in mice plasma. *Biosensors & Bioelectronics*, Vol. 86, 2016, pp. 714–719.

[42] Hu, X.-S., Y. Shen, Y.-T. Zhang, and J.-J. Nie. Preparation of flower-like CuS/reduced graphene oxide(RGO) photocatalysts for enhanced photocatalytic activity. *Journal of Physics and Chemistry of Solids*, Vol. 103, 2017, pp. 201–208.

[43] Zhang, X.-F., Y. Chen, Y. Feng, X. Zhang, J. Qiu, M. Jia, and J. Yao. Facile preparation of Zn0.5Cd0.5S@RGO nanocomposites as efficient visible light driven photocatalysts. *Journal of Alloys and Compounds*, Vol. 705, 2017, pp. 392–398.

[44] Prashantha Kumar, H. G., and M. Anthony Xavior. Processing and Characterization of Al 6061 – Graphene Nanocomposites. *Materials Today: Proceedings*, Vol. 4, No. 2, 2017, pp. 3308–3314.

[45] Mokhalingam, A., D. Kumar, and A. Srivastava. Mechanical Behaviour of Graphene Reinforced Aluminum Nano composites. *Materials Today: Proceedings*, Vol. 4, No. 2, 2017, pp. 3952–3958.

[46] Borkar, T., H. Mohseni, J. Hwang, T. W. Scharf, J. S. Tiley, S. H. Hong, and R. Banerjee. Excellent strength–ductility combination in nickel-graphite nanoplatelet (GNP/Ni) nanocomposites. *Journal of Alloys and Compounds*, Vol. 646, 2015, pp. 135–144.

[47] El-Ghazaly, A., G. Anis, and H.G. Salem. Effect of graphene addition on the mechanical and tribological behavior of nanostructured AA2124 self-lubricating metal matrix composite. *Composites Part A: Applied Science and Manufacturing*, Vol. 95, 2017,

pp. 325-336.

[48] Rashad, M., F. Pan, J. Zhang, and M. Asif. Use of high energy ball milling to study the role of graphene nanoplatelets and carbon nanotubes reinforced magnesium alloy. *Journal of Alloys and Compounds*, Vol. 646, 2015, pp. 223–232.

[49] Yue, H., L. Yao, X. Gao, S. Zhang, E. Guo, H. Zhang, X. Lin, and B. Wang. Effect of ball-milling and graphene contents on the mechanical properties and fracture mechanisms of graphene nanosheets reinforced copper matrix composites. *Journal of Alloys and Compounds*, Vol. 691, 2017, pp. 755–762.

[50] Reddy, K. S., D. Sreedhar, K. D. Kumar, and G. P. Kumar. Role of Reduced Graphene Oxide on Mechanical-thermal Properties of Aluminum Metal Matrix Nano Composites. *Materials Today: Proceedings*, Vol. 2, No. 4-5, 2015, pp. 1270–1275.

[51] Gao, X., H. Yue, E. Guo, H. Zhang, X. Lin, L. Yao, and B. Wang. Mechanical properties and thermal conductivity of graphene reinforced copper matrix composites. *Powder Technology*, Vol. 301, 2016, pp. 601–607.

[52] Yang, M., L. Weng, H. Zhu, T. Fan, and D. Zhang. Simultaneously enhancing the strength, ductility and conductivity of copper matrix composites with graphene nanoribbons. *Carbon*, Vol. 118, 2017, pp. 250–260.

[53] Li, M., H. Gao, J. Liang, S. Gu, W. You, D. Shu, J. Wang, and B. Sun. Microstructure evolution and properties of graphene nanoplatelets reinforced aluminum matrix composites. *Materials Characterization*, Vol. 140, 2018, pp. 172–178.

[54] Tabandeh-Khorshid, M., J. B. Ferguson, B. F. Schultz, C.-S. Kim, K. Cho, and P. K. Rohatgi. Strengthening mechanisms of graphene- and Al2O3-reinforced aluminum nanocomposites synthesized by room temperature milling. *Materials & Design*, Vol. 92, 2016, pp. 79–87.

[55] Zhang, H., C. Xu, W. Xiao, K. Ameyama, and C. Ma. Enhanced mechanical properties of Al5083 alloy with graphene nanoplates prepared by ball milling and hot extrusion. *Materials Science and Engineering A*, Vol. 658, 2016, pp. 8–15.

[56] Shin, S. E., H. J. Choi, J. H. Shin, and D. H. Bae. Strengthening behavior of few-layered graphene/aluminum composites. *Carbon*, Vol. 82, 2015, pp. 143–151.

[57] Li, J. L., Y. C. Xiong, X. D. Wang, S. J. Yan, C. Yang, W. W. He, J. Z. Chen, S. Q. Wang, X. Y. Zhang, and S. L. Dai. Microstructure and tensile properties of bulk nanostructured aluminum/graphene composites prepared via cryomilling. *Materials Science and Engineering A*, Vol. 626, 2015, pp. 400–405.

[58] Liu, J., U. Khan, J. Coleman, B. Fernandez, P. Rodriguez, S. Naher, and D. Brabazon. Graphene oxide and graphene nanosheet reinforced aluminium matrix composites: Powder synthesis and prepared composite characteristics. *Materials & Design*, Vol. 94, 2016, pp. 87–94.

[59] Dasari, B. L., M. Morshed, J. M. Nouri, D. Brabazon, and S. Naher. Mechanical properties of graphene oxide reinforced aluminium matrix composites. *Composites. Part B, Engineering*, Vol. 145, 2018, pp. 136–144.

[60] Hu, Z., G. Tong, Q. Nian, R. Xu, M. Saei, F. Chen, C. Chen, M. Zhang, H. Guo, and J. Xu. Laser sintered single layer graphene oxide reinforced titanium matrix nanocomposites. *Composites. Part B, Engineering*, Vol. 93, 2016, pp. 352–359.

[61] Liu, Y., Y. Liu, Q. Zhang, C. Zhang, J. Wang, Y. Wu, P. Han, Z. Gao, L. Wang, and X. Wu. Control of the microstructure and mechanical properties of electrodeposited graphene/Ni composite. *Materials Science and Engineering A*, Vol. 727, 2018, pp. 133–139.

[62] Kuang, D., L. Xu, L. Liu, W. Hu, and Y. Wu. Graphene–nickel composites. *Applied Surface Science*, Vol. 273, 2013, pp. 484–490.

[63] Dutkiewicz, J., P. Ozga, W. Maziarz, J. Pstruś, B. Kania, P. Bobrowski, and J. Stolarska. Microstructure and properties of bulk copper matrix composites strengthened with various kinds of graphene nanoplatelets. *Materials Science and Engineering A*, Vol. 628, 2015, pp. 124–134.

[64] ng, L. Yao, X. Lin, B. Wang, and E. Guan. Tribological properties of copper matrix composites reinforced with homogeneously dispersed graphene nanosheets. *Journal of Materials Science and Technology*, Vol. 34, No. 10, 2018, pp. 1925-1931.

[65] Kavimani, V., and K. S. Prakash. Tribological behaviour predictions of r-GO reinforced Mg composite using ANN coupled Taguchi approach. *Journal of Physics and Chemistry of Solids*, Vol. 110, 2017, pp. 409–419.

[66] Ponraj, N. V., A. Azhagurajan, S. C. Vettivel, X. Sahaya Shajan, P. Y. Nabhiraj, and M. Sivapragash. Graphene nanosheet as reinforcement agent in copper matrix composite by using powder metallurgy method. *Surfaces and Interfaces*, Vol. 6, 2017, pp. 190–196.

[67] Zhao, C. Enhanced strength in reduced graphene oxide/nickel composites prepared by molecular-level mixing for structural applications. *Applied Physics. A, Materials Science & Processing*, Vol. 118, No. 2, 2015, pp. 409–416.

[68] Gao, X., H. Yue, E. Guo, H. Zhang, X. Lin, L. Yao, and B. Wang. Preparation and tensile properties of homogeneously dispersed graphene reinforced aluminum matrix composites. *Materials & Design*, Vol. 94, 2016, pp. 54–60.

[69] Ju, J. M., G. Wang, and K.-H. Sim. Facile synthesis of graphene reinforced Al matrix composites with improved dispersion of graphene and enhanced mechanical properties. *Journal of Alloys and Compounds*, Vol. 704, 2017, pp. 585–592.

[70] Kwon, H., J. Mondal, K. A. AlOgab, V. Sammelselg, M. Takamichi, A. Kawaski, and M. Leparoux. Graphene oxide-reinforced aluminum alloy matrix composite materials fabricated by powder metallurgy. *Journal of Alloys and Compounds*, Vol. 698, 2017, pp. 807–813.

[71] Jiang, R., X. Zhou, Q. Fang, and Z. Liu. Copper–graphene bulk composites with homogeneous graphene dispersion and enhanced mechanical properties. *Materials Science and Engineering A*, Vol. 654, 2016, pp. 124–130.

[72] Hwang, J., T. Yoon, S. H. Jin, J. Lee, T. S. Kim, S. H. Hong, and S. Jeon. Enhanced mechanical properties of graphene/copper nanocomposites using a molecular-level mixing process. *Advanced Materials*, Vol. 25, No. 46, 2013, pp. 6724–6729.

[73] Wang, J., Z. Li, G. Fan, H. Pan, Z. Chen, and D. Zhang. Reinforcement with graphene nanosheets in aluminum matrix composites. *Scripta Materialia*, Vol. 66, No. 8, 2012, pp. 594–597.

[74] Geim, A. K. Graphene prehistory. *Physica Scripta*, Vol. 2012(T146), 2012, pp. 014003.

[75] Yin, S., Z. Zhang, E. J. Ekoi, J. J. Wang, D. P. Dowling, V. Nicolosi, and R. Lupoi. Novel cold spray for fabricating graphene-reinforced metal matrix composites. *Materials Letters*, Vol. 196, 2017, pp. 172–175.

[76] Brodie, B. C. On the atomic weight of graphite. *Philosophical Transactions*, Vol. 149, 1859, pp. 249-259.

[77] Hummers, W. S., and R. E. Offeman. Preparation of Graphitic Oxide. *Journal of the American Chemical Society*, Vol. 80, No. 6, 1958, p. 1339.

[78] Pei, S., and H.-M. Cheng. The reduction of graphene oxide. *Carbon*, Vol. 50, No. 9, 2012, pp. 3210–3228.
[79] SHANG, Y., D. ZHANG, Y. LIU, and C. GUO. Preliminary comparison of different reduction methods of graphene oxide. *Bulletin of Materials Science*, Vol. 38, 2015, pp. 7-12.
[80] Johnson, D. W., B. P. Dobson, and K. S. Coleman. A manufacturing perspective on graphene dispersions. *Curr. Opin. Colloid Interface*, Vol. 20, No. 5-6, 2015, pp. 367–382.
[81] Jia, X., J. Campos-Delgado, M. Terrones, V. Meunier, and M. S. Dresselhaus. Graphene edges: A review of their fabrication and characterization. *Nanoscale*, Vol. 3, No. 1, 2011, pp. 86–95.
[82] Snook, I., and A. Barnard. *Physics and Applications of Graphene edited by Dr.* Sergey Mikhailov, InTech, 2011, Chapter 13, pp. 277–302.
[83] Han, M. Y., B. Özyilmaz, Y. Zhang, and P. Kim. Energy band-gap engineering of graphene nanoribbons. *Physical Review Letters*, Vol. 98, 2007, pp. 206805.
[84] Campos-Delgado, J., J. M. Romo-Herrera, X. Jia, D. A. Cullen, H. Muramatsu, Y. A. Kim, T. Hayashi, Z. Ren, D. J. Smith, Y. Okuno, T. Ohba, H. Kanoh, K. Kaneko, M. Endo, H. Terrones, M. S. Dresselhaus, and M. Terrones. Bulk production of a new form of sp(2) carbon: Crystalline graphene nanoribbons. *Nano Letters*, Vol. 8, No. 9, Sep. 2008, pp. 2773–2778.
[85] Jiao, L., L. Zhang, X. Wang, G. Diankov, and H. Dai. Narrow graphene nanoribbons from carbon nanotubes. *Nature*, Vol. 458, No. 7240, Apr. 16, 2009, pp. 877–880.
[86] Avouris, P., and C. Dimitrakopoulos. Graphene: synthesis and applications. *Materials Today*, Vol. 15, 2012, pp. 86-97.
[87] Shao, P., W. Yang, Q. Zhang, Q. Meng, X. Tan, Z. Xiu, J. Qiao, Z. Yu, and G. Wu. Microstructure and tensile properties of 5083 Al matrix composites reinforced with graphene oxide and graphene nanoplates prepared by pressure infiltration method. *Composites Part A: Applied Science and Manufacturing*, Vol. 109, 2018, pp. 151-162.
[88] Chen, Y., X. Zhang, E. Liu, C. He, Y. Han, Q. Li, P. Nash, and N. Zhao. Fabrication of three-dimensional graphene/Cu composite by in-situ CVD and its strengthening mechanism. *Journal of Alloys and Compounds*, Vol. 688, 2016, pp. 69–76.
[89] Jiang, J., X. He, J. Du, X. Pang, H. Yang, and Z. Wei. In-situ fabrication of graphene-nickel matrix composites. *Materials Letters*, Vol. 220, 2018, pp. 178–181.
[90] Fu, K., X. Zhang, C. Shi, E. Liu, F. He, J. Li, N. Zhao, and C. He. An approach for fabricating Ni@graphene reinforced nickel matrix composites with enhanced mechanical properties. *Materials Science and Engineering A*, Vol. 715, 2018, pp. 108–116.
[91] Zhong, Y., Z. Zhen, and H. Zhu. Graphene: Fundamental research and potential applications. *FlatChem*, Vol. 4, 2017, pp. 20–32.
[92] Dasari, B. L., J. M. Nouri, D. Brabazon, and S. Naher. Graphene and derivatives – Synthesis techniques, properties and their energy applications. *Energy*, Vol. 140, 2017, pp. 766–778.
[93] Chu, K., F. Wang, X. Wang, and D. Huang. Anisotropic mechanical properties of graphene/copper composites with aligned graphene. *Materials Science and Engineering A*, Vol. 713, 2018, pp. 269–277.
[94] Yang, W., Q. Zhao, L. Xin, J. Qiao, J. Zou, P. Shao, Z. Yu, Q. Zhang, and G. Wu. Microstructure and mechanical properties of graphene nanoplates reinforced pure Al matrix composites prepared by pressure infiltration method. *Journal of Alloys and Compounds*, Vol. 732, 2018, pp. 748–758.
[95] Jiang, Y., Z. Tan, R. Xu, G. Fan, D.-B. Xiong, Q. Guo, Y. Su, Z. Li, and D. Zhang. Tailoring the structure and mechanical properties of graphene nanosheet/aluminum composites by flake powder metallurgy via shift-speed ball milling. *Composites Part A: Applied Science and Manufacturing,* Vol. 111, 2018, pp. 73-82.
[96] Si, X., M. Li, F. Chen, P. Eklund, J. Xue, F. Huang, S. Du, and Q. Huang. Effect of carbide interlayers on the microstructure and properties of graphene-nanoplatelet-reinforced copper matrix composites. *Materials Science and Engineering A*, Vol. 708, 2017, pp. 311–318.
[97] Chen, F., J. Ying, Y. Wang, S. Du, Z. Liu, and Q. Huang. Effects of graphene content on the microstructure and properties of copper matrix composites. *Carbon*, Vol. 96, 2016, pp. 836–842.
[98] Khodabakhshi, F., M. Nosko, and A. P. Gerlich. Effects of graphene nano-platelets (GNPs) on the microstructural characteristics and textural development of an Al-Mg alloy during friction-stir processing. *Surface and Coatings Technology*, Vol. 335, 2018, pp. 288–305.
[99] Tabandeh-Khorshid, M., E. Omrani, P. L. Menezes, and P. K. Rohatgi. Tribological performance of self-lubricating aluminum matrix nanocomposites: Role of graphene nanoplatelets. *Eng. Sci. Technol. Int. J.*, Vol. 19, No. 1, 2016, pp. 463–469.
[100] Kim, W. J., T. J. Lee, and S. H. Han. Multi-layer graphene/copper composites: Preparation using high-ratio differential speed rolling, microstructure and mechanical properties. *Carbon*, Vol. 69, 2014, pp. 55–65.
[101] Jang, H., S. Yoo, M. Quevedo, and H. Choi. Effect of processing route on mechanical and thermal properties of few-layered graphene (FLG)-reinforced copper matrix composites. *Journal of Alloys and Compounds*, Vol. 754, 2018, pp. 7–13.
[102] Ghasali, E., P. Sangpour, A. Jam, H. Rajaei, K. Shirvanimoghaddam, and T. Ebadzadeh. Microwave and spark plasma sintering of carbon nanotube and graphene reinforced aluminum matrix composite. *Archives of Civil and Mechanical Engineering*, Vol. 18, No. 4, 2018, pp. 1042–1054.
[103] Chen, L. Y., H. Konishi, A. Fehrenbacher, C. Ma, J. Q. Xu, H. Choi, H. F. Xu, F. E. Pfefferkorn, and X. C. Li. Novel nanoprocessing route for bulk graphene nanoplatelets reinforced metal matrix nanocomposites. *Scripta Materialia*, Vol. 67, No. 1, 2012, pp. 29–32.
[104] Rashad, M., F. Pan, A. Tang, Y. Lu, M. Asif, S. Hussain, J. She, J. Gou, J. Mao, and J. Magnes. Effect of graphene nanoplatelets (GNPs) addition on strength and ductility of magnesium-titanium alloys. *Alloy.*, Vol. 1, No. 3, 2013, pp. 242–248.
[105] Rashad, M., F. Pan, H. Hu, M. Asif, S. Hussain, and J. She. Enhanced tensile properties of magnesium composites reinforced with graphene nanoplatelets. *Materials Science and Engineering A*, Vol. 630, 2015, pp. 36–44.
[106] Rashad, M., F. Pan, A. Tang, M. Asif, J. She, J. Gou, J. Mao, and H. Hu. Development of magnesium-graphene nanoplatelets composite. *Journal of Composite Materials*, Vol. 49, No. 3, 2014, pp. 285–293.
[107] Rashad, M., F. Pan, M. Asif, and A. Tang. Powder metallurgy of Mg–1%Al–1%Sn alloy reinforced with low content of graphene nanoplatelets (GNPs). *Journal of Industrial and Engineering Chemistry*, Vol. 20, No. 6, 2014, pp. 4250–4255.
[108] Turan, M. E., Y. Sun, Y. Akgul, Y. Turen, and H. Ahlatci. The effect of GNPs on wear and corrosion behaviors of pure magnesium. *Journal of Alloys and Compounds*, Vol. 724, 2017, pp. 14–23.

[109] Das, A., and S. P. Harimkar. Effect of Graphene Nanoplate and Silicon Carbide Nanoparticle Reinforcement on Mechanical and Tribological Properties of Spark Plasma Sintered Magnesium Matrix Composites. *Materials Science and Technology*, Vol. 30, No. 11, 2014, pp. 1059–1070.

[110] Rashad, M., F. Pan, and M. Asif. Exploring mechanical behavior of Mg–6Zn alloy reinforced with graphene nanoplatelets. *Materials Science and Engineering A*, Vol. 649, 2016, pp. 263–269.

[111] Rashad, M., F. Pan, D. Lin, and M. Asif. High temperature mechanical behavior of AZ61 magnesium alloy reinforced with graphene nanoplatelets. *Materials & Design*, Vol. 89, 2016, pp. 1242–1250.

[112] Hu, Z., G. Tong, D. Lin, Q. Nian, J. Shao, Y. Hu, M. Saeib, S. Jin, and G. J. Cheng. Laser sintered graphene nickel nanocomposites. *Journal of Materials Processing Technology*, Vol. 231, 2016, pp. 143–150.

[113] Tang, Y., X. Yang, R. Wang, and M. Li. Enhancement of the mechanical properties of graphene–copper composites with graphene–nickel hybrids. *Materials Science and Engineering A*, Vol. 599, 2014, pp. 247–254.

[114] Mu, X. N., H. N. Cai, H. M. Zhang, Q. B. Fan, Z. H. Zhang, Y. Wu, Y. X. Ge, and D. D. Wang. Interface evolution and superior tensile properties of multi-layer graphene reinforced pure Ti matrix composite. *Materials & Design*, Vol. 140, 2018, pp. 431–441.

[115] Mu, X. N., H. M. Zhang, H. N. Cai, Q. B. Fan, Z. H. Zhang, Y. Wu, Z. J. Fu, and D. H. Yu. Microstructure evolution and superior tensile properties of low content graphene nanoplatelets reinforced pure Ti matrix composites. *Materials Science and Engineering A*, Vol. 687, 2017, pp. 164–174.

[116] Mu, X. N., H. N. Cai, H. M. Zhang, Q. B. Fan, F. C. Wang, Z. H. Zhang, Y. Wu, Y. X. Ge, S. Chang, R. Shi, Y. Zhou, and D. D. Wang. Uniform dispersion of multi-layer graphene reinforced pure titanium matrix composites via flake powder metallurgy. *Materials Science and Engineering A*, Vol. 725, 2018, pp. 541–548.

[117] Cao, Z., X. Wang, J. Li, Y. Wu, H. Zhang, J. Guo, and S. Wang. Reinforcement with graphene nanoflakes in titanium matrix composites. *Journal of Alloys and Compounds*, Vol. 696, 2017, pp. 498–502.

[118] Yan, S. J., S. L. Dai, X. Y. Zhang, C. Yang, Q. H. Hong, J. Z. Chen, and Z. M. Lin. Investigating aluminum alloy reinforced by graphene nanoflakes. *Materials Science and Engineering A*, Vol. 612, 2014, pp. 440–444.

[119] Bastwros, M., G.-Y. Kim, C. Zhu, K. Zhang, S. Wang, X. Tang, and X. Wang. Effect of ball milling on graphene reinforced Al6061 composite fabricated by semi-solid sintering. *Composites. Part B, Engineering*, Vol. 60, 2014, pp. 111–118.

[120] Zhang, Z. W., Z. Y. Liu, B. L. Xiao, D. R. Ni, and Z. Y. Ma. High efficiency dispersal and strengthening of graphene reinforced aluminum alloy composites fabricated by powder metallurgy combined with friction stir processing. *Carbon*, Vol. 135, 2018, pp. 215–223.

[121] Wang, L., Y. Cui, S. Yang, B. Li, Y. Liu, P. Dong, J. Bellah, G. Fan, R. Vajtai, and W. Fei. Microstructure and properties of carbon nanosheet/copper composites processed by particle-assisted shear exfoliation. *RSC Advances*, Vol. 5, 2015, pp. 19321-19328.

[122] Kim, Y., J. Lee, M. S. Yeom, J. W. Shin, H. Kim, Y. Cui, J. W. Kysar, J. Hone, Y. Jung, S. Jeon, and S. M. Han. Strengthening effect of single-atomic-layer graphene in metal-graphene nanolayered composites. *Nature Communications*, Vol. 4, No. 1, 2013, p. 2114.

[123] Liu, X., D. Wei, L. Zhuang, C. Cai, and Y. Zhao. Fabrication of high-strength graphene nanosheets/Cu composites by accumulative roll bonding. *Materials Science and Engineering A*, Vol. 642, 2015, pp. 1–6.

[124] Wang, X., J. Li, and Y. Wang. Improved high temperature strength of copper-graphene composite material. *Materials Letters*, Vol. 181, 2016, pp. 309–312.

[125] Zhang, X., K. Wu, M. He, Z. Ye, S. Tang, and Z. Jiang. Facile synthesis and characterization of reduced graphene oxide/copper composites using freeze-drying and spark plasma sintering. *Materials Letters*, Vol. 166, 2016, pp. 67–70.

[126] Li, J. F., L. Zhang, J. K. Xiao, K. c. Zhou. Sliding wear behavior of copper-based composites reinforced with graphene nanosheets and graphite. *Transactions of Nonferrous Metals Society of China*, Vol. 25, 2015, pp. 3354-3362.

[127] Zhang, D., and Z. Zhan. Preparation of graphene nanoplatelets-copper composites by a modified semi-powder method and their mechanical properties. *Journal of Alloys and Compounds*, Vol. 658, 2016, pp. 663–671.

[128] Chu, K., F. Wang, Y. Li, X. Wang, D. Huang, and H. Zhang. Interface structure and strengthening behavior of graphene/CuCr composites. *Carbon*, Vol. 133, 2018, pp. 127–139.

[129] Asgharzadeh, H., and M. Sedigh. Synthesis and mechanical properties of Al matrix composites reinforced with few-layer graphene and graphene oxide. *Journal of Alloys and Compounds*, Vol. 728, 2017, pp. 47–62.

[130] Rashad, M., F. Pan, A. Tang, M. Asif, S. Hussain, J. Gou, and J. Mao. Improved strength and ductility of magnesium with addition of aluminum and graphene nanoplatelets (Al+GNPs) using semi powder metallurgy method. *Journal of Industrial and Engineering Chemistry*, Vol. 23, 2015, pp. 243–250.

[131] Song, Y., Y. Chen, W. W. Liu, W. L. Li, Y. G. Wang, D. Zhao, and X. B. Liu. Microscopic mechanical properties of titanium composites containing multi-layer graphene nanofillers. *Materials & Design*, Vol. 109, 2016, pp. 256–263.

[132] Ashwath, P., and M. A. Xavior. The effect of ball milling & reinforcement percentage on sintered samples of aluminium alloy metal matrix composites. *Procedia Engineering*, Vol. 97, 2014, pp. 1027-1032.

[133] Hu, Z., F. Chen, J. Xu, Q. Nian, D. Lin, C. Chen, X. Zhu, Y. Chen, and M. Zhang. 3D printing graphene-aluminum nanocomposites. *Journal of Alloys and Compounds*, Vol. 746, 2018, pp. 269–276.

[134] Zhang, D., and Z. Zhan. Strengthening effect of graphene derivatives in copper matrix composites. *Journal of Alloys and Compounds*, Vol. 654, 2016, pp. 226–233.

[135] Yang, Z., L. Wang, Z. Shi, M. Wang, Y. Cui, B. Wei, S. Xu, Y. Zhu, and W. Fei. Preparation mechanism of hierarchical layered structure of graphene/copper composite with ultrahigh tensile strength. *Carbon*, Vol. 127, 2018, pp. 329–339.

[136] Wang, L., Y. Cui, B. Li, S. Yang, R. Li, Z. Liu, R. Vajtai, and W. Fei. High apparent strengthening efficiency for reduced graphene oxide in copper matrix composites produced by molecule-lever mixing and high-shear mixing. *RSC Advances*, Vol. 5, 2015, pp. 51193-51200.

[137] Ayyappadas, C., A. Muthuchamy, A. Raja Annamalai, and D. K. Agrawal. An investigation on the effect of sintering mode on various properties of copper-graphene metal matrix composite. *Advanced Powder Technology*, Vol. 28, No. 7, 2017, pp. 1760–1768.

[138] Du, X., W. Du, Z. Wang, K. Liu, and S. Li. Ultra-high strengthening efficiency of graphene nanoplatelets reinforced magnesium matrix composites. *Materials Science and Engineering A*, Vol.

711, 2018, pp. 633–642.

[139] Dixit, S., A. Mahata, D. R. Mahapatra, S. V. Kailas, and K. Chattopadhyay. Multi-layer graphene reinforced aluminum – Manufacturing of high strength composite by friction stir alloying. *Composites. Part B, Engineering*, Vol. 136, 2018, pp. 63–71.

[140] Yolshina, L. A., R. V. Muradymov, I. V. Korsun, G. A. Yakovlev, and S. V. Smirnov. Novel aluminum-graphene and aluminum-graphite metallic composite materials: Synthesis and properties. *Journal of Alloys and Compounds*, Vol. 663, 2016, pp. 449–459.

[141] Venkatesan, S., and M. Anthony Xavior. Tensile behavior of aluminum alloy (AA7050) metal matrix composite reinforced with graphene fabricated by stir and squeeze cast processes. *Science and Technology of Materials,* Vol. 30, 2018, pp. 74-85.

[142] Chen, Y. X., X. Zhang, E. Z. Liu, C. N. He, C. S. Shi, J. J. Li, P. Nash, and N. Q. Zhao. Fabrication of in-situ grown graphene reinforced Cu matrix composites. *Scientific Reports*, Vol. 6, 2016, pp. 1-9.

[143] Liu, X., J. Li, J. Sha, E. Liu, Q. Li, C. He, C. Shi, and N. Zhao. In-situ synthesis of graphene nanosheets coated copper for preparing reinforced aluminum matrix composites. *Materials Science and Engineering A*, Vol. 709, 2018, pp. 65–71.

[144] Liu, G., N. Zhao, C. Shi, E. Liu, F. He, L. Ma, Q. Li, J. Li, and C. He. In-situ synthesis of graphene decorated with nickel nanoparticles for fabricating reinforced 6061Al matrix composites. *Materials Science and Engineering A*, Vol. 699, 2017, pp. 185–193.

[145] Sruti, A. N., and K. Jagannadham. Electrical Conductivity of Graphene Composites with In and In-Ga Alloy. *Journal of Electronic Materials*, Vol. 39, No. 8, 2010, pp. 1268–1276.

[146] Meyers, M. A., A. Mishra, and D. J. Benson. Mechanical properties of nanocrystalline materials. *Progress in Materials Science*, Vol. 51, No. 4, 2006, pp. 427–556.

[147] Suryanarayana, C. Mechanical alloying and milling. *Progress in Materials Science*, Vol. 46, No. 1-2, 2001, pp. 1–184.

[148] Mishra, R. S., and Z. Y. Ma. Friction stir welding and processing. *Materials Science and Engineering R*, Vol. 50, 2005, pp. 1-78.

[149] Simar, A., Y. Bréchet, B. de Meester, A. Denquin, C. Gallais, and T. Pardoen. Integrated modeling of friction stir welding of 6xxx series Al alloys: Process, microstructure and properties. *Progress in Materials Science*, Vol. 57, No. 1, 2012, pp. 95–183.

[150] Liu, Z. Y., B. L. Xiao, W. G. Wang, and Z. Y. Ma. Singly dispersed carbon nanotube/aluminum composites fabricated by powder metallurgy combined with friction stir processing. *Carbon*, Vol. 50, No. 5, 2012, pp. 1843–1852.

[151] Ma, Z. Y., A. L. Pilchak, M. C. Juhas, and J. C. Williams. Microstructural refinement and property enhancement of cast light alloys via friction stir processing. *Scripta Materialia*, Vol. 58, No. 5, 2008, pp. 361–366.

[152] Srinivasan, D., R.S. Kadadeveramath, S. Rajendran, and E. N. Ganesh. State-of-art review of ceramic reinforced aluminum metal matrix composite and it's machining characteristics. *Journal of Chemical and Pharmaceutical Sciences*, No. 11, 2017, pp. 154-164.

[153] Hu, Z., F. Chen, J. Xu, Z. Ma, H. Guo, C. Chen, Q. Nian, X. Wang, and M. Zhang. Fabricating graphene-titanium composites by laser sintering PVA bonding graphene titanium coating: Microstructure and mechanical properties. *Composites. Part B, Engineering*, Vol. 134, 2018, pp. 133–140.

[154] Khodabakhshi, F., S. M. Arab, P. Švec, and A. P. Gerlich. Fabrication of a new Al-Mg/graphene nanocomposite by multi-pass friction-stir processing: Dispersion, microstructure, stability, and strengthening. *Materials Characterization*, Vol. 132, 2017, pp. 92–107.

[155] Fadavi Boostani, A., S. Yazdani, R. Taherzadeh Mousavian, S. Tahamtan, R. Azari Khosroshahi, D. Wei, D. Brabazon, J. Z. Xu, X. M. Zhang, and Z. Y. Jiang. Strengthening mechanisms of graphene sheets in aluminium matrix nanocomposites. *Materials & Design*, Vol. 88, 2015, pp. 983–989.

[156] Bartolucci, S. F., J. Paras, M. A. Rafiee, J. Rafiee, S. Lee, D. Kapoor, and N. Koratkar. Graphene–aluminum nanocomposites. *Materials Science and Engineering A*, Vol. 528, No. 27, 2011, pp. 7933–7937.

[157] Kim, Y., J. Lee, M. S. Yeom, J. W. Shin, H. Kim, Y. Cui, J. W. Kysar, J. Hone, Y. Jung, S. Jeon, and S. M. Han. Strengthening effect of single-atomic-layer graphene in metal-graphene nanolayered composites. *Nature Communications*, Vol. 4, No. 1, 2013, p. 2114.

[158] Feng, S., Q. Guo, Z. Li, G. Fan, Z. Li, D.-B. Xiong, Y. Su, Z. Tan, J. Zhang, and D. Zhang. Strengthening and toughening mechanisms in graphene-Al nanolaminated composite micro-pillars. *Acta Materialia*, Vol. 125, 2017, pp. 98–108.

[159] Cao, M., D.-B. Xiong, Z. Tan, G. Ji, B. Amin-Ahmadi, Q. Guo, G. Fan, C. Guo, Z. Li, and D. Zhang. Aligning graphene in bulk copper: Nacre-inspired nanolaminated architecture coupled with in-situ processing for enhanced mechanical properties and high electrical conductivity. *Carbon*, Vol. 117, 2017, pp. 65–74.

[160] Wejrzanowski, T., M. Grybczuk, M. Chmielewski, K. Pietrzak, K. J. Kurzydlowski, and A. Strojny-Nedza. Thermal conductivity of metal-graphene composites. *Materials & Design*, Vol. 99, 2016, pp. 163–173.

[161] Chu, K., X. Wang, Y. Li, D. Huang, Z. Geng, X. Zhao, H. Liu, and H. Zhang. Thermal properties of graphene/metal composites with aligned graphene. *Materials & Design*, Vol. 140, 2018, pp. 85–94.

[162] Boden, A., B. Boerner, P. Kusch, I. Firkowska, and S. Reich. Nanoplatelet size to control the alignment and thermal conductivity in copper-graphite composites. *Nano Letters*, Vol. 14, No. 6, 2014, pp. 3640–3644.

[163] Cao, M., D.-B. Xiong, L. Yang, S. Li, Y. Xie, Q. Guo, Z. Li, H. Adams, J. Gu, T. Fan, X. Zhang, and D. Zhang. Ultrahigh Electrical Conductivity of Graphene Embedded in Metals. *Advanced Functional Materials*, Vol. 29, No. 17, 2019, p. 1806792.

[164] Jin, B., D.-B. Xiong, Z. Tan, G. Fan, Q. Guo, Y. Su, Z. Li, and D. Zhang. Enhanced corrosion resistance in metal matrix composites assembled from graphene encapsulated copper nanoflakes. *Carbon*, Vol. 142, 2019, pp. 482–490.

[165] Schriver, M., W. Regan, W. J. Gannett, A. M. Zaniewski, M. F. Crommie, and A. Zettl. Graphene as a long-term metal oxidation barrier: Worse than nothing. *ACS Nano*, Vol. 7, No. 7, 2013, pp. 5763–5768.

[166] Chen, S., L. Brown, M. Levendorf, W. Cai, S.-Y. Ju, J. Edgeworth, X. Li, C. W. Magnuson, A. Velamakanni, R. D. Piner, J. Kang, J. Park, and R. S. Ruoff. Oxidation resistance of graphene-coated Cu and Cu/Ni alloy. *ACS Nano*, Vol. 5, No. 2, 2011, pp. 1321–1327.